

# Faculteit Industriële Ingenieurswetenschappen

master in de industriële wetenschappen: energie

## **Masterthesis**

***Modelling the impact of microclimate conditions on moisture absorption in PV modules***

**Klaartje Dirckx  
Jason 's Jongers**

Scriptie ingediend tot het behalen van de graad van master in de industriële wetenschappen: energie

### **PROMOTOR :**

Prof. dr. ir. Michael DAENEN

### **PROMOTOR :**

dr. Ismail KAAYA

### **COPROMOTOR :**

dr. Nikoleta KYRANAKI

Gezamenlijke opleiding UHasselt en KU Leuven



Universiteit Hasselt | Campus Diepenbeek | Faculteit Industriële Ingenieurswetenschappen | Agoralaan Gebouw H - Gebouw B | BE 3590 Diepenbeek

Universiteit Hasselt | Campus Diepenbeek | Agoralaan Gebouw D | BE 3590 Diepenbeek  
Universiteit Hasselt | Campus Hasselt | Martelarenlaan 42 | BE 3500 Hasselt



**2022**  
**2023**

# Faculteit Industriële Ingenieurswetenschappen

master in de industriële wetenschappen: energie

## ***Masterthesis***

***Modelling the impact of microclimate conditions on moisture absorption in PV modules***

**Klaartje Dirckx**

**Jason 's Jongers**

Scriptie ingediend tot het behalen van de graad van master in de industriële wetenschappen: energie

### **PROMOTOR :**

Prof. dr. ir. Michael DAENEN

### **PROMOTOR :**

dr. Ismail KAAYA

### **COPROMOTOR :**

dr. Nikoleta KYRANAKI



**KU LEUVEN**



## Foreword

The master's thesis is created by Hasselt University in collaboration with KU Leuven and EnergyVille for the master's degree in industrial engineering. In today's society and in the future, renewable energy is necessary. Research on the lifetime of renewable energy systems is therefore very important. As students, this topic was relevant to our studies, Energy and Electromechanical Engineering, to get a better idea of the impact that moisture can have on PV modules. This topic was also interesting because of the combination of many skills including modelling and developing an in-house made test setup. The fact that the topic is about renewable energy is an advantage.

Finally, a few words of appreciation. We would like to thank EnergyVille for making the thesis possible and for allowing us to use the lab facilities. We would also like to thank dr. Ismail Kaaya and dr. Nikoleta Kyranaki for their guidance, advice, and support. Next, we thank Daniel Jimenez Pelarda for the COMSOL simulations and his supervisors dr. Malte Ruben Vogt and ir. Youri Blom. Finally, we would like to thank our supervisor Prof. dr. ir. Michaël Daenen.



## Table of content

<b>Foreword</b> .....	<b>1</b>
<b>Tables</b> .....	<b>5</b>
<b>Figures</b> .....	<b>7</b>
<b>Abstract</b> .....	<b>9</b>
<b>Abstract Nederlands</b> .....	<b>11</b>
<b>1 Introduction</b> .....	<b>13</b>
1.1 Imec .....	13
1.2 Lifetime of PV modules .....	13
1.3 Problem statement.....	13
1.4 Objective 1.....	14
1.5 Objective 2.....	16
<b>2 Moisture inside cavity</b> .....	<b>17</b>
2.1 Reference study.....	17
2.1.1 Importance of longevity .....	17
2.1.2 Material properties .....	17
2.1.3 Ventilation .....	17
2.1.4 Thermal model .....	18
2.1.5 Cavity wall.....	19
2.2 Analytical model.....	20
2.2.1 Moisture transport through the air.....	21
2.2.2 Moisture transport through a solid material .....	23
2.2.3 Parameters of the model and surroundings .....	24
2.3 Sensitivity analysis.....	25
2.4 Measurements and results.....	27
2.4.1 Temperature measurements .....	27
2.4.2 Relative humidity measurements .....	28
2.4.3 Average values for different sensor locations.....	29
2.4.4 Difference between STMW and OMWT.....	29
2.4.5 Model validation.....	30
2.4.6 Analysing the model on longterm data .....	31
2.4.7 Errors .....	33
2.4.8 PVGIS .....	36
2.5 Conclusion cavity model.....	38
<b>3 Moisture ingress into PV modules</b> .....	<b>41</b>

3.1	Reference study.....	41
3.1.1	Different type of failures .....	41
3.1.2	Fick's law.....	42
3.1.3	Using FEM analysis for moisture ingress .....	42
3.1.4	Moisture pathways.....	43
3.1.5	Measurements .....	44
3.1.6	Humidity indicator cards calibration .....	45
3.2	Analytical model .....	46
3.2.1	Breathable backsheet.....	47
3.2.2	Glass backsheet PV module.....	47
3.2.3	Parameters .....	47
3.3	Validation analytical model .....	48
3.3.1	Backsheet and encapsulant.....	49
3.3.2	Module with breathable backsheet .....	53
3.3.3	Glass backsheet PV module.....	55
3.3.4	BIPV module .....	58
3.4	Measurements .....	60
3.4.1	Indicator cards.....	60
3.4.2	Lamination process.....	61
3.4.3	Measurement setup .....	61
3.4.4	Climatic chamber.....	62
3.4.5	Image processing.....	64
3.4.6	Calibration curve humidity cards .....	65
3.4.7	Results .....	67
3.5	Conclusion BIPV module.....	76
<b>4</b>	<b>Conclusion .....</b>	<b>79</b>
	<b>References .....</b>	<b>81</b>
	<b>Appendices .....</b>	<b>83</b>

# Tables

- Table 1: Range input parameters ..... 26
- Table 2: Average values for the different locations of the sensors ..... 29
- Table 3: Difference between the STMW and OMWB panels ..... 29
- Table 4: Table of six months ..... 33
- Table 5: One-year average humidities for Singapore, Kuwait and Brussels ..... 38
- Table 6: Parameters Arrhenius equations ..... 48
- Table 7: Moving average ..... 48
- Table 8: Explanation samples ..... 68





## Figures

Figure 1: Tested PV modules in EnergyVille .....	14
Figure 2: Different sensors .....	15
Figure 3: Boxplot of the relative humidity for the different segments.....	18
Figure 4: PV elements and thermal elements of ventilated BIPV module.....	19
Figure 5: Thermal model .....	19
Figure 6: Heat transport modelling in ventilated cavity walls .....	19
Figure 7: Moisture transport modelling in ventilated cavity walls .....	20
Figure 8: Different moisture paths for a ventilated BIPV module.....	21
Figure 9: Cross section of the BIPV module setup with dimensions.....	25
Figure 10: Pareto chart.....	26
Figure 11: Temperature measurements .....	27
Figure 12: Relative humidity measurements .....	28
Figure 13: Analytical model relative humidity for June 2022 .....	30
Figure 14: Analytical model relative humidity for July 2022.....	31
Figure 15: Analytical model relative humidity for October 2022.....	31
Figure 16: Analytical model relative humidity for November 2022.....	32
Figure 17: Analytical model relative humidity for December 2022 .....	32
Figure 18: Errors analytical model with inside parameters .....	34
Figure 19: Errors analytical model without inside parameters.....	35
Figure 20: Errors atmosphere .....	36
Figure 21: Simulated cavity relative humidity and ambient relative humidity for Singapore .....	37
Figure 22: Simulated cavity relative humidity and ambient relative humidity for Kuwait .....	37
Figure 23: Simulated cavity relative humidity and ambient relative humidity for Brussels .....	38
Figure 24: Non-breathable backsheet.....	43
Figure 25: Breathable backsheet.....	43
Figure 26: Pathways of a PV module with breathable backsheet.....	44
Figure 27: Indicator cards.....	45
Figure 28: Points where the moisture ingress is simulated .....	49
Figure 29: Results backsheet and encapsulant compared with Figure 1 of [19] .....	50
Figure 30: One-year results backsheet in point B1 .....	51
Figure 31: One-year results backsheet at different thicknesses.....	51
Figure 32: One-year results encapsulant in point E1 .....	52
Figure 33: One-year average moisture concentrations backsheet and encapsulant .....	52
Figure 34: Five-year results pathway two breathable backsheet module time depended .....	53
Figure 35: Results pathway two breathable backsheet module distance depended .....	54
Figure 36: Five-year average moisture concentrations pathway two breathable model.....	54
Figure 37: Five-year results Singapore glass backsheet model time depended .....	55
Figure 38: Results Singapore glass backsheet model distance depended .....	56
Figure 39: Five-year results Brussels glass backsheet model time depended .....	56
Figure 40: Results Brussels glass backsheet model distance depended .....	57
Figure 41: Five-year average moisture concentrations Singapore glass backsheet model .....	57
Figure 42: Five-year average moisture concentrations Brussels glass backsheet model .....	58
Figure 43: Half-year results BIPV module pathway 1.....	59
Figure 44: Fifteen-year results BIPV module pathway 2 .....	59
Figure 45: Indicator card lamination .....	60
Figure 46: Lay-out lamination .....	61
Figure 47: Measurement setup .....	62

Figure 48: Damp heat chamber .....	63
Figure 49: Calibration planning .....	63
Figure 50: Picture G4 210h .....	64
Figure 51: Picture G4 1222h .....	64
Figure 52: Zoomed in G4 .....	65
Figure 53: Lay-out calibration modules .....	65
Figure 54: C3 before damp heat .....	66
Figure 55: C3 40% .....	66
Figure 56: C3 50% .....	66
Figure 57: C3 60% .....	66
Figure 58: C3 70% .....	66
Figure 59: C3 85% .....	66
Figure 60: Example colour plot .....	67
Figure 61: C4 30% dot .....	68
Figure 62: C4 40% dot .....	68
Figure 63: C4 30% without 70% RH .....	69
Figure 64: C4 40% without 70% RH .....	69
Figure 65: B3 30% dot .....	70
Figure 66: B3 40% dot .....	70
Figure 67: B4 30% dot .....	71
Figure 68: B4 40% dot .....	71
Figure 69: G3 30% dot .....	72
Figure 70: G3 40% dot .....	72
Figure 71: G4 30% dot .....	73
Figure 72: G4 40% dot .....	73
Figure 73: G1 TU delft .....	74
Figure 74: G2 TU Delft .....	74
Figure 75: G3 .....	74
Figure 76: G4 .....	74
Figure 77: RMC levels B3 and B4 30% .....	75
Figure 78: RMC levels B3 and B4 40% .....	76

## Abstract

Imec's Energy Systems team, situated in Genk, developed a framework to simulate the photovoltaic (PV) lifetime energy production using a physics-based approach. This framework uses degradation rate models which are based on validated thermal models. However, the framework does not consider the moisture ingress in a PV module, which has been shown to affect the expected lifetime of a PV module significantly. In other studies, about moisture ingress, the microclimate (cavity, atmosphere, etc...) around building integrated photovoltaics (BIPV) modules has not been entirely investigated.

Therefore, this master's thesis has two main objectives. The first objective is to create an analytical model for calculating the relative humidity in the cavity and to test if this model is more accurate than considering the atmospheric humidity. The second objective is to create an analytical model for the moisture ingress in a PV module. The mentioned models are generated with Python. The model of the first goal is validated with measurement data of the cavity. This model is compared to a COMSOL model developed by TU Delft.

The measurements of the humidity in the cavity indicate that the model of the cavity is more accurate than when assuming that the humidity in the cavity is identical to the atmospheric humidity. The analytical model for the moisture ingress in the module reveals that the bill of materials plays a significant role on the moisture ingress. Especially, the use of different backsheets. This was also proven by the experiments.



## Abstract Nederlands

Het Energy Sytem Team van Imec, gevestigd in Genk, heeft een framework ontwikkeld om de energieproductie van photovoltaic (PV) modules te simuleren met behulp van een fysisch gebaseerd model. Dit framework gebruikt degradatiemodellen die gebaseerd zijn op gevalideerde thermische modellen. Het framework houdt geen rekening met de indringing van vocht in een PV-module. Dit heeft een belangrijke invloed op de verwachte levensduur. In andere studies over vochtindringing is het microklimaat (spouwmuur, atmosfeer, enz...) rond building integrated photovoltaics (BIPV) modules niet volledig onderzocht.

Daarom heeft deze masterproef twee hoofddoelstellingen. De eerste doelstelling stelt een analytisch model op om de relatieve vochtigheid in de spouwmuur te berekenen en te testen of dit model nauwkeuriger is dan de luchtvochtigheid. De tweede doelstelling maakt een analytisch model voor de indringing van vocht in een PV-module. Voorgaande modellen worden gegenereerd met Python. Het eerste model wordt gevalideerd met meetgegevens van de spouwmuur. Dit model wordt vergeleken met een COMSOL model ontwikkeld door TU Delft.

De metingen van de relatieve vochtigheid in de spouwmuur geven aan dat het model nauwkeuriger is dan de aanname dat de vochtigheid in de spouwmuur identiek is aan de luchtvochtigheid. Uit het analytische model voor de vochtindringing in de module blijkt dat de gebruikte materialen, voornamelijk de backsheets, een significante invloed hebben op de vochtindringing. Dit is ook het resultaat van het experiment.



# 1 Introduction

## 1.1 Imec

Imec is a research center that focuses on the innovation of nano and digital technology. It was founded in 1984 and it cooperates with UHasselt on solar energy, energy storage, etc [1]. The company has locations in Leuven, Antwerp, Brussels, and Genk and has other offices across the world. This master's thesis takes place in collaboration with EnergyVille in Genk. EnergyVille is a cooperation between the Belgian research teams of KU Leuven, VITO, imec, and UHasselt [2]. They focus on renewable and sustainable energy systems. Imec has more than 30 years of experience in the development of silicon and thin-film photovoltaics (PV). Currently, imec mostly focuses on research and development of thin photovoltaic panels. Additionally, they develop PV panels for applications such as building-integrated photovoltaics and lightweight solutions (for automotive). They have partnerships with the European R&D cluster Solliance. Together they work on the development of perovskite solar cells and their goal is to achieve world-record conversion efficiencies on cell and module level [1].

## 1.2 Lifetime of PV modules

Durability is an important factor in the study of PV modules. To simulate the lifetime of a PV module, a framework simulation program is used that was created by imec. The degradation rate is highly dependent on the bill of materials and the conditions of the environment. The framework simulation uses physics-based models. Imec's framework is capable of simulating the thermal behaviour for most of these new applications using pre-validated thermal models. This simulation framework, however, is currently unable to simulate the effect that environmental conditions have on moisture ingress inside the PV module. In this thesis, a model for the estimation of this effect will be developed with the purpose to be added to the simulation. In the simulation framework, both accuracy and speed are important. In today's research, a finite element method is used to simulate moisture ingress into the PV module. However, it is not possible to integrate a finite element model in the framework.

## 1.3 Problem statement

There are two main problems when calculating the lifetime of a PV module. The first problem is that these calculations do not incorporate the moisture ingress. The second problem when calculating the moisture ingress is using the ambient relative humidity instead of the humidity in the cavity. Together these two simplifications can cause a significant inaccuracy when calculating the expected lifetime of a PV module. Both problems require an analytical model instead of a model which uses finite element software. This is to ensure an easy incorporation into imec's simulation framework.



## 1.4 Objective 1

The first objective is to evaluate the microclimate around a building-integrated PV module (BIPV). The most important microclimate around a BIPV module is the cavity. This is an air gap that is connected to the backsheet of a PV module. The cavity, shown in Figure 1 can heavily affect the humidity inside the PV module. Therefore, the main goal for the first objective is to create an analytical model for the relative humidity inside the cavity. In most circumstances the moisture ingress is calculated by using the atmospheric conditions (outdoor conditions). In this thesis, the simulation will be carried out by using an analytical model for the cavity. The difference in accuracy between using the atmospheric or cavity conditions will be analysed. After that, the model will be validated with measurements from EnergyVille. Then, the ambient data of Brussels, Kuwait, and Singapore will be used to test the model for different climates.

Firstly, moisture ingress will be investigated for BIPV. For this purpose, the four different BIPV modules on the roof of EnergyVille are used and shown in Figure 1.

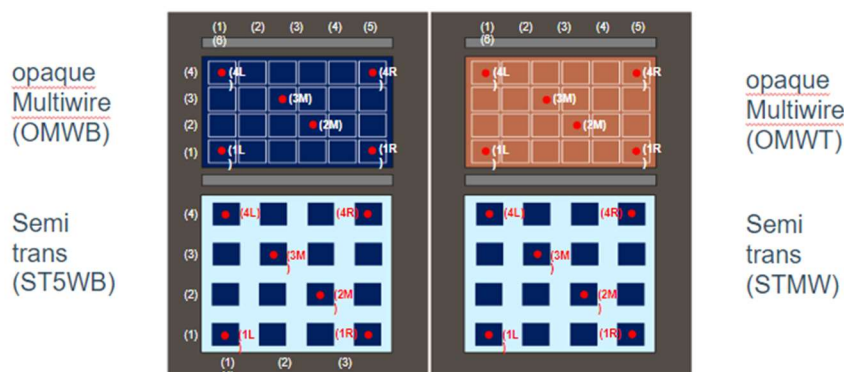


Figure 1: Tested PV modules in EnergyVille

The two PV modules at the top of Figure 1 are non-transparent, ventilated, and have a different colour. The colour of the left PV panel is black, and of the right is terracotta. The heat absorption from solar radiation depends on this colour. The bottom two PV modules are semi-transparent. The STMW (semi-transparent multi-wire) uses multi-wires to conduct electricity and the ST5WB (semi-transparent five-wire busbar) uses five busbars. The measurement setup has several sensors that measure the temperature, wind speed, relative humidity, and heat flux at different places. This is done respectively with a thermocouple, anemometer, relative humidity meter, and heat flux meter. Most of the temperature and humidity sensors are placed in proximity of the BIPV. Figure 2 shows the placement of these sensors.

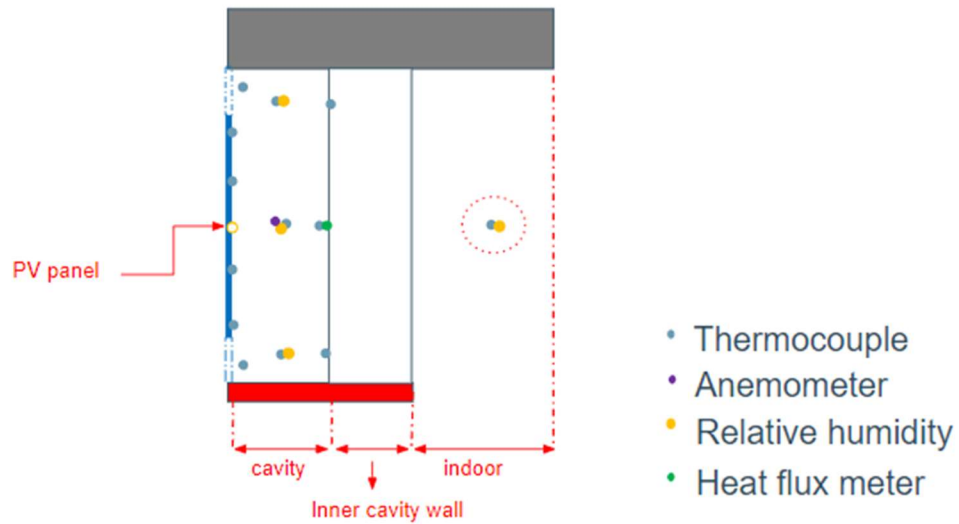


Figure 2: Different sensors

The data from the sensors in Figure 2 will be processed into various graphs using the matplotlib function in Python. This function is an efficient way of plotting due to the large quantity of data. These graphs will give an idea about the evolution of humidity during a given period. After that, the humidity around the PV module will be evaluated. For this, a literature study is conducted. With this information, the analytical model is developed.

## 1.5 Objective 2

After objective 1, the analytical model for moisture concentration inside the PV module is created, consisting of two different analytical models. The first analytical model is made for a PV module with a breathable backsheets. In this PV module, moisture enters through the backsheets. The second model is developed for a glass backsheets PV module. Here, the moisture can only enter from the sides. The two different PV modules and their pathways will be explained in more detail in 3.1.4.

The analytical model is compared with the use of the finite element software COMSOL Multiphysics. This COMSOL model is made by TU delft. Both models need the temperature and relative humidity to calculate the moisture ingress. For the breathable backsheets module, the module temperature and the ambient humidity of Delft is used. The glass backsheets PV module uses ambient data of Singapore and Brussels because of their different climates. After that, the analytical model from objective 1 is used to simulate the moisture ingress in a BIPV module. In this thesis, an analytical model is chosen over a COMSOL model because an analytical model is easier to integrate and use.

Lastly, a glass backsheets PV module and a module with breathable backsheets are manufactured. The moisture ingress into these two PV modules is compared by using humidity indicator cards. The use and working principles of these cards will be explained in 3.1.6. Accelerated aging test is carried out to ensure full moisture integration. Accelerated aging methods include tests that can simulate the long-term effect on PV modules. The method used in this thesis is the damp heat test. The conditions applied are a temperature of 85 °C and a relative humidity of 85% for an uninterrupted duration of 1000 hours [3].

## 2 Moisture inside cavity

### 2.1 Reference study

Firstly, a literature study is done to ensure a better understanding of the microclimate around the BIPV module. For this, the influence of cavity ventilation on the relative humidity is researched. After that, the heat and moisture transport in the cavity will be explained. Also, the importance of the lifetime of a PV module and some material properties are shortly discussed.

#### 2.1.1 Importance of longevity

Degradation is one of the most crucial factors in the design and maintenance of a PV module. This is because the durability of a PV module largely contributes to the total amount of solar energy produced and therefore the return on investment for the owner. In this paper, the importance and impact of the different types of degradation are explained.

An encapsulant like ethylene vinyl acetate (EVA) is an essential packaging material that embeds the solar cell and delivers electrical isolation and protection from mechanical loads and corrosive environments. For this purpose, EVA is the most used encapsulant due to its lower cost of material, good adhesive properties with glass and backsheets, and the low glass transition temperature which protects the PV module from thermal cycling loads [4].

#### 2.1.2 Material properties

The material properties of the PV module components have the most influence on degradation and failure of PV modules. In the following paper, the advantages and disadvantages of the chosen materials are explained. In the current state of encapsulant materials, EVA is the most preferred option due to its cost-effectiveness. EVA however is liable to acetic acid production in the presence of moisture and has a high-water vapour transmission rate. Other polymeric encapsulants have their advantages but are limited in one way or the other. Polymeric materials for PV modules need to have strong adhesion, low diffusivity, and low solubility to protect the PV module over its lifetime against the ingress of gaseous species. A disadvantage of EVA is its very high diffusion coefficient [5].

#### 2.1.3 Ventilation

There are different ways of ventilation. Examples are forced ventilation, natural ventilation, and no ventilation. In this part of the thesis, these different ventilation methods are discussed. Ventilation has also many benefits. Due to ventilation, the operating temperature of the PV module will be lower compared to an unventilated installation. According to [6], the efficiency of a crystalline silicon solar cell will drop by 0.5% per degree Celsius the temperature increases. It is therefore better to keep the operating temperature as low as possible [7].

In [6] four different ventilation methods are compared. These are forced intermediate and natural ventilation, forced high and natural ventilation, natural ventilation, and no ventilation. These different setups were investigated over three years. Energy measurements indicate that forced high and natural ventilation has the highest energy output and no ventilation the lowest. After three years, the energy output of the naturally ventilated PV module is 82% higher than for the non-ventilated PV module monthly. This percentage depends on the ambient temperature. In the summer months, this percentage will be higher than in the winter months.

Figure 3 shows a boxplot of the relative humidity of the forced intermediate and natural ventilated PV module (segment 1), the forced high and natural ventilated PV module (segment 2), and the non-ventilated PV module (segment 4). The naturally ventilated PV module is not shown because the sensor failed during the measurements [6, p. 398].

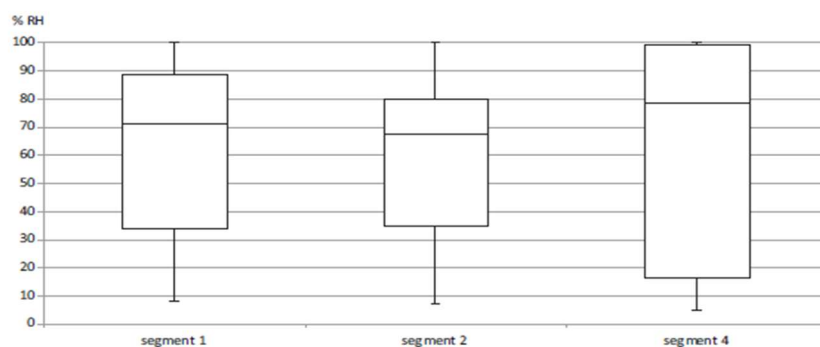


Figure 3: Boxplot of the relative humidity for the different segments

Figure 3 shows that the humidity has the largest range in the non-ventilated PV module. The humidity will also be close to 100% here, creating an elevated risk of condensation [6]. When the boxplots of Figure 3 are compared, it is noticeable that the average relative humidity increases as the ventilation decreases. Since the ventilation rate of natural ventilation ranges between forced intermediate and natural ventilation and no ventilation, the mean relative humidity of natural ventilation will also be in between them. From the previous paragraph, it can be concluded that forced high and natural ventilation ensures a longer module lifetime and higher yields. But forced ventilation has a few disadvantages compared to natural ventilation, for example, the use of energy, the investment, and the noise increases [7].

This thesis uses only natural ventilation or no ventilation. So, the predicted humidity in the PV module is supposed to be lower in the case of natural ventilation. This will also be better for the PV module's durability.

#### 2.1.4 Thermal model

The framework already consists of a model for the temperature. This thermal model is studied to understand the method of making an analytical model. The thermal model is shown in Figure 4 and Figure 5.

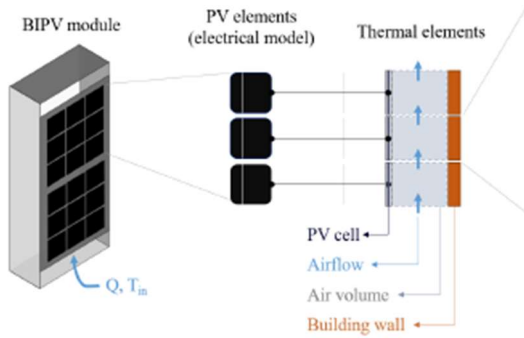


Figure 4: PV elements and thermal elements of ventilated BIPV module [7, p. 4395]

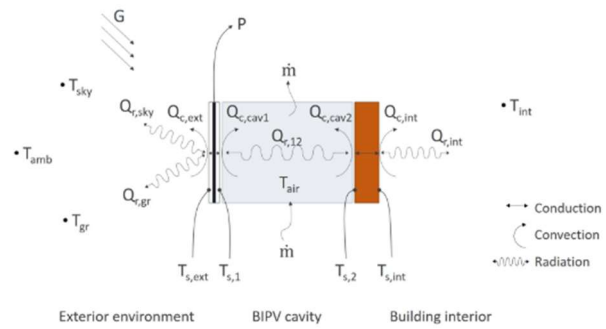


Figure 5: Thermal model [8, p.11]

First, the PV module is divided into smaller elements. Here, an electrical and thermal model are created. Each PV element from the electrical model corresponds to a thermal element. The PV elements have each their temperature and irradiance inputs so that shading and temperature gradients can be modelled. Figure 4 shows a ventilated building integrated module with the PV elements, thermal elements, and the thermal model [7]. The thermal model of Figure 5 shows the conduction, convection, and radiation through the element. Also, the different temperatures, solar irradiance ( $G$ ), and airmass ( $\dot{m}$ ) are shown.

The same method has been used in this thesis.

### 2.1.5 Cavity wall

The cavity plays a significant role in this thesis. One of the main objectives is to model the humidity inside the cavity. For this, a basic understanding of the layout of the cavity is necessary. M. Van Belleghem et al. [9] delivers a useful explanation of the functions and layout of the cavities in European buildings. The layout of a cavity wall with the given heat transport is shown in Figure 6.

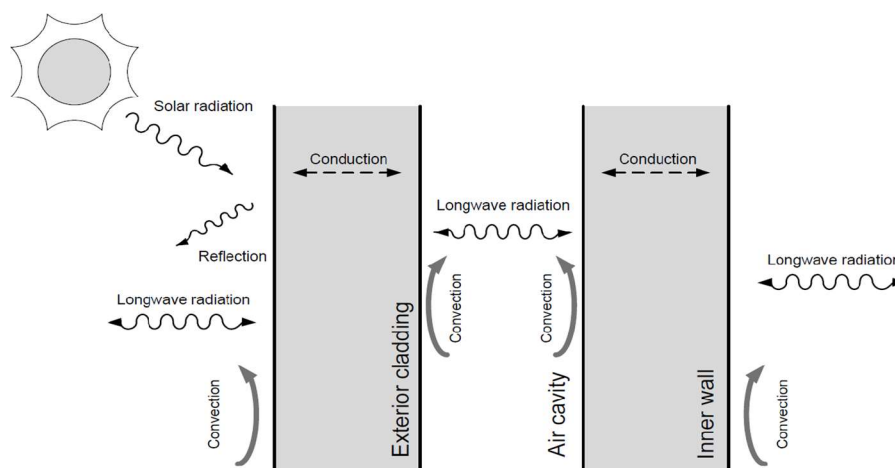


Figure 6: Heat transport modelling in ventilated cavity walls [9, p. 5]

In most European houses a cavity is implemented between the inner and outer wall of the house. This cavity is hollow and provides an air layer between the outer and inner wall. Figure 6 shows the

different heat transfer methods for a normal wall or cavity without the implementation of a PV module. The heat is transported using three transport mechanisms: radiation, conduction, and convection. Heat transfer by radiation is the main contributor to heat transport from the outside wall to the cavity. This radiation is due to solar radiation on sunny days. The amount of radiation that is absorbed is dependent on the material and colouring. The wall will also exchange radiant heat with the sky, this radiation can cause heat loss or gain depending on the outside temperature. Convection is caused by the transportation of heat due to the flow of air. The heat transfer inside the materials is due to conduction, this is strongly dependent on the used materials and the thickness [9]. Beside heat transport another important factor is moisture ingress, this is shown in Figure 7.

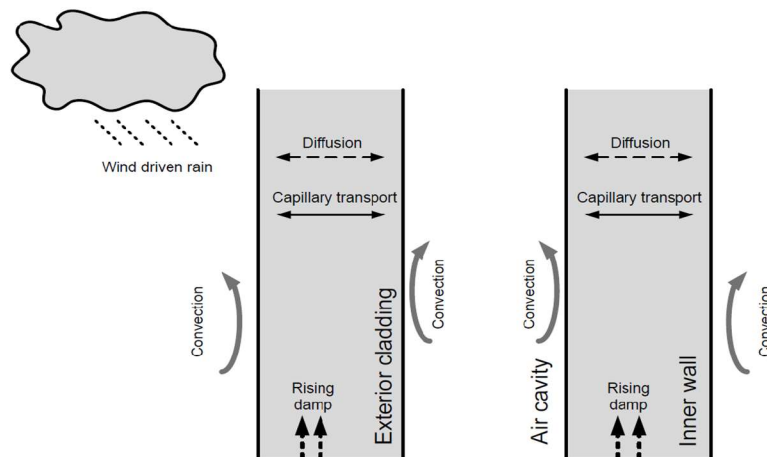


Figure 7: Moisture transport modelling in ventilated cavity walls [9, p. 5]

The outer wall is in Europe mostly built out of masonries like brick or cinder block. This masonry is an absorbent material that over time can draw rainwater or even humidity into the wall. One of the functions of the cavity is to drain water and prevent moisture from the outside penetrating on the inside wall. The cavity uses weep holes or ventilation grills at the base that serves to drain water. These weepholes let air inside the cavity. The moisture pathway is like the heat pathway in that it has many different types of flow paths. The main flow that will be used in this thesis is the diffusion through the walls. The moisture flow is highly dependent on the outside parameters. These include temperature, relative humidity, pressure, and wind speed. Figure 7 shows the different pathways of moisture [9].

## 2.2 Analytical model

The analytical model is based on the law of conservation of energy in which the incoming moisture is equal to the outgoing moisture. Figure 8 shows the different moisture paths for a ventilated BIPV module.

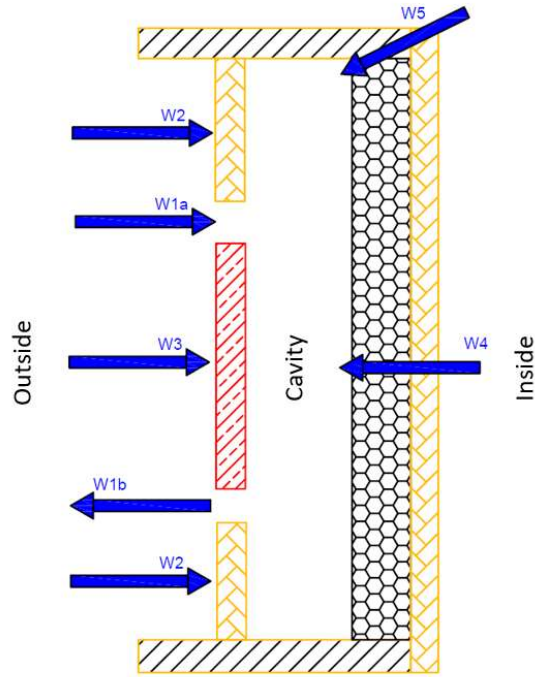


Figure 8: Different moisture paths for a ventilated BIPV module

In Figure 8,  $w_{1,a}$  is the moisture transport through the ventilation inlet,  $w_{1,b}$  is the moisture transport through the ventilation outlet,  $w_2$  is the moisture transport through the wall between the outside and the cavity,  $w_3$  is the moisture transport through the BIPV module,  $w_4$  is the moisture transport through the wall between the cavity and the inside, and  $w_5$  is the moisture transport through gaps in the inner wall. According to the law of conservation of energy can be assumed that the moisture ingress is equal to the moisture egress:

$$w_{1,a} - w_{1,b} + w_2 + w_3 - w_4 - w_5 = 0 \quad (1)$$

Formula (1) will be used to describe the relative humidity in the cavity. For this, each moisture path of (1) will be written as function of the relative humidity.

In this thesis, two different types of transport can be defined, moisture transport through a solid material and through the air.

### 2.2.1 Moisture transport through the air

This section discusses moisture transport through the air. According to [4] the moisture load through an opening can be described as:

$$w_{opening} = A \cdot \rho \cdot 60 \cdot v_{air} \cdot (M_{out} - M_{in}) \quad (2)$$

with:  $w_{opening}$ , the moisture load through the opening [g/h];  
 $A$ , the area of the opening [m<sup>2</sup>];  
 $\rho$ , the density of the air [kg/m<sup>3</sup>];  
 $v_{air}$ , the air velocity through the opening [m/min];



$M_{out}$ , the moisture content outside [g/kg];

$M_{in}$ , the moisture content inside [g/kg].

This formula is used to calculate the difference of moisture through the ventilation ( $w_{1,a} - w_{1,b}$ ) and the moisture transport through the gaps ( $w_5$ ). For  $w_{1,a} - w_{1,b}$  [g/s], this results in (3).

$$w_{1,a} - w_{1,b} = A_{vent} \cdot \rho \cdot v_{air} \cdot (M_{out} - M_{cav}) \quad (3)$$

With:  $A_{vent}$ , the ventilation area [m<sup>2</sup>];

$\rho$ , the density of the air [kg/m<sup>3</sup>];

$v_{air}$ , the air velocity through the opening [m/s];

$M_{out}$ , the moisture content outside [g/kg];

$M_{cav}$ , the moisture content in the cavity [g/kg].

Since  $w_{1,a} - w_{1,b}$  is in [g/s] and  $v_{air}$  is in [m/s], the factor 60 [min/h] in (3) is not needed. For  $w_5$  [g/s], this results in (4).

$$w_5 = A_{gap} \cdot \rho \cdot v_{air} \cdot (M_{cav} - M_{in}) \quad (4)$$

With:  $A_{gap}$ , the total area of the gaps [m<sup>2</sup>];

$M_{in}$ , the moisture content inside [g/kg].

According to [11], the air density in (2) depends on the pressure. Since this pressure is not completely constant, the air density is calculated in this thesis. This is more accurate than working with a constant value. The density is then equal to:

$$\rho = \frac{P_d}{R_d \cdot T} + \frac{P_V}{R_V \cdot T} \quad (5)$$

with:  $P_d$ , the partial pressure of dry air [Pa];

$P_V$ , the partial water vapour pressure [Pa];

$R_d$ , the specific gas constant of dry air [J/kg · K];

$R_V$ , the specific gas constant of water vapour [J/kg · K];

$T$ , the temperature of the air [K].

The partial pressure of dry air in (5) can be written as [12]:

$$P_d = P_{tot} - P_V \quad (6)$$

with  $P_{tot}$  the ambient pressure given in Pa. The partial vapour pressure in (6) can be described as [12]:

$$P_V = \frac{P_{sat} \cdot RH}{100} \quad (7)$$

with:  $P_{sat}$ , the saturation pressure [hPa];

$RH$ , the humidity [%].

Here the saturation pressure is equal to [12]:

$$P_{sat} = 6.11 \cdot 100 \cdot 10^{\frac{a \cdot T}{b+T}} \quad (8)$$

with: 6.11, the saturation pressure of water at 0°C [hPa];

$a$ , the Magnus and Tetens coefficient (7.5) [°C];

$b$ , the Magnus and Tetens coefficient (237.3) [°C];

$T$ , the temperature [°C].

Combining formulas (5)-(8) gives the formula for the air density (9):

$$\rho = \frac{P_{tot} - RH_{out} \cdot 6.11 \cdot 10^{\frac{7.5 \cdot T_{out}}{237.3 + T_{out}}}}{R_d \cdot (T_{out} + 273)} + \frac{RH_{out} \cdot 6.11 \cdot 10^{\frac{7.5 \cdot T_{out}}{237.3 + T_{out}}}}{R_v \cdot (T_{out} + 273)} \quad (9)$$

with:  $RH_{out}$ , the outside humidity [%];  
 $T_{out}$ , the outside temperature [°C].

The moisture content in a specific location ( $M_x$ ) is defined in [12] as:

$$M_x \approx 37.95/P \cdot RH_x \cdot 10^{\frac{a \cdot T_x}{b + T_x}} \quad (10)$$

with:  $P$ , the ambient pressure [hPa];  
 $RH_x$ , the humidity in x [%];  
 $T_x$ , the temperature in x [°C].

In this thesis, the moisture content of three different places is needed. These are given by equations (11)-(13):

$$M_{out} \approx 3795/P_{tot} \cdot RH_{out} \cdot 10^{\frac{7.5 \cdot T_{out}}{237.3 + T_{out}}} \quad (11)$$

$$M_{cav} \approx 3795/P_{tot} \cdot RH_{cav} \cdot 10^{\frac{7.5 \cdot T_{cav}}{237.3 + T_{cav}}} \quad (12)$$

$$M_{in} \approx 3795/P_{tot} \cdot RH_{in} \cdot 10^{\frac{7.5 \cdot T_{in}}{237.3 + T_{in}}} \quad (13)$$

with:  $P_{tot}$ , the ambient pressure [Pa];  
 $RH_{cav}$ , the humidity in the cavity [%];  
 $T_{cav}$ , the temperature in the cavity [°C];  
 $RH_{in}$ , the inside humidity [%];  
 $T_{in}$ , the inside temperature [°C].

Here the pressure is given in Pascal. Therefore, the constant 37.95 is multiplied by 100.

## 2.2.2 Moisture transport through a solid material

This section will discuss moisture transport through a solid material. This moisture transport can be described using (14) [13].

$$W_{solid,material} = \frac{(P_1 - P_2)}{\sum z_{solid,material}} \quad (14)$$

With:  $w_{solid,material}$ , the moisture transport through a solid material [kg/s · m<sup>2</sup>]  
 $P_1$ , the partial vapour pressure on one side of the solid material [Pa];  
 $P_2$ , the partial vapour pressure on the other side of the solid material [Pa];  
 $\sum z_{solid,material}$ , the sum of the diffusion coefficients for the solid materials [Pa · s · m<sup>2</sup>/kg].

This formula is used to calculate the moisture transport through the walls and through the BIPV module. This results in (15), (16), (17):

$$w_2 = \frac{(P_{out} - P_{cav}) \cdot A_{wall,out}}{\frac{\sum z_2}{1000} \cdot d_2} \quad (15)$$

$$w_3 = \frac{(P_{out} - P_{cav}) \cdot A_{BIPV}}{\frac{\sum z_3}{1000} \cdot d_3} \quad (16)$$

$$w_4 = \frac{(P_{cav} - P_{in}) \cdot A_{wall,in}}{\frac{\sum z_4}{1000} \cdot d_4} \quad (17)$$

with:  $P_{out}$ , the outside partial vapour pressure [Pa];  
 $P_{cav}$ , the partial vapour pressure of the cavity [Pa];  
 $P_{in}$ , the inside partial vapour pressure [Pa];  
 $A_{wall,out}$ , the surface area of the outside wall [m<sup>2</sup>];  
 $A_{BIPV}$ , the surface area of the BIPV module [m<sup>2</sup>];  
 $A_{wall,in}$ , the surface area of the inside wall [m<sup>2</sup>];  
 $d$ , the thickness of the material [m].

The diffusion coefficients in (15)-(17) are shown in Appendix A. These coefficients are given in [GPa s m<sup>2</sup>/kg m] and the diffusion coefficient in (14) is given in [Pa s m<sup>2</sup>/kg]. Therefore, the diffusion coefficients in (15)-(17) are multiplied by the thickness of the solid material ( $d$ ). Also, the moisture flow in (14) is given in [kg/s m<sup>2</sup>], while (1) requires [g/s]. Therefore, (14) is multiplied by the area of the solid material and the diffusion coefficient in (15)-(17) is divided by 1000. The partial vapour pressures  $P_{out}$ ,  $P_{cav}$ , and  $P_{in}$  are written in function of the relative humidity by using formulas (7) and (8). Appendix A shows that the diffusion coefficient for glass is infinite. Therefore,  $\sum z_3$  is infinite and  $w_3$  is negligible. For  $z_2$  the diffusion coefficient of soft wallboard is used. This is done for a worst-case scenario.  $\sum z_4$  is a combination of soft wallboard ( $z_{4,a}$ ) and isolation ( $z_{4,b}$ ). For the isolation, the value of gypsum is taken as an approach because no other diffusion coefficients for isolation can be found.

### 2.2.3 Parameters of the model and surroundings

The model uses various parameters of the PV module and the surroundings to calculate the humidity. Many of these parameters are directly linked to the humidity and have a large influence on the result the model delivers. This will later be shown in the sensitivity analysis. The parameters were measured on-site at the existing test facility on the roof of EnergyVille 2 using a measuring tape. In Figure 9 a representation of the setup is given with a legend including the existing materials. The dimensions of the PV module are in millimetres. The right side of the picture gives a representation of the front side of the PV module and the cross-section is presented on the left side of the picture. The thickness of the PV module is not given. This is because the front PV panel of a PV module is made of glass which has an infinite high diffusion coefficient, this can be found in Appendix A. Therefore, the water penetration is negligible and so is the thickness.

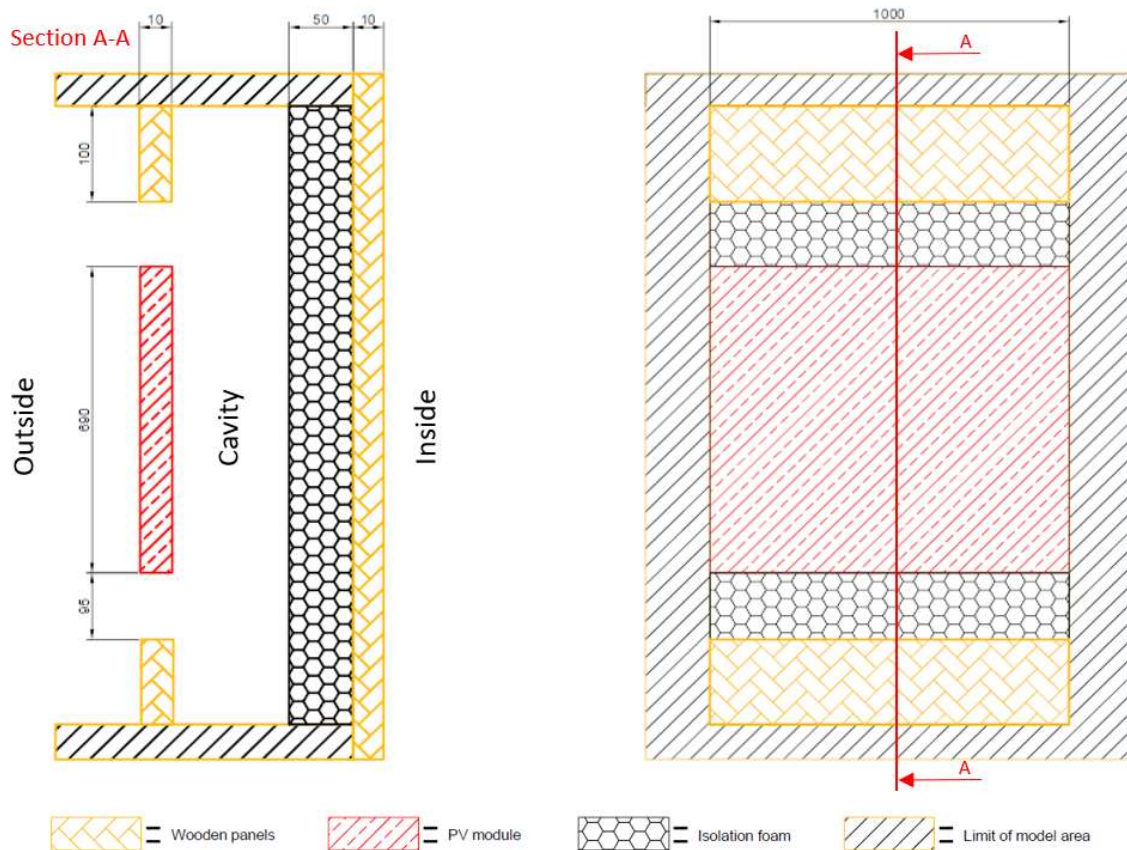


Figure 9: Cross section of the BIPV module setup with dimensions

The moisture ingress is proportional to the surface area of the surrounding. This surface area is calculated by multiplying the height and the width. The thickness of the surroundings is inversely proportional to the moisture ingress. The type of material used also plays a large role in moisture ingress. This is due to a material characteristic named: “diffusion coefficient” and can be found in Appendix A. The used materials can be found in the legend at the bottom of Figure 9. As previously explained, the left side is the outside atmosphere and the right side the inside of the building. This building uses a double layer of isolation and wood. This is to minimise heat loss and reduce moisture transport. Due to human error, there may be gaps in the connections between the cavity and the inside. This was also noticed by testing for air leaks. This can play a key role in moisture ingress.

### 2.3 Sensitivity analysis

A sensitivity analysis is done on the analytical model in section 2.2. In this analysis, the response of the output by a change in the input is evaluated. This is done to analyse which inputs have the biggest influence on the output. Here, the input parameters are set high (maximum value) and low (minimum value) according to a certain pattern. This pattern comes from an engineering statistics handbook and is shown in Appendix B [14]. For this model a  $2^{6-2}$  – experiment is done. This is a fractional factorial experiment with six input parameters. A fractional factorial experiment was chosen instead of a full factorial experiment so that the number of experiments could be reduced. Now 16 experiments were done. Table 1 shows the input parameters with their minimum and maximum value.

Table 1: Range input parameters

Input parameter	Minimum value	Maximum value
$RH_{out}$ [%]	0	100
$RH_{in}$ [%]	10	80
$T_{out}$ [°C]	-20	45
$T_{cav}$ [°C]	-20	60
$T_{in}$ [°C]	15	35
$v_{air}$ [m/s]	0	25

Table 1 is used to get the output. This is the relative humidity in the cavity. The sensitivity analysis is shown in Appendix B. The experiments are evaluated with a regression analysis. With these studies, the effect of a parameter on the output can be calculated. This effect is twice the coefficient from the regression analysis. The different effects are plotted as a percentage of the total effect. This is shown in Figure 10.

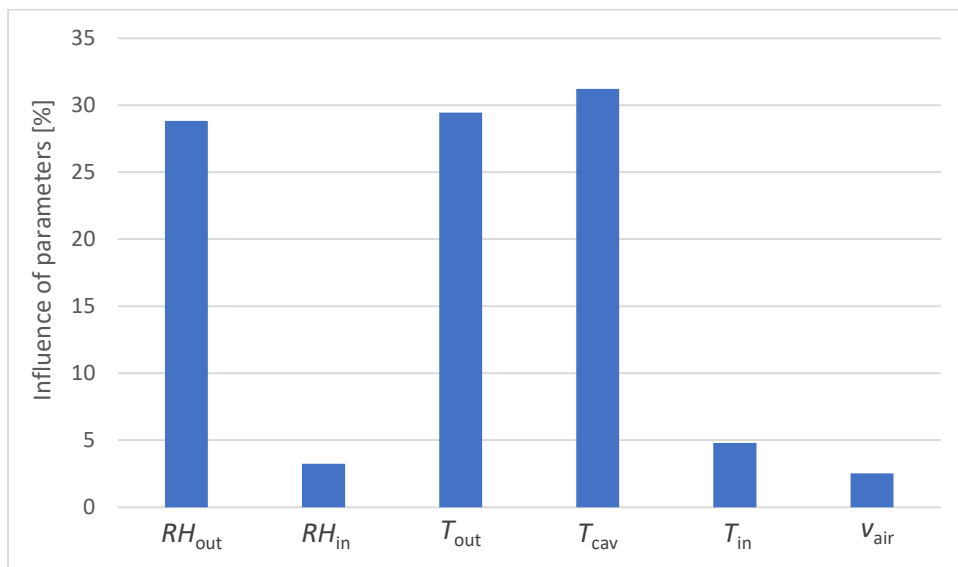


Figure 10: Pareto chart

Figure 10 shows that the outside relative humidity, the outside temperature, and the temperature in the cavity are the most important parameters. The inside relative humidity, the inside temperature, and the speed of the air through the opening are approximately 25% less important. The relative humidity and the temperature in the building are not always known. This is because the lifetime simulation of the BIPV module is mostly done for different geographical places and not for a specific building. In this case, the moisture pathways caused by the inside area ( $w_4$  and  $w_5$ ) can be neglected. The analytical model will be compared with the measurements with or without using these inside parameters.

## 2.4 Measurements and results

This paragraph will discuss the measurements and the results of objective 1. Firstly, the measurements of the temperature and humidity sensors of the different locations are compared. After that, the difference between the semi-transparent multi-wire (STMW) and the opaque multi-wire (OMWT) PV modules are discussed. Finally, the analytical model is validated.

### 2.4.1 Temperature measurements

In the first instance a dataset of the measurements from both the cavity and PV module was plotted for providing a better understanding of the physics of the PV modules and differences between each of the different types of PV modules. This dataset was provided with measurements from the test setup on the roof of the EnergyVille 2 building. This test setup consists of four different types of PV modules with sensors for both the temperature and relative humidity at different locations. This test setup is fully explained in section 1.4 of this thesis. The measurements are shown in Figure 11.

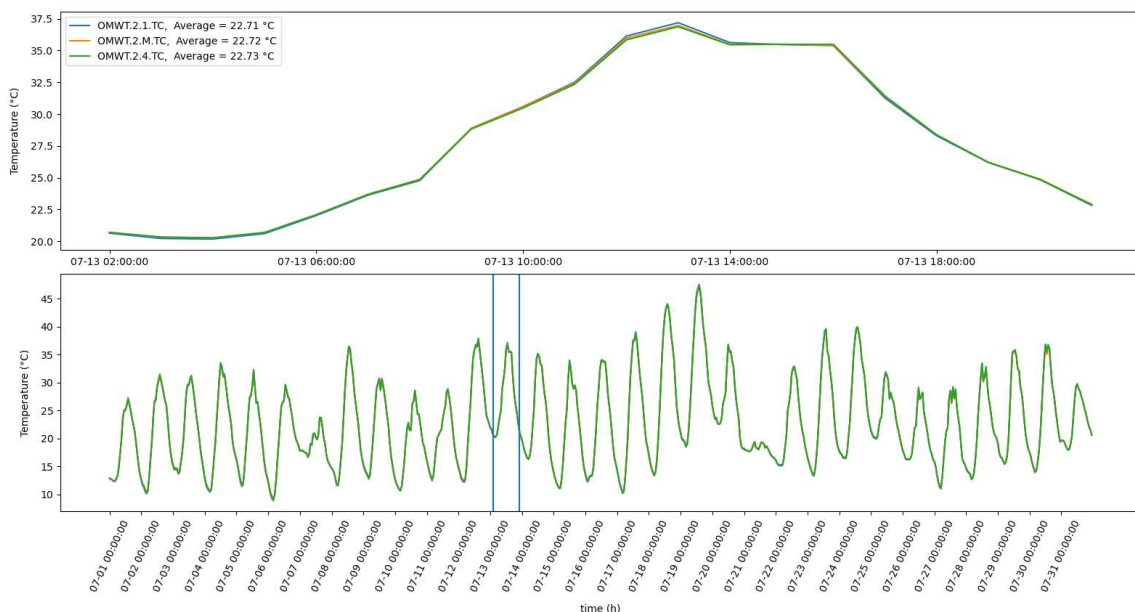


Figure 11: Temperature measurements

Figure 11 shows the temperature inside the cavity for the OMWT module. The plot shows the measurements for the month of July, other months were also plotted but will be discussed later. The graph at the bottom of the figure shows the entire month while the top graph shows 24 hours. The vertical lines on the bottom graph indicate the time at which was zoomed in. This zoom-in is shown in the top graph. This graph shows that the temperature is the highest just before 14:00. This can be explained by the fact that at this time the incident solar irradiation is higher so that the PV panel produces the most amount of energy. There are three different graphs given for three different placements of the sensor. The difference between them is negligible. In the next sections, the average between these three sensors is used as the temperature in the cavity. Furthermore, the average values for the whole month are given in the top left of the graph. On the bottom graph, it is

visible that the temperature is not constant over time and varies each day. This is explained by the outside parameters. These outside parameters consist of the temperature, wind speed, solar radiation, etc.

2.4.2 Relative humidity measurements

In Figure 12 the graphs of the relative humidity inside the cavity for the month of July are shown.

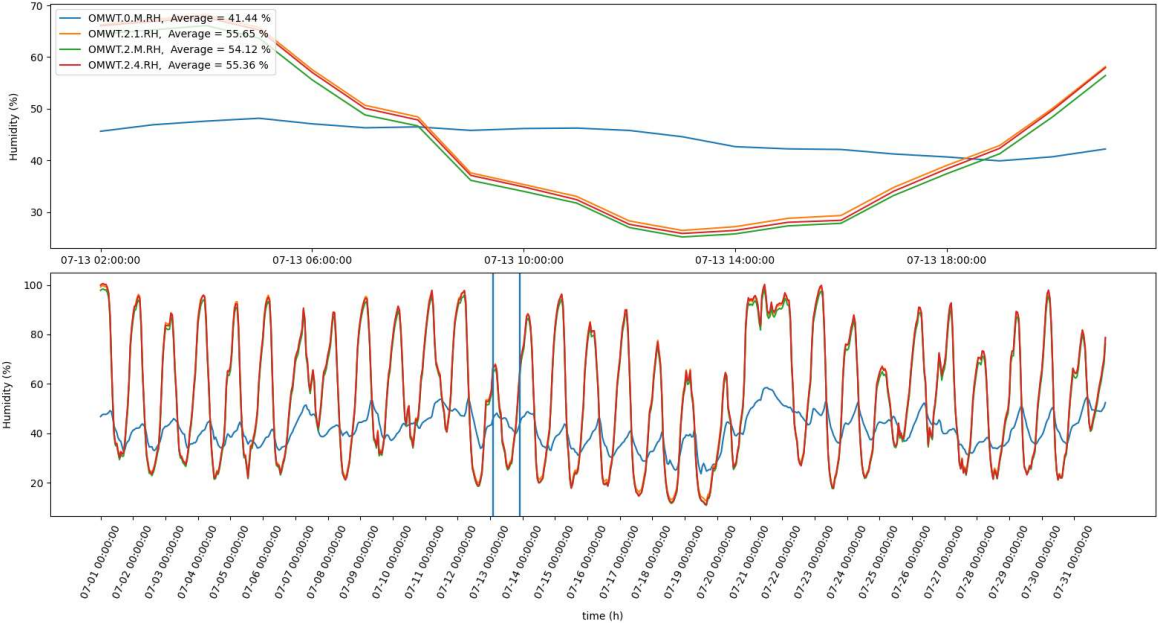


Figure 12: Relative humidity measurements

The plot method is identical to the method used in 2.4.1. Therefore, the top graph of Figure 12 is the graph for 24 hours and the bottom graph is for the entire month. The averages are also shown on the top left. In this instance, the difference between the different locations of the sensors is more noticeable. In this graph, the relative humidity of the middle cavity sensor is the lowest because this sensor is further away from the ventilation area. The extra blue graph shown is the humidity inside the building. The humidity inside has less amplitude than inside the cavity. This is because the atmosphere has more impact on the cavity due to the ventilation holes whereas inside the building the moisture ingress is much lower.

### 2.4.3 Average values for different sensor locations

Table 2 shows the average values of the different locations of sensors for the OMWT module.

Table 2: Average values for the different locations of the sensors

Location	0: indoor	1: inner cavity			2: cavity wall			3: PV module						IN	OUT
Placement	M	1.1	1.M	1.4	2.1	2.M	2.4	3.1L	3.1R	3.2M	3.3M	3.4L	3.4R		
Temperature (°C)	25.06	23.05	23.53	23.54	22.71	22.72	22.73	25.38	26.47	25.72	25.5	25.38	25.65	23.22	23.66
Humidity (%)	41.44				55.65	54.12	55.36								

Table 2 shows some extra sensors that are not shown in the graphs in the earlier parts. These sensors are the temperature sensors at the cavity wall (location 2), the PV module itself (location 3), and the in and outlet temperature. The positive difference between the in and outlet sensor show that there is a heat transfer. This shows that the PV module is cooled by the ventilation area. This difference is not significant. When the PV module has the highest temperature, this difference is more significant. In this situation, the delta can reach up to two degrees difference indicating that the PV module is being effectively cooled.

### 2.4.4 Difference between STMW and OMWT

This section describes the difference between an all-black non-transparent panel that is being cooled by a ventilation area and a semi-transparent panel that has no cooling capabilities. These differences can be observed by the average temperatures in Table 3 of both the STMW and the OMWT panels.

Table 3: Difference between the STMW and OMWB panels

	STMW				OMWT			
Location	0	1	2	3	0	1	2	3
Placement	M	M	M	3.2M	M	M	M	3.2M
Temperature (°C)	24.6	33.5	32.17	32.08	25.06	23.53	22.72	25.72
Humidity (%)	45.03		29.44		41.44		54.12	

As shown in Table 3 the temperatures of the STMW are significantly higher than the OMWT temperatures. The energy production of the STMW is even lower due to the smaller cells that are



used so that the PV module is semi-transparent. Due to the semi-transparency, the amount of radiant heat being absorbed is less than the OMWT. This indicates that the ventilation area that the OMWB and OWMT have, significantly reduces the temperatures. If these PV panels were installed without ventilation then the temperatures would be significantly higher than the temperatures in the STMW and could have a negative effect on the lifetime of the PV module. Therefore, most PV modules that are used as BIPV modules are equipped with a ventilation area. For this reason, the next chapters will focus on these types of PV modules. The humidity inside the non-ventilated PV modules is lower than the ventilated PV module, this indicates that there is a relation between the temperature and humidity.

#### 2.4.5 Model validation

As previously mentioned, the objective is to model the relative humidity inside the cavity. The analytical model as described in part 2.2 is compared with the measurements. The model was first tested for the month of June, where the model uses inside parameters as input. This can be seen in Figure 13.

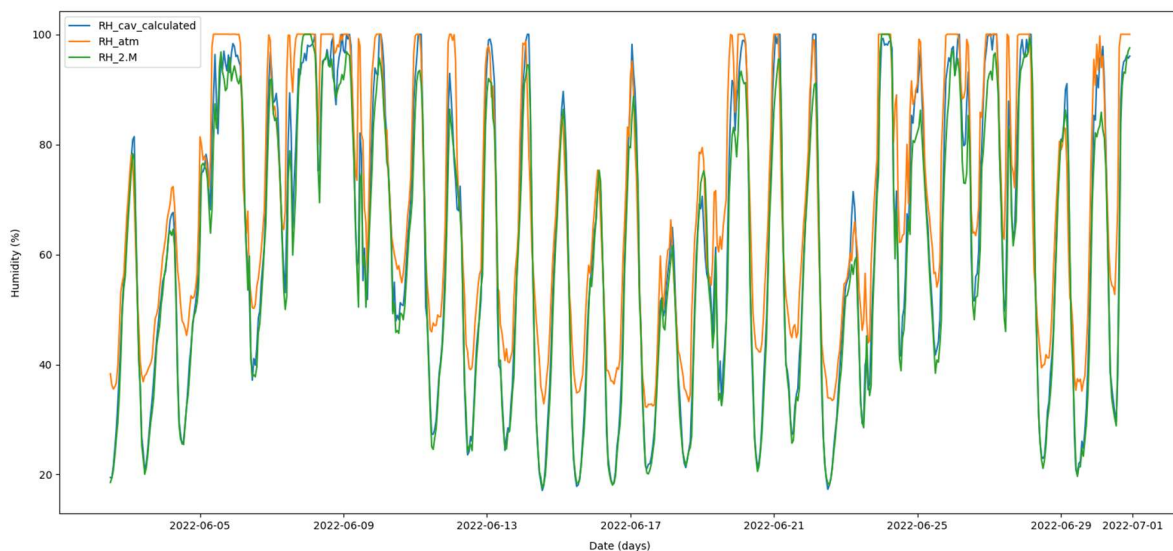


Figure 13: Analytical model relative humidity for June 2022

The graph in Figure 13 shows the results of the analytical model and the measured atmospheric and cavity relative humidity in blue, orange, and green respectively. The relative humidity of the analytical model is limited to 100%. This is done to ensure that the results stay within the 0-100% range like the sensor data. The model follows the pattern of the cavity measurements. More specifically, the model provides good predictions at low relative humidity. For higher relative humidity, the analytical model is overpredicting.

The visible difference in the atmospheric relative humidity compared to cavity relative humidity is a clear indication that the simplification to use atmospheric humidity as cavity humidity in lifetime models could increase the uncertainties in the predictions. It is therefore better to calculate the humidity in the cavity using models like the one developed in this thesis.

## 2.4.6 Analysing the model on longterm data

To ensure accuracy and repeatability, the model is used to simulate the relative humidity inside the cavity. This model is then compared to the actual measurements of the relative humidity inside the cavity and in the atmosphere. This is done for a period of six months to ensure an accurate testing of the model. Four of these months are shown in Figure 14, Figure 15, Figure 16, and Figure 17. The model is tested with and without using the inside parameters (i.e room temperature and relative humidity) since these inside variables are not usually available.

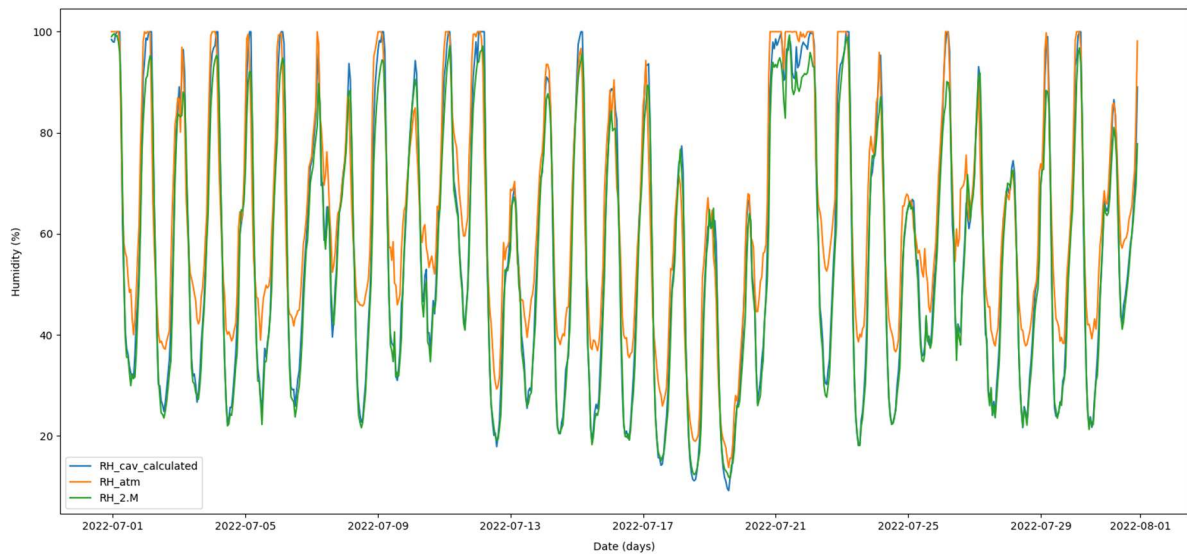


Figure 14: Analytical model relative humidity for July 2022

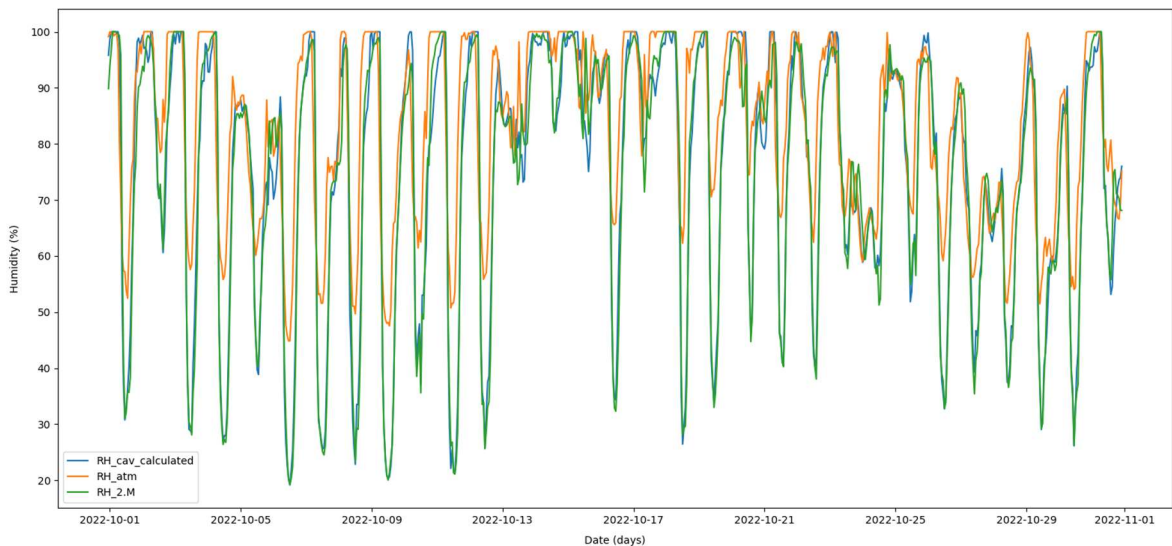


Figure 15: Analytical model relative humidity for October 2022

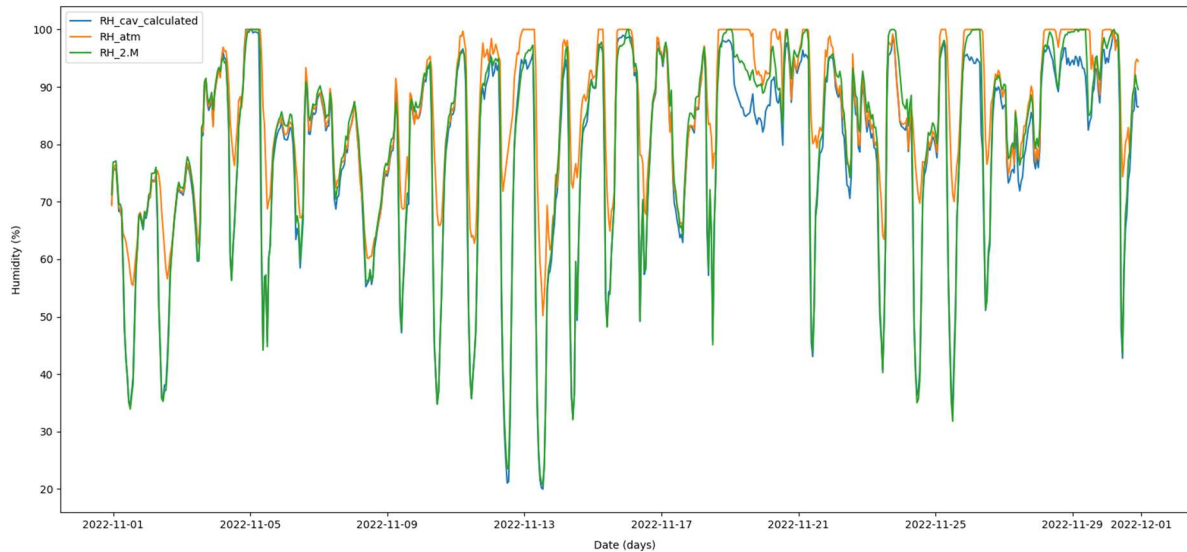


Figure 16: Analytical model relative humidity for November 2022

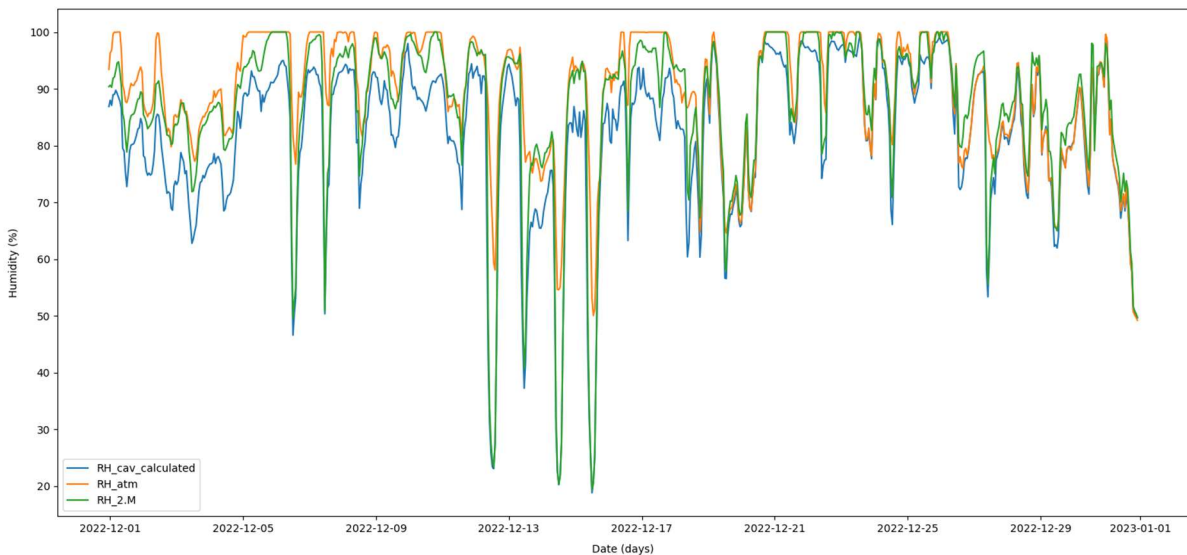


Figure 17: Analytical model relative humidity for December 2022

The first month that was tested was June, this is shown in section 2.4.5. The results for July are shown in Figure 14. This month is comparable to June and delivers similar results. The model shows a better representation of the true values, this is especially noticeable for the low humidity levels.

The graph for the month of August is not shown. This is because the sensor data was interrupted. Due to this, there was a data loss of 1.5 weeks in the middle of the month. Therefore, this graph is not included in the thesis. The parts that were not interrupted were modelled and averaged. This delivers the average data that can be found in Table 4.

September is also not shown due to a fault in the data. The humidity in the cavity for this month was very low, due to a fault in the measurements. Due to this, the entire month is not included in this thesis.

The next month shown is October. This month shows higher humidity levels compared to June and July for the humidity in the cavity and atmosphere. This is expected due to the climatic difference

between summer and autumn. The difference between the modelled relative humidity in the cavity and the atmosphere is here lower than in earlier months. This is shown in Table 4.

The analytical model of the beginning of the month November responds well with the measurements. However, at the end of November, it loses accuracy.

In December, the average relative humidity is the highest compared with the other months. The analytical model shows an undervaluing characteristic in the colder months.

Table 4 shows the average relative humidity of the model for each month with and without the use of these inside parameters. Additionally, the average measured relative humidity of the different months are shown.

Table 4: Table of six months

OMWT	June	July	August	October	November	December	Average
RH_atm (%)	69.59	63.26	62.1	82.98	85.14	89.44	
RH_measured (%)	59.9	55.04	54.53	74.79	80.02	87	
RH_atm - RH_measured (%)	-9.69	-8.22	-7.57	-8.19	-5.12	-2.44	-6.87
RH_Cav with inside (%)	62.36	57.04	55.73	75	78.32	82.62	
RH_measured - RH_cav with inside (%)	-2.46	-2	-1.2	-0.21	1.7	4.38	
Percent error (%)	-4.11	-3.63	-2.21	-0.28	2.12	5.03	-0.51
RH_Cav without inside (%)	62.42	57.1	55.78	75.04	78.18	82.05	
RH_measured - RH_cav without inside(%)	-2.25	-2.06	-1.25	-0.25	1.84	4.95	
Percent error (%)	-4.21	-3.74	-2.29	-0.33	2.3	5.69	-0.43

The percent error ( $\delta$ ) in Table 4 can be calculated with [15]:

$$\delta = \frac{y_i - \hat{y}_i}{y_i} \cdot 100\% \quad (18)$$

with:  $y_i$ , the measured relative humidity in the cavity [%];  
 $\hat{y}_i$ , the predicted humidity in the cavity [%].

The total average of the six months indicates that the percent error when using the humidity of the atmosphere for  $\hat{y}_i$  delivers an overestimation of 6.87%. When the modelled humidity is used for  $\hat{y}_i$  the percent error is between 0.51 and 0.43%. This indicates that using the modelled humidity as a representation of the humidity in the cavity delivers more accurate results than using the humidity in the atmosphere. Section 2.4.7 explains this in more detail. An important factor to consider is that using both the model and the atmosphere deliver an average overestimation. This is important because an underestimation could deliver false information when the humidity is used to calculate the lifetime of the PV module. An overvaluation on the other hand delivers a shorter lifespan, which is more desirable for the use of a lifespan simulation. At first glance the difference between using the inside parameters or not seems negligible. This is also explained in section 2.4.7.

#### 2.4.7 Errors

The analytical model is validated by calculating three different errors [16]. These are the normalized root mean square error (NRMSE), the mean absolute error (MAE), and the mean absolute percentage error (MAPE). The NRMSE can be calculated with:

$$NRMSE = \frac{\sqrt{\frac{1}{n} \sum_{i=1}^n (y_i - \hat{y}_i)^2}}{y_{i,max} - y_{i,min}} \cdot 100\% \quad (19)$$

The MAE is defined by:

$$MAE = \frac{1}{n} \sum_{i=1}^n |y_i - \hat{y}_i| \quad (20)$$

The MAPE is calculated using:

$$MAPE = \frac{1}{n} \sum_{i=1}^n \frac{|y_i - \hat{y}_i|}{y_i} \cdot 100\% \quad (21)$$

with:  $n$ , the sample size [/];

$y_i$ , the measured relative humidity in the cavity [%];

$\hat{y}_i$ , the modelled relative humidity [%];

$y_{i,max}$ , the maximum measured relative humidity in the cavity [%];

$y_{i,min}$ , the minimum measured relative humidity in the cavity [%].

Figure 18 represents the three different errors for six months, where the analytical model uses the inside parameters. In Figure 19 the errors of the analytical model without the parameters inside the building are shown.

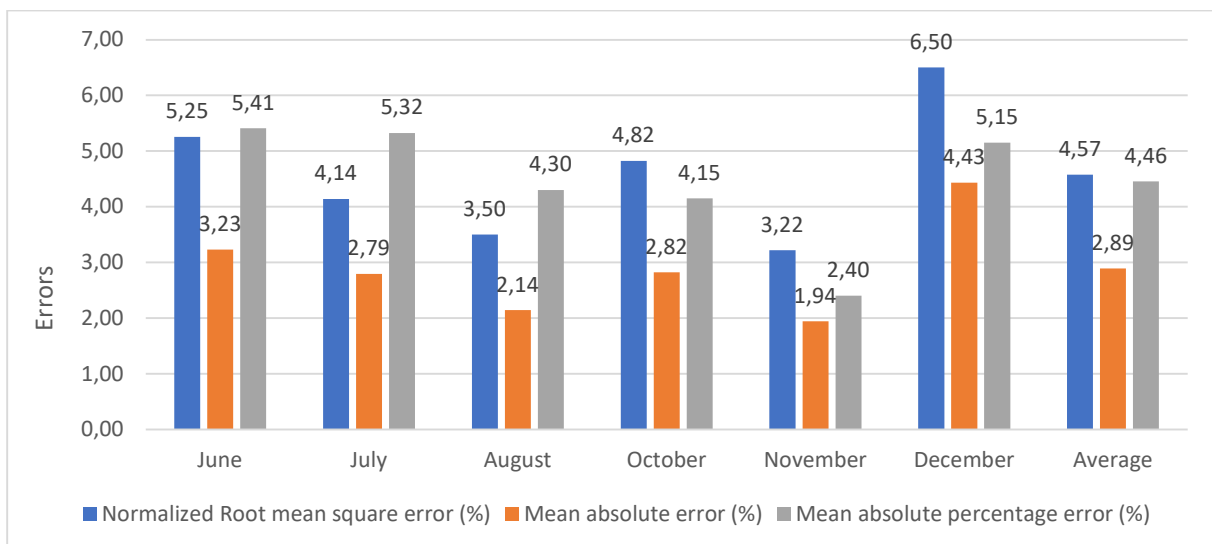


Figure 18: Errors analytical model with inside parameters

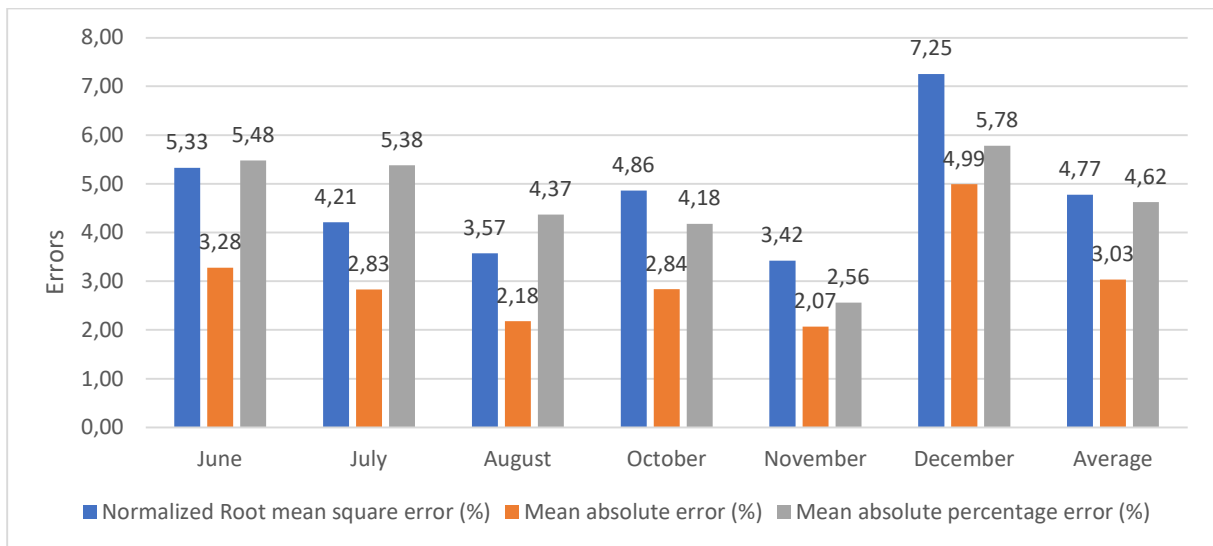


Figure 19: Errors analytical model without inside parameters

The errors in Figure 18 and Figure 19 are given in percent where the percentage in the NRMSE and the MAPE expresses a fraction of 100. The percentage in the MAE is derived from the dimension of the relative humidity, so it is an absolute value. The NRMSE and the MAPE are considered the more important errors because these errors are normalized and consider the ratio of the difference. As the non-normalized differences can give a false representation of high values. These figures show that the model is the most accurate in the month of November and least accurate in the month of December. The difference between these two months is approximately 3%. The average errors are below 5% (predetermined by EnergyVille). Therefore, the analytical model is considered a good way to predict the relative humidity in the cavity.

Figure 19 shows that the analytical model without the parameters from inside the building is less accurate than the model which includes these parameters. The difference between the average errors is approximately 0.17%. This is a small difference. So, the parameters inside the building have a small influence on the modelled humidity. This was also the conclusion of the sensitivity in section 2.3.

The formulas (19)-(21) are also used to compare the relative humidity of the atmosphere ( $\hat{y}_i$ ) with the measured relative humidity in the cavity ( $y_i$ ). The faults are shown in Figure 20.

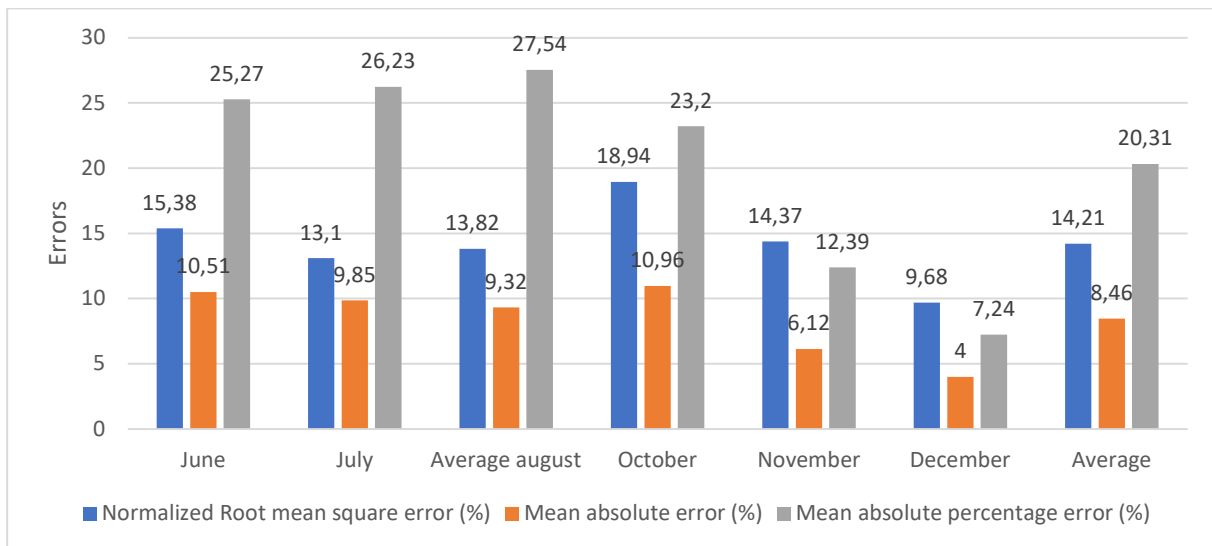


Figure 20: Errors atmosphere

The average NRMSE in Figure 20 is about 9.4% greater than compared with the average NRMSE of the model. The MAE and the MAPE are respectively 5.4% and 15.7% higher. Here, the difference between the NRMSE and the MAPE is also greater compared with the model. In the model the difference between these two errors is neglectable.

#### 2.4.8 PVGIS

In the previous sections measurement data from EnergyVille was used. This section uses data from the Photovoltaic geographical information system (PVGIS). This is an online tool that provides information about solar system performance and solar radiation, for different locations around the world. For this thesis, the PVGIS generator 'typical meteorological year' (TMY) is used. TMY generates hourly meteorological data for a chosen location [17]. In this thesis, the used locations are Singapore, Kuwait, and Brussels. For these locations, the relative humidity in the cavity was compared with the outside relative humidity. This is done for a whole year with data ranging from 2005 up to 2020. PVGIS looks for every month which year has the most data that is representative of typical conditions and then this year is used for that particular month. As explained in section 2.2 the analytical model of the cavity uses outdoor parameters. These parameters are the windspeed, the temperature, relative humidity, and the pressure of the atmosphere. These parameters are taken from the TMY tool. For the constant parameters, for example, the area of the ventilation and the diffusion coefficients, the values of the measurement setup in EnergyVille are assumed. The temperature in the cavity and the inside parameters are not available in PVGIS. Therefore, the temperature in the cavity is calculated using the temperature model of EnergyVille. The moisture pathways caused by the inside area ( $w_4$  and  $w_5$ ) are neglected in this part. Figure 21 shows the humidity in Singapore, where the blue graph is the relative humidity in the cavity according to the analytical model and the orange graph is the humidity in the atmosphere. In Figure 22 and Figure 23 the humidity in Kuwait and Brussels is shown.



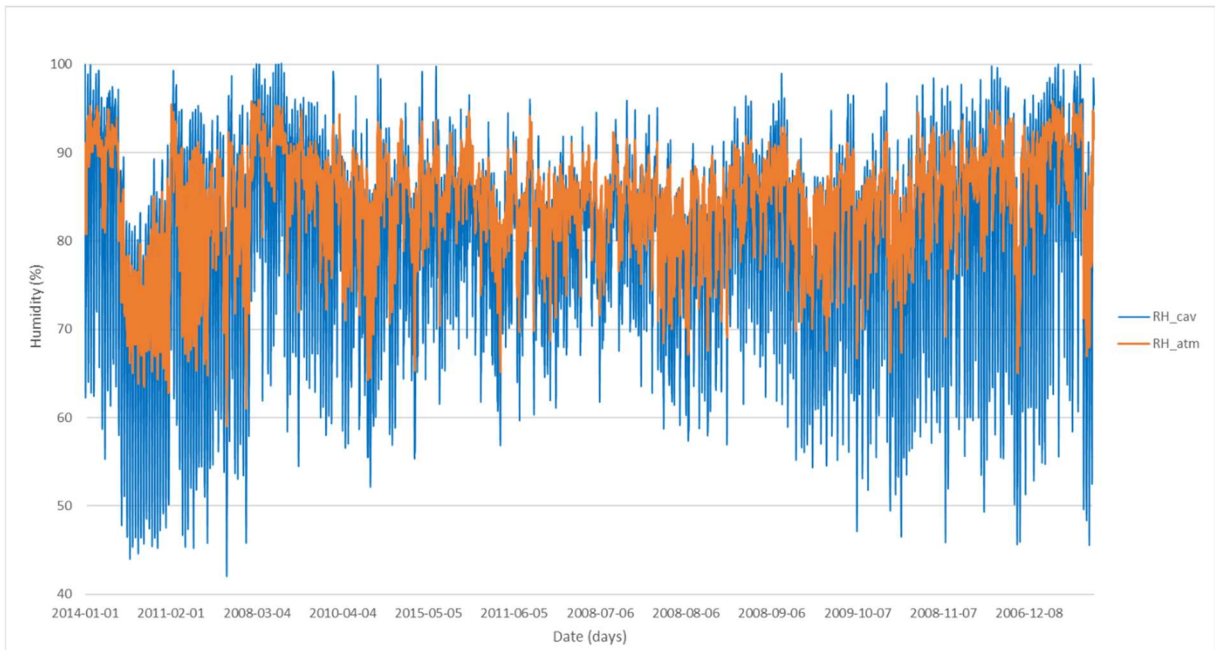


Figure 21: Simulated cavity relative humidity and ambient relative humidity for Singapore

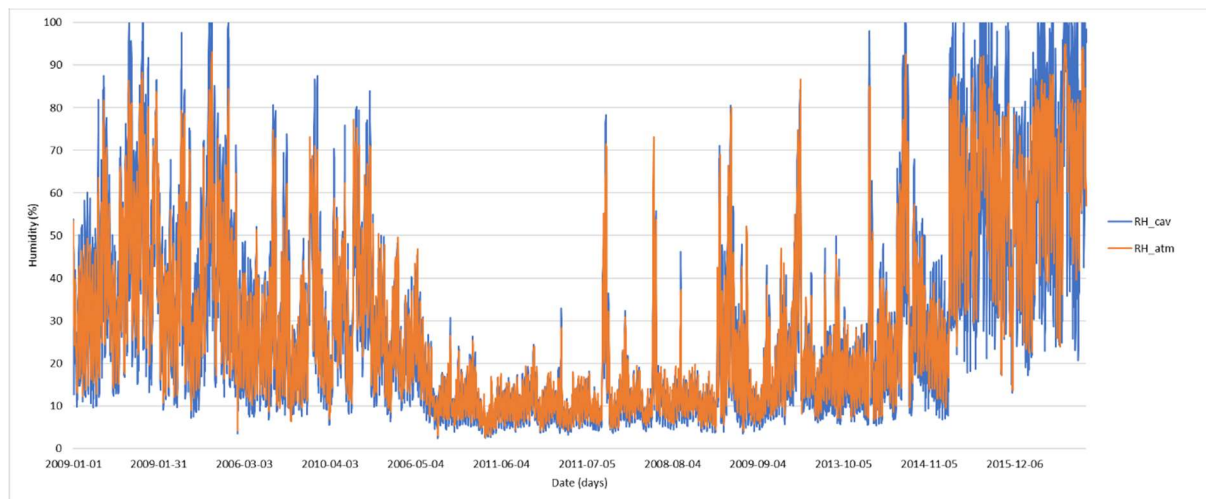


Figure 22: Simulated cavity relative humidity and ambient relative humidity for Kuwait



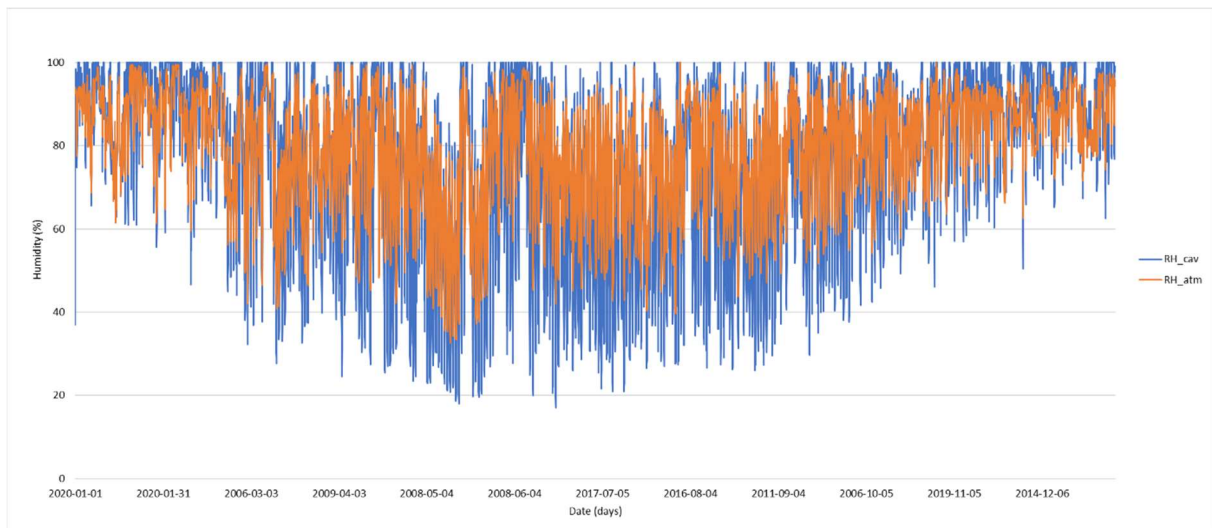


Figure 23: Simulated cavity relative humidity and ambient relative humidity for Brussels

Figure 21, Figure 22, and Figure 23 shows that the modelled humidity follows the same pattern as the atmospheric humidity. This was also the case in the measurements of EnergyVille. In Kuwait, the two graphs are very similar. In Singapore and Brussels, the two graphs correspond to higher humidity values. The humidity of the atmosphere shows less fluctuations than the humidity of the model. This was similar to what was seen from the measurements explained in section 2.4. This was also the case for the measurements in EnergyVille. In these graphs, the humidity is also limited to 100%. Table 5 shows the one-year average humidities for the three different places.

Table 5: One-year average humidities for Singapore, Kuwait and Brussels

	Singapore	Kuwait	Brussels
<b>RH_atm (%)</b>	84.53	29.40	79.55
<b>RH_cav (%)</b>	79.69	28.60	76.75
<b>RH_atm - RH_cav (%)</b>	4.84	0.81	2.79

Table 5 shows that the average relative humidities in Singapore and Brussels are in the same range, while the relative humidity in Kuwait is much lower. This was also illustrated in the graphs before.

## 2.5 Conclusion cavity model

The relative humidity in the cavity can be calculated using the law of conservation of energy, where two different types of transport can be defined. These are moisture transport through the air and through the walls. The analytical model uses parameters that depend on the type of materials used and the dimensions. This can therefore be easily changed for different type of PV panels. The runtime of the model delivers results in less than two minutes.

The sensitivity analysis shows that the outside relative humidity, the outside temperature, and the temperature in the cavity are the most important parameters. The inside relative humidity, the inside temperature, and the speed of the air through the opening are approximately 25% less

important. The relative humidity and the temperature in the building (inside parameters) are not always known when the BIPV is installed. This is because the lifetime simulation of the BIPV module is mostly performed before the BIPV modules are installed and therefore before the inside parameters can be affected by the BIPV. In this case, the moisture pathways caused by the inside area can be neglected. By neglecting these parameters, the analytical model reduces the over-estimation of the cavity humidity. This is shown in section 2.4.6 by a difference of 0.08% in percent error. In section 2.4.7 the error data shows that the model that incorporates the inside room parameters is slightly better. For later use the model without the inside parameters will be used. This is because this uses less parameters and is therefore faster to simulate.

The average percent error for the six months that were tested, shows that the analytical model is slightly overpredicting. The results show that the model is underpredicting in November and December. It will be expected that the model will also underpredict in January and February. For the rest of the year an overprediction is assumed, this results in an average year data that is slightly overvalued.

Beside the percent error, three other errors were calculated. These are the normalized root mean square error (NRMSE), the mean absolute error (MAE), and the mean absolute percentage error (MAPE). The average of these errors is below 5%. Therefore, the analytical model is considered a good way to predict the relative humidity in the cavity.

The NRMSE, the MAE and the MAPE of the relative humidity in the atmosphere compared to the humidity measurements in the cavity are respectively 9.4%, 5.4%, and 15.7% higher than the errors of using the modelled relative humidity. Therefore, it is more accurate to use the analytical model to calculate the humidity in the cavity than using the humidity of the atmosphere.

The analytical model has been applied to simulate timeseries of relative humidity in three locations: Kuwait, Brussels and Singapore. For Kuwait, the simulated cavity relative humidity is very similar to the atmospheric relative humidity. This is due to the low relative humidity which makes the difference between the two graphs negligible. For Singapore and Brussels, the analytical model predicts lower relative humidity compared to the atmospheric humidity. This was also noticed with the measurements of EnergyVille. Further research is needed to investigate if the model is an accurate representation of the relative humidity inside the cavity for Singapore and Kuwait.



## 3 Moisture ingress into PV modules

### 3.1 Reference study

Also, for the analytical model of the moisture ingress into the PV module, a literature study is done. First the different failure types of a PV module are discussed. Next, the different moisture pathways are described. Finally, different moisture measurement methods are compared.

#### 3.1.1 Different type of failures

Moisture ingress into PV modules is often regarded as one of the most contributing factors in shortening the lifespan of a PV module. The moisture can contribute to different types of failure modes of the PV cell and encapsulant.

The PV cell is encapsulated between two layers of encapsulant. The encapsulant uses an adhesion to ensure full protection against moisture ingress. This adhesion is achieved by implementing a high temperature on the encapsulant and due to variation between atmospheric pressure and vacuum. The loss of adhesion in the PV module due to environmental conditions or mechanical stress can result in delamination at the polymer/cell interface which has a negative impact on the efficiency and lifespan. This can occur due to moisture ingress and can account for a  $\leq 4\%$  loss in produced power [5]. Also, the glass/encapsulant interface is sensitive for delamination.

Another degradation type caused by moisture ingress is discolouration of the PV cell, this discolouration often results in an orange colour. Discolouration is most of the time caused by the chemical reaction of the moisture or gaseous by-products and the encapsulation (adhesion, ultraviolet (UV), and thermal stabilizers). This discolouration can take varying colouring forms depending on the reactions with moisture or UV radiation. Discoloration degradation can account for around 0.5% of the 0.8% power production losses per year for PV plants. This type of degradation can usually be detected by a visual inspection [5].

Delamination and discolouration cause power losses, but a bigger factor to consider is that they create cavities in the PV module which serve as a reservoir for gas and moisture accumulation. This enhances the chances of corrosion of the metal interconnections in the PV modules which can cause power loss. This form of material degradation is often found around cell metallization and cell interconnect ribbons. The water trapped within the encapsulant behaves as an optical barrier which decreases the quantum efficiency of the model. This degradation however can be partially reversed by the drying effect that the environment can have on the PV module. This drying period can be achieved by a high temperature and low environmental humidity [5].

Potential induced degradation also known as PID can play a contributing role in the overall loss of efficiency. PID can be caused by a high potential difference between the frame and the solar cells of a PV module. This can be caused by electrochemical interactions. Due to the potential difference, there are leakage currents from the cells to the frame. This can lead to PID. The high humidity, high temperature, and UV radiation drive moisture into a PV module. Due to the electrochemical reaction of the anti-reflection coating and/or the reduced bulk resistivity of the encapsulants, this can lead to PID. PID can also be caused due to the migration of  $\text{Na}^+$  molecules from the glass toward the bulk of the cell [4].

As earlier stated, corrosion, delamination, and discolouration are more common in high temperatures and humidity. However, moisture ingress can also be influenced by the pressure and concentration gradients of the diffusion. These parameters are dependent on humidity and temperature. Also, UV radiation has a significant influence on moisture ingress. Therefore, encapsulants with an high UV stability can be used [5].

Moisture can be transported inside a PV module in different ways. One of the ways is diffusion through a backsheet and encapsulant. This diffusion is dependent on material properties and outside parameters. Different type of models can be used to calculate diffusion of moisture through materials. One of these models is Fick's diffusion law described below.

### 3.1.2 Fick's law

Fick's first law is given by formula (22) [18].

$$J = -D \nabla c \quad (22)$$

with:  $J$ , the mass flux of moisture [ $\text{kg}/\text{m}^2 \cdot \text{s}$ ];  
 $D$ , the diffusion coefficient [ $\text{m}^2/\text{s}$ ];  
 $c$ , the concentration [ $\text{kg}/\text{m}^3$ ].

Fick's second law is given by formula (23) [18].

$$\frac{\partial c}{\partial t} = D \nabla^2 c \quad (23)$$

The second law can be simplified to one dimension. This can be done by assuming that moisture can only penetrate the backsheet through the stack. This assumption takes into account that the moisture ingress through the edges is considered negligible due to the low surface area of the edges in comparison to the backsheet [18].

### 3.1.3 Using FEM analysis for moisture ingress

A finite element method program is often used to simulate the moisture concentration and the moisture ingress into a PV module. These methods can deliver adequately results in comparison to measurements, although a slight overestimation or underestimation can be observed depending on the different type of materials. These models can use a 1D or 2D type of simulation depending on the moisture pathway and the desirable accuracy [18].

In most instances Henry's law is used to calculate the saturation moisture concentration. Henry's law states that the moisture a material absorb is proportional to the relative humidity of the environment, depending on the henry-coefficient, which gives the solubility (3.2).

### 3.1.4 Moisture pathways

The components and configuration of a PV module contribute to its moisture ingress and therefore the lifetime of the PV module. It is therefore important to analyse the different types of configurations and the different components. Two different types of PV modules are shown in Figure 24 and Figure 25.

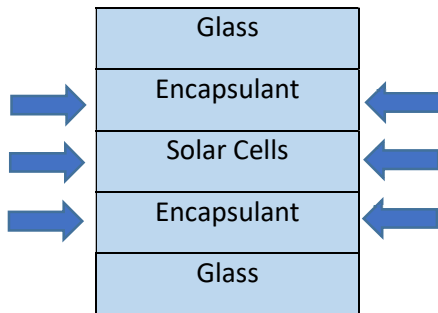


Figure 24: Non-breathable backsheet

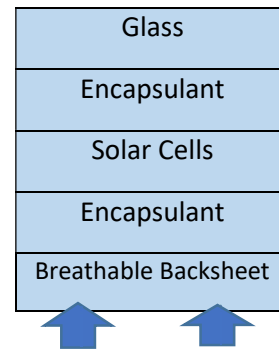


Figure 25: Breathable backsheet

There are two different configurations. PV modules with permeable and impermeable backsheets. The impermeable backsheet (often referred to as glass backsheet configuration) allows moisture vapour diffusion through the edges of the PV module and not the back as shown in Figure 24. This configuration is often used for thin film PV modules and other emerging technologies. Permeable configuration (often referred to as glass-to-polymer or “breathable backsheet”) is universally associated with traditional silicon crystalline technologies and is shown in Figure 25. This type of configuration is more prone to moisture ingress. It is impossible to completely prevent moisture ingress into PV modules. Even the PV modules with perfectly sealed configurations are liable to moisture ingress through voids of the PV module created in the manufacturing or due to mechanical or climatic stressors [5].

According to Marwaha and Ghosh, the moisture in a PV module with a breathable backsheet can be described by two different pathways. These pathways are shown in Figure 26.

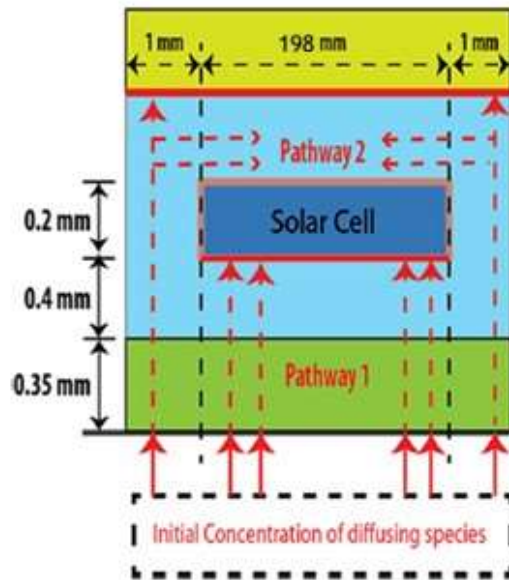


Figure 26: Pathways of a PV module with breathable backsheet [19, p. 4758]

Figure 26 shows that there is a vertical pathway (Pathway 1) and a lateral pathway (Pathway 2). The moisture along pathway 1 moves from the environment through the backsheet (green) and the encapsulant (blue). Pathway 1 will stop underneath the solar cell or underneath the glass plate depending on the location in the PV module. So at the left and right sides of the module, pathway one will stop underneath the glass plate. Here, most of the diffusing species will change direction just before reaching the glass plate. These species will follow pathway 2. The moisture that enters the breathable module from the sides is much smaller than the moisture that moves along pathway one. Therefore, the moisture that enters from the sides is negligible.

### 3.1.5 Measurements

To measure the moisture ingress inside the encapsulation different type of methodologies are available [18], [20]. Some of these methods can be used with or without a solar cell inside the PV module. Doing measurements without a solar cell can simplify the lamination process but can also affect the accuracy of the measurement. Measuring with a solar cell encapsulated ensures a more real-world representation of the moisture pathways, this is because moisture is unable to move through the solar cell. When laminating a sensor directly to a cell it is possible to permanently damage the cell due to the high pressure of the lamination machine. Due to this, the encapsulation of sensors or other embedded measuring devices is more prone to cause cracks in the solar cell than not implementing a measuring device. These cracks can cause moisture to move through the solar cell instead of around it. However, by using an extra lamination layer between the cell and the measurement device such stresses on the cell can be lowered. This extra lamination layer needs to have small incisions on the location of the measurement devices ensuring that it measures the moisture content at the level of the cell.

For measuring the moisture ingress, different types of sensors or measuring devices are available [20], [21]. Each sensor has its strengths and weaknesses. One common sensor widely used is embedding digital humidity sensors that are laminated into the encapsulant. However, these sensors

are designed to measure the relative humidity in the atmosphere and are not calibrated for measuring the moisture content of polymers. These sensors therefore need to be recalibrated for this use. Also, these sensors often have a cable which needs to exit the stack. This can affect the moisture concentration and therefore the accuracy [18].

Beside the use of sensors, it is also possible to weigh the samples before and after the moisture absorption. The difference between the start and end values of the weighing is then the moisture that was absorbed by the PV module. This method however delivers a total result of the moisture absorbed but cannot be adapted to measure at one dept or distance.

There is however a new method that uses embedded indicator cards [18]. These cards are embedded inside the lamination and change colour depending on the moisture concentration inside the lamination. This method is low cost and can be used for different type of PV cells and model structures. The colour changes on these cards however needs to be analysed with a code to deliver readable results. These cards do not introduce additional moisture pathways such as the digital sensors causes with its connection cables. This is due to the fact that the humidity indicator cards can be analysed optically and so do not need any cable connection [18]. This method however cannot directly measure the moisture content. However, the method can be combined with other polymer characterisation methods such as water vapour transmission rate (WVTR) measurements.

The indicator cards are used in this thesis to measure the relative humidity in the PV module. These cards are chosen because this method is cost effective and does not create additional moisture pathways.

### 3.1.6 Humidity indicator cards calibration

Figure 27 shows the humidity indicator cards used in the literature. These cards offer multiple different dots with different concentrations of cobaltous chloride on a blotting paper. The cards work by absorbing a specific amount of moisture from the humidity. The amount of moisture absorbed is linked to the relative humidity in the atmosphere. The colours will change gradually over a range of different humidity levels [18].

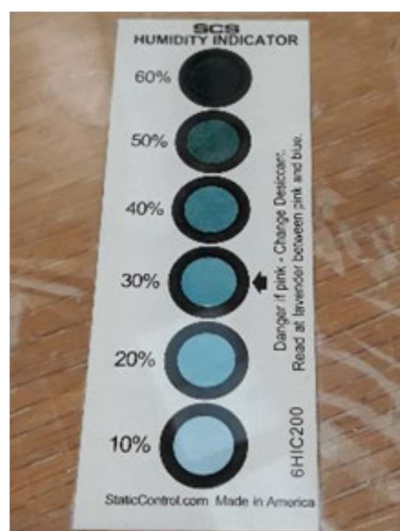


Figure 27: Indicator cards [18, p.17]



Calibration of the indicator cards, shown in Figure 27, was necessary for the representation of relative moisture content, also known as RMC. This calibration is necessary to see what colour shades of the dots is equivalent to what RMC level. This will later be explained in section 3.4.6.

### 3.2 Analytical model

The analytical model for the moisture ingress in a PV module can be described by Fick's diffusion laws. These are explained in 3.1.2. Solving Fick's second law (23) gives the moisture concentration ( $C$ ) in function of the distance ( $x$ ) and time ( $t$ ) [22]:

$$C(x, t) = C_s + \frac{4 \cdot C_s}{\pi} \sum_{m=0}^{\infty} \frac{1}{2m+1} \sin \left[ \frac{(2m+1)\pi x}{l} \right] e^{\left( -\frac{D(2m+1)^2 \pi^2 t}{l^2} \right)} \quad (24)$$

with:  $C$ , the moisture concentration [ $\text{kg}/\text{m}^3$ ];  
 $x$ , the distance [m];  
 $t$ , the time [s];  
 $C_s$ , the saturation moisture concentration [ $\text{kg}/\text{m}^3$ ];  
 $l$ , the length/width/thickness of the PV module [m];  
 $D$ , the diffusion coefficient [ $\text{m}^2/\text{s}$ ].

The diffusion coefficient expresses the rate at which molecules can move through a material. Here, the molecules move from an area with a high concentration to an area with a low concentration [23]. The saturation concentration in (24) can be calculated using Henry's law [19]:

$$C_s = S_{H_2O} \cdot p_{H_2O} \cdot RH_m \quad (25)$$

with:  $S_{H_2O}$ , the solubility of water vapour in the material [ $\text{kg}/\text{m}^3 \cdot \text{Pa}$ ];  
 $p_{H_2O}$ , the vapour pressure of moisture [Pa];  
 $RH_m$ , the module relative humidity [%].

The solubility expresses how easily water vapour can dissolve in the material. The relation between the diffusion coefficient and the solubility is given by [5]:

$$P = D \cdot S \quad (26)$$

here, the permeability ( $P$ ) expresses how easily a porous material can transmit a fluid [24]. The moisture vapour pressure can be described by the Arden Buck equation [25]:

$$p_{H_2O} = 6.1121 e^{\left( (18.678 - \frac{T_m}{234.5}) \left( \frac{T_m}{257.14 + T_m} \right) \right)} \cdot 100 \quad (27)$$

Here,  $T_m$  is the module temperature in degrees Celsius. The diffusion coefficient and the solubility are temperature depended. These parameters can be described by the Arrhenius equations [26]:

$$D = D_0 \cdot e^{\left( \frac{-E_{a,D}}{R \cdot (T_m + 273.15)} \right)} \quad (28)$$

$$S_{H_2O} = S_{H_2O,0} \cdot e^{\left( \frac{-E_{a,S}}{R \cdot (T_m + 273.15)} \right)} \quad (29)$$

with:  $D_0$ , the pre-exponential factor of the diffusion coefficient [ $\text{m}^2/\text{s}$ ];  
 $E_{a,D}$ , the activation energy of the process for the diffusion coefficient [kJ/mol];  
 $R$ , the universal gas constant [kJ/mol · K];  
 $S_{H_2O,0}$ , the solubility of water vapour in the material [ $\text{kg}/\text{m}^3$ ];

$S_{H_2O,0}$ , the pre-exponential factor of the diffusion coefficient [kg/m<sup>3</sup>];  
 $E_{a,s}$ , the activation energy of the process for the solvability [kJ/mol].

The solubility in equation (29) is in [kg/m<sup>3</sup>] and is taking into account the moisture vapour pressure. Therefore, the moisture vapour pressure in equation (25) is not needed. When equation (29) is used, the saturation moisture concentration is equal to:

$$C_s = S_{H_2O} \cdot RH_m \quad (30)$$

### 3.2.1 Breathable backsheet

The calculation of the moisture concentration in the module with the breathable backsheet is based on Figure 26. Here, pathway 1 is calculated with two different formulas. One for the moisture concentration in the backsheet and one for the moisture concentration in the encapsulant. For the concentration in the backsheet, formula (24) is used. Here, 'l' is the thickness of the backsheet. The concentration in the encapsulant is calculated using:

$$C_{ENC} = \frac{S_{ENC}}{S_{BS}} \cdot C(x, t) \quad (31)$$

with:  $C_{ENC}$ , the moisture concentration in the encapsulant [kg/m<sup>3</sup>];  
 $S_{ENC}$ , the solubility of the encapsulant [kg/m<sup>3</sup>];  
 $S_{BS}$ , the solubility of the backsheet [kg/m<sup>3</sup>].

In formula (31),  $C(x,t)$  can be calculated with (24). Here, 'l' is the thickness of the encapsulant and  $C_s$  is the moisture concentration at the transition of the backsheet and the encapsulant. Now, pathway 2 (Figure 26) can be calculated. This is done with formula (24). Here,  $C_s$  is equal to the moisture concentration at the end of Pathway 1 (Figure 26), in the middle of the distance between the top of the solar cell and the glass plate. Pathway 2 (Figure 26) is calculated with a one-dimensional (1D) equation because a squared PV module is used.

### 3.2.2 Glass backsheet PV module

The analytical model for the glass backsheet PV module is less complex than the analytical model for the module with the breathable backsheet. This model also uses equation (24). Here, 'l' is the width of the PV module.

### 3.2.3 Parameters

The parameters that are used for equation (28) and (29) are the activation energy of the process, the pre-exponential factor of the diffusion coefficient and solubility. Table 6 shows these parameters for the materials used in this thesis.

Table 6: Parameters Arrhenius equations [27], [28]

Material	$E_{a,D}$ [kJ/mol]	$D_0$ [m <sup>2</sup> /s]	$E_{a,S}$ [kJ/mol]	$S_{H_2O,0}$ [kg/m <sup>3</sup> ]
EVA	38.97	$2.46 \cdot 10^{-4}$	12.58	$2.91 \cdot 10^2$
TPO	-17.35	$7.57 \cdot 10^{-12}$	113.9	$6.45 \cdot 10^{15}$
PET <sub>b</sub>	35.2	$5.1 \cdot 10^{-7}$	12.26	1048
PIB	55	$50 \cdot 10^{-4}$	7.5	52

The first two materials (ethylene vinyl acetate (EVA) and Thermoplastic polyolefin (TPO)) in Table 6 can be used for the encapsulant. Polyethylene Terephthalate black (PET<sub>b</sub>) is used for the backsheet and polyisobutylene (PIB) for the edge seals. For the temperature and relative humidity the PV module parameters are needed. These can be provided by the simulation framework of imec. For the dimensions of the PV module, the suggested dimensions of [19] are used as shown in Figure 26. In this thesis, zero thickness is taken at the transition of the environment and the backsheet. The width and length of the PV module are both 0.2 m. Because of symmetry, a 1D model can be used instead of a 2D model. This will reduce the complexity and the simulation time. Because of this, the glass backsheet model will only be simulated for half the width (0.1 m).

### 3.3 Validation analytical model

As mentioned before, the analytical model is validated by comparing it to the finite element software COMSOL Multiphysics. This is carried out for the breathable backsheet, the encapsulant, the breathable module and the glass backsheet PV module.

The analytical model shows more variation than the model made with COMSOL Multiphysics. Also, the amplitude of the COMSOL model reduces when the penetration depth increases. Where, the amplitude of the analytical model remains constant. Therefore, the analytical model will use a moving average. The moving average takes the average of 'n' values in a dataset with 'm' elements at a specific time 't'. Here, 'n' is also called the window. At 't = 0', the average is taken for the first 'n' values. After that, the window moves one value so that the initial value of the window is at 't=1' and the end value is at 't=1+n'. Here, a new average value is taken. This is repeated until the end of the dataset is reached. Table 7 show an example of the moving average [29].

Table 7: Moving average

Time	0	1	2	3	4	Moving average
Value	1	2	3	7	9	2

Time	0	1	2	3	4	Moving average
Value	1	2	3	7	9	2, 4

In this thesis, two different moving averages are used. For the first moving average, the input values (the relative humidity and the temperature) are averaged. The moisture concentration is then calculated with the averaged input. The second moving average will average the output values of the analytical model (the moisture concentration). All the graphs of the analytical model that are shown in 3.3 use a moving average, except Figure 29, Figure 34, and Figure 37.

The moisture ingress is simulated at different places in the module. These places are shown in Figure 28.

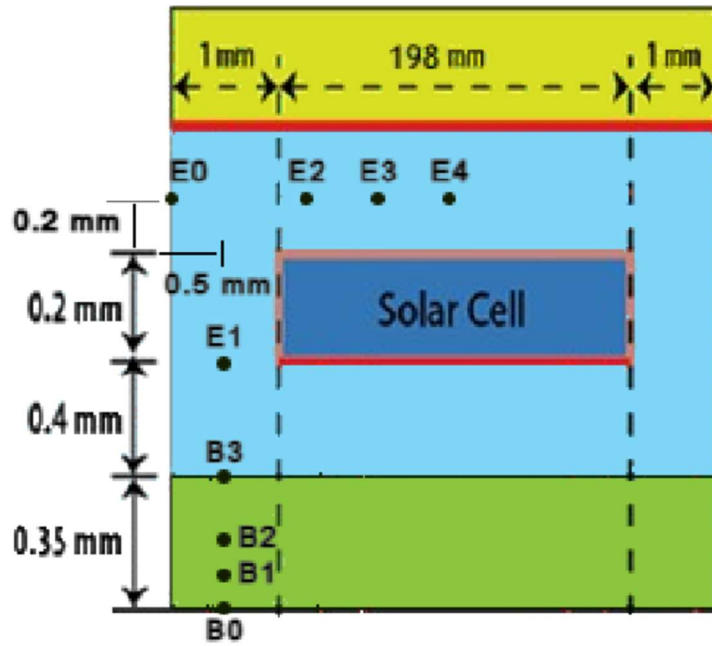


Figure 28: Points where the moisture ingress is simulated

In Figure 28, the points 'B' are situated in the backsheet and the point 'E' is situated in the encapsulant. Here, point B1, B2 and B3 are located at respectively 0.0875 mm, 0.175 mm, and 0.35 mm from the transition of the atmosphere and the backsheet. Point E2, E3, and E4 are respectively at 0.025 mm, 0.05 mm and 0.1 mm.

### 3.3.1 Backsheet and encapsulant

First, the analytical model and the model made in COMSOL Multiphysics are compared with the results of [19]. For this, the same parameters as in the paper are used. In this paper the diffusion coefficient and the solubility are kept constant. The results can be seen in Figure 29.

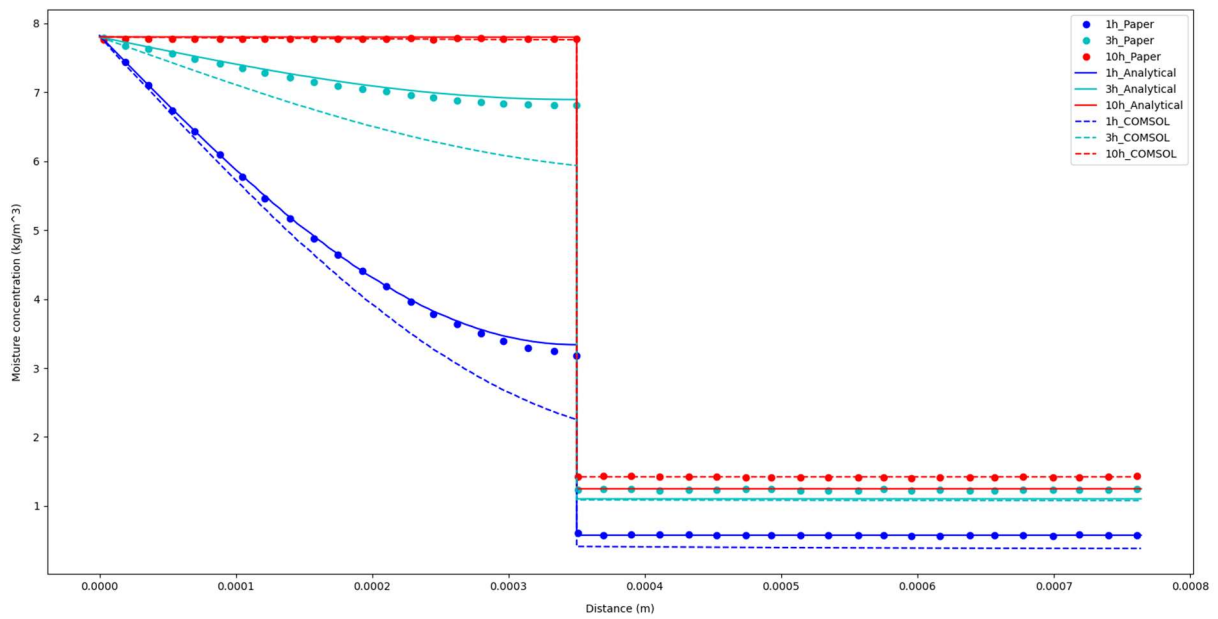


Figure 29: Results backsheet and encapsulant compared with Figure 1 of [19]

Figure 29 shows the moisture concentration in function of the thickness of the breathable backsheet and the encapsulant. Here, the backsheet has a thickness of 0.35 mm and the encapsulant has a thickness of 0.4 mm. The results of the analytical model (straight line) correspond well with the results in the paper (dotted line). Only at ten hours, the analytical model for the encapsulant has an underestimation of  $0.19 \text{ kg/m}^3$ . COMSOL deviates from the absolute values in the paper. For one hour, COMSOL has an underestimation of  $0.93 \text{ kg/m}^3$  for the backsheet. After three hours, this underestimation is  $0.87 \text{ kg/m}^3$ . Since the COMSOL model has the same trend as the analytical model, COMSOL will be used to validate the analytical model.

After that, the models for the breathable backsheet and the encapsulant are plotted in function of time. For this, one-year measurement data of Delft (Netherlands) is used. This data provides module temperatures and the ambient humidity. Here, the diffusion coefficient and the solubility vary with the temperature. Figure 30 shows the results in point B1.

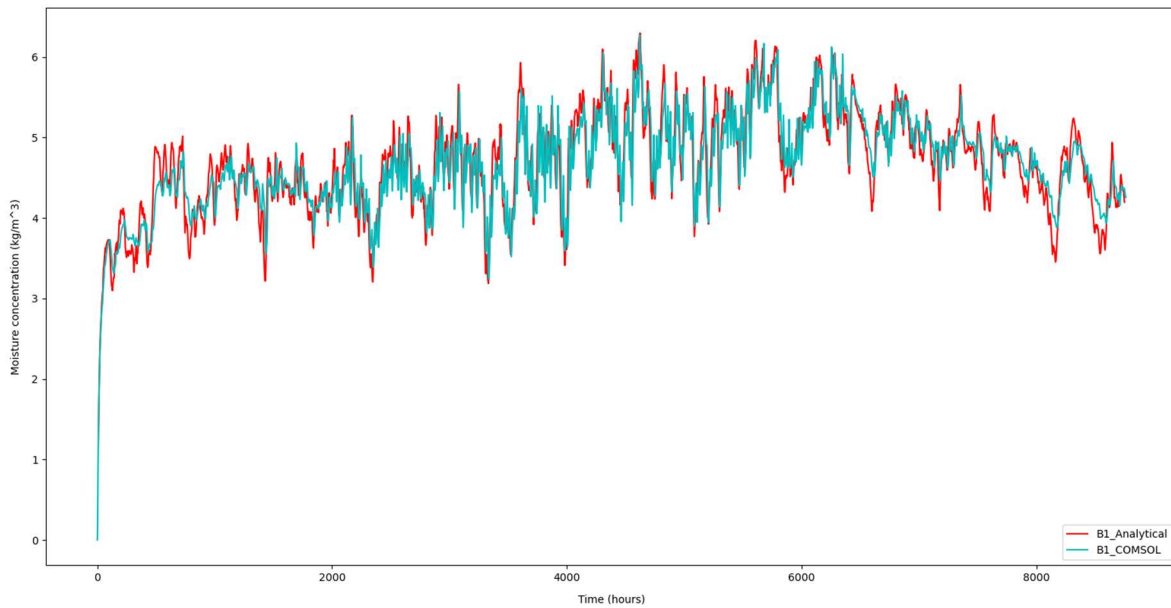


Figure 30: One-year results backsheet in point B1

Figure 30 plots the moisture concentration in function of the time. Here, the red graph shows the results for the analytical model and the blue graph shows the results of COMSOL. Both graphs have the same trend. At the beginning and at the end, the analytical model has more variation than the results of COMSOL. In this graph a moving average is used to reduce the variation of the analytical model. Figure 31 plots the results of the analytical model for four different places in the backsheet using the moving average.

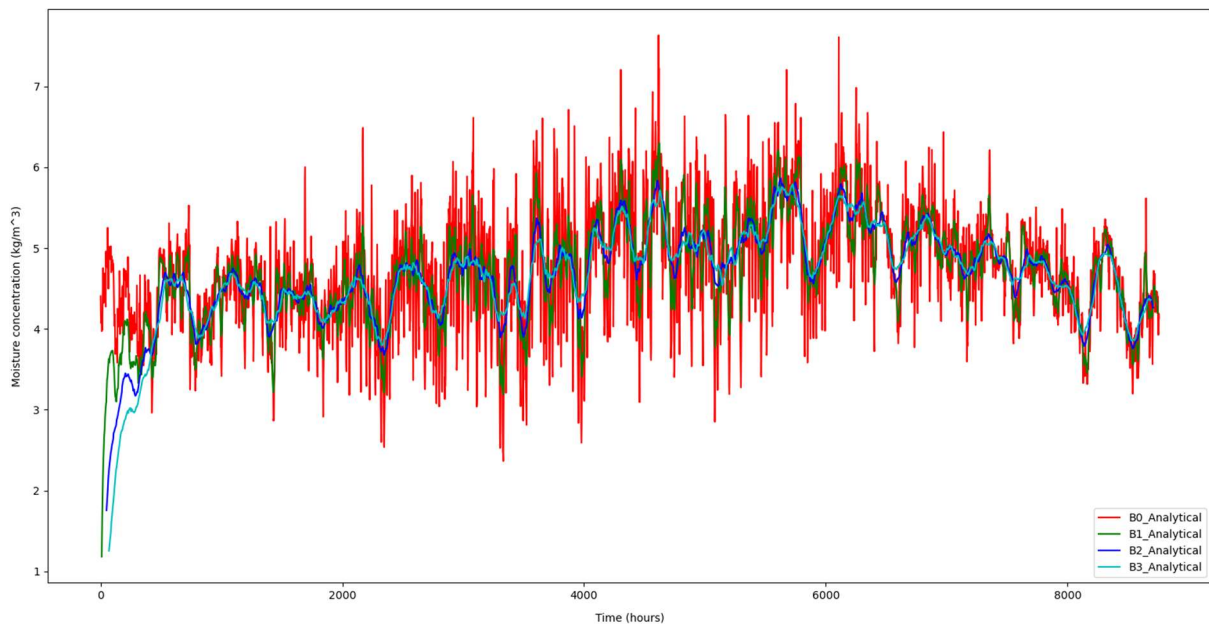


Figure 31: One-year results backsheet at different thicknesses

Figure 31 shows that in point B0 (transition of the backsheet to the environment), the backsheet immediately reaches the saturation concentration. The other three graphs reach the saturation concentration at approximately 450 hours. Furthermore, the saturation concentration is reached faster at a lower thickness. Afterwards, the results for the encapsulant in point E1 are shown in Figure 32.

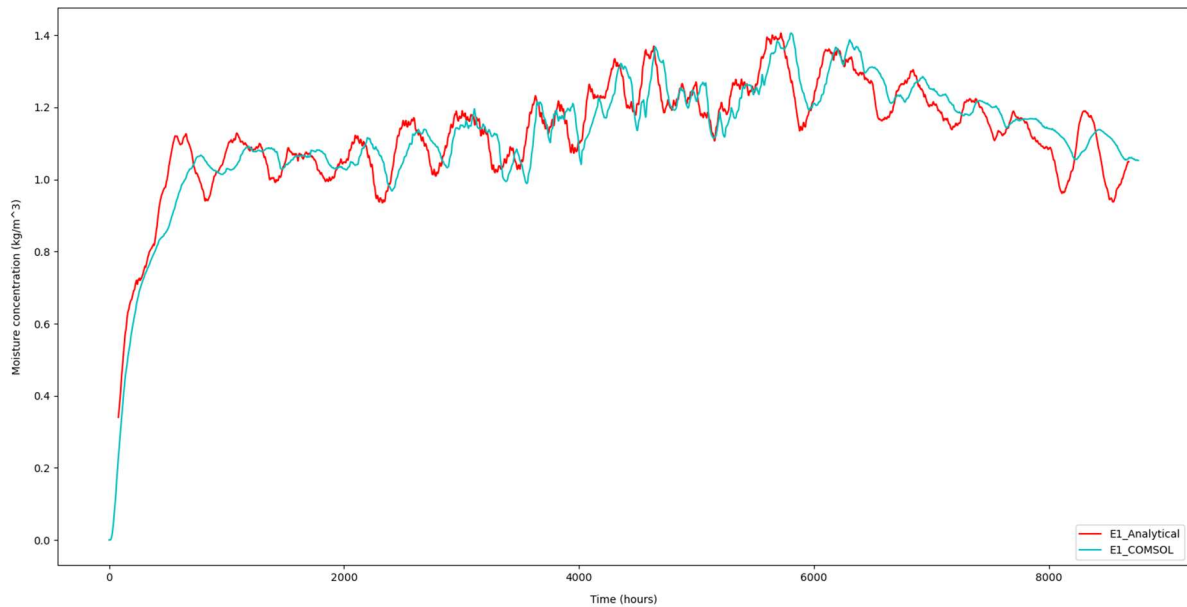


Figure 32: One-year results encapsulant in point E1

Figure 32 shows that the analytical model reaches the saturation concentration after approximately 501 h, while the model developed with COMSOL reaches saturation concentration after around 565 h. The moisture concentration in the encapsulant is approximately a quarter of the concentration in the backsheet. Finally, Figure 33 plots the one-year average moisture concentrations for a full year at the different places.

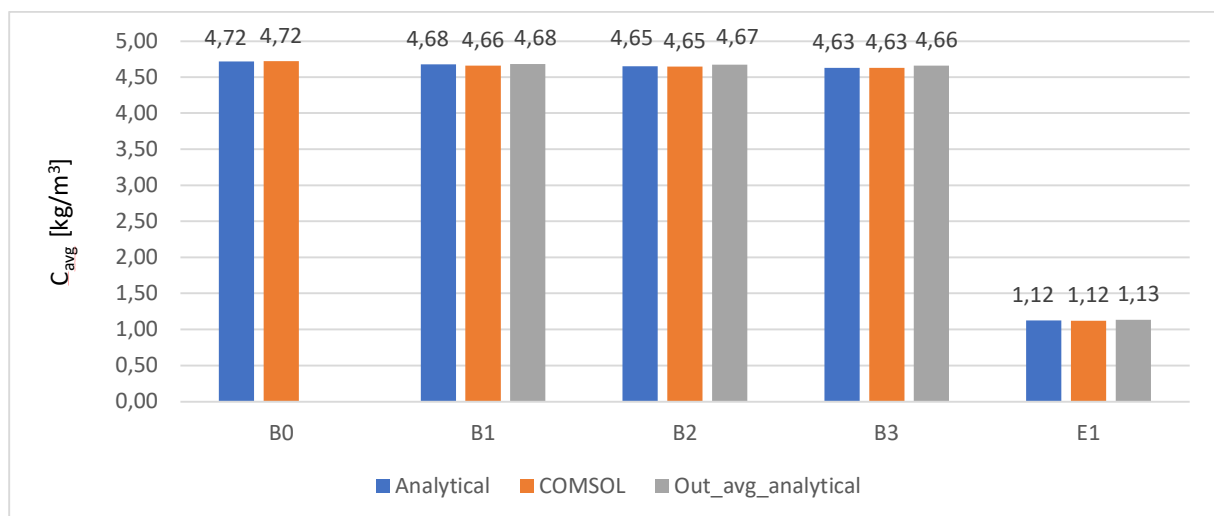


Figure 33: One-year average moisture concentrations backsheet and encapsulant

In Figure 33, the grey bars represent the average values for the averaged output of the analytical model. So, 'Out\_avg\_analytical' plots the one-year average moisture concentrations when the output is averaged. At zero thickness the amplitudes of both models corresponded well. Therefore, no moving average was needed.

### 3.3.2 Module with breathable backsheet

This section discusses the results of pathway 2 in Figure 26. For this, five-year data from Delft is used. Figure 34 shows the results in point E2, E3, and E4 in function of the time.

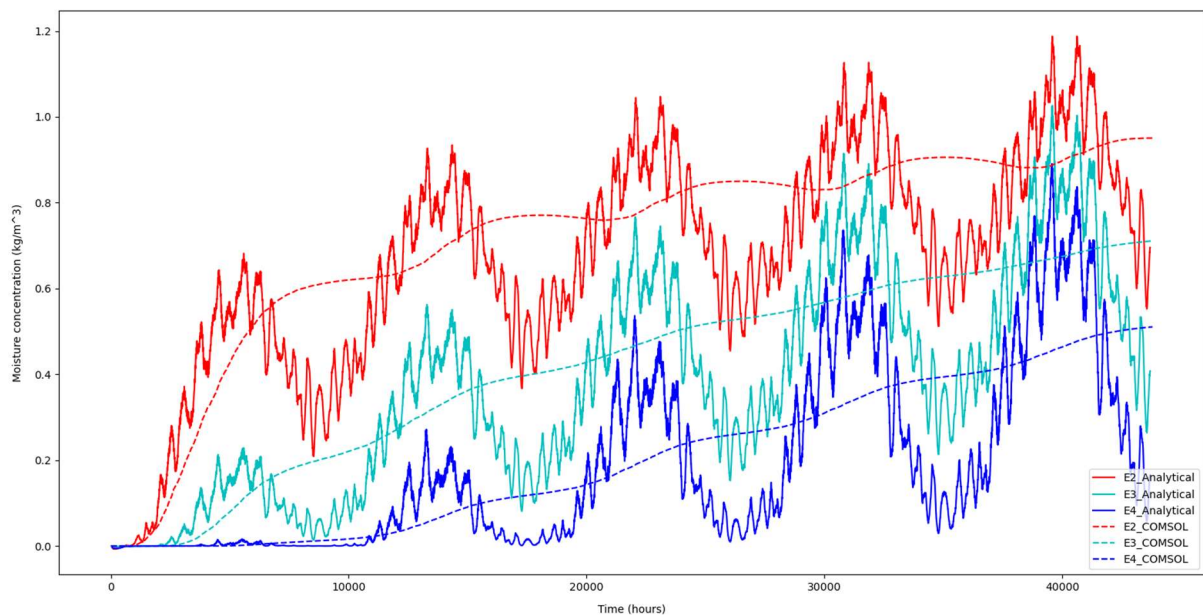


Figure 34: Five-year results pathway two breathable backsheet module time depended

Figure 34 shows that the analytical model has more variation than the COMSOL model. Near the edge of the PV module (E2), the moisture concentration will increase faster than in the middle of the PV module (E4). After five years, the moisture concentration of the three graphs keeps increasing, so the saturation concentration is not reached yet. Figure 35 plots the moisture concentration of pathway 2 in function of the distance. Here, 0 m is at the edge of the PV module and 0.1 m is in the middle of the PV module.



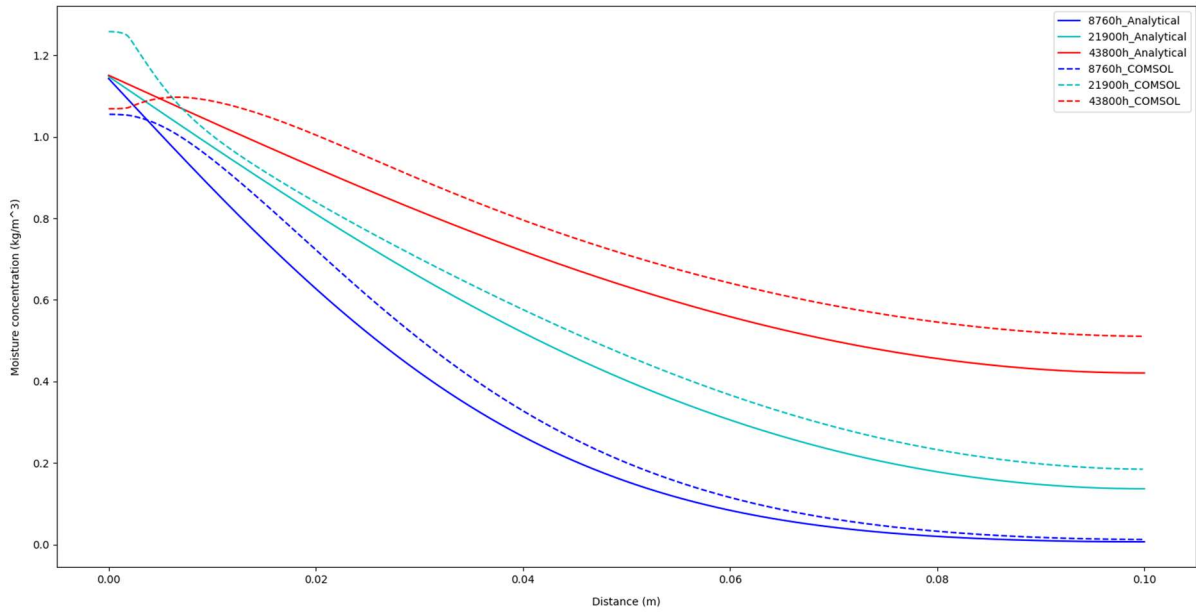


Figure 35: Results pathway two breathable backsheet module distance depended

Figure 35 plots the moisture concentration for 1 year (8 760 h), 2.5 years (21 900 h) and for 5 years (43 800 h). Here, the moisture concentration decreases if the distance from the edge increases. The moisture concentration simulated by the analytical model is lower than the moisture concentrations simulated by COMSOL. This is also shown by the five-year average concentrations in Figure 36.

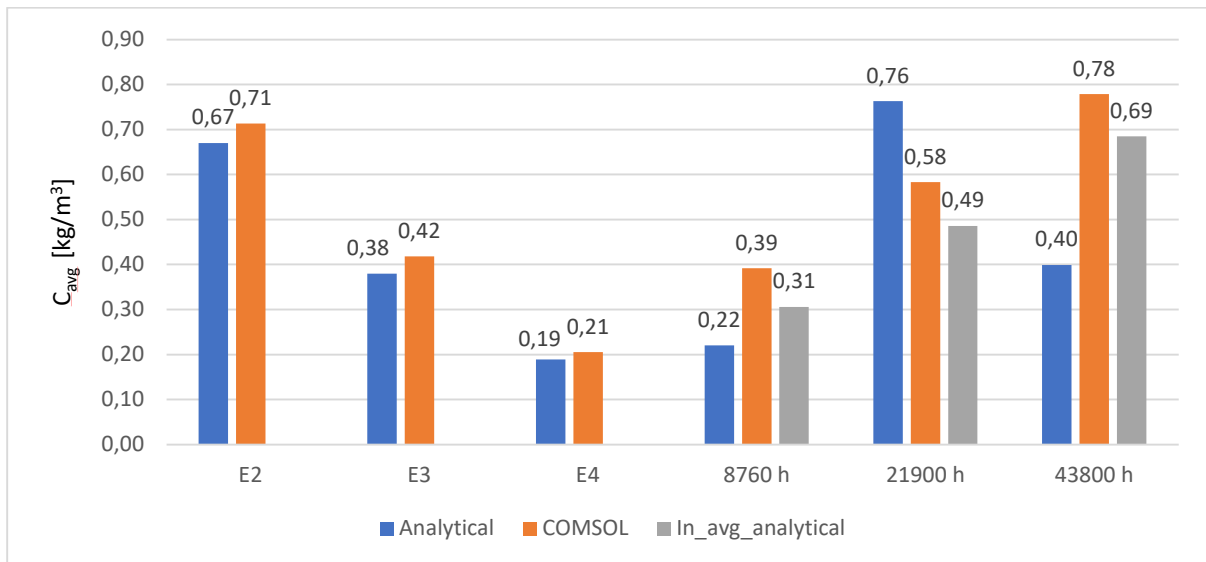


Figure 36: Five-year average moisture concentrations pathway two breathable model

The grey bars in Figure 36 'In\_avg\_analytical' plots the five-year average moisture concentrations when the input is averaged. The average moisture concentrations for the analytical model varies from the average values of COMSOL. The reason for this can be that the analytical model uses a 1D model, while COMSOL uses a 2D model. For the next simulations both the analytical model and COMSOL will use a 1D model.

### 3.3.3 Glass backsheet PV module

The glass backsheet PV module is validated with data of Singapore and Brussels. These two locations are chosen because of their different climates. Singapore has a tropical climate, while Brussels has a temperate climate. In Singapore the temperature is almost constant during the year with an average temperature of 31 °C, while the temperature in Brussels varies from around 6.2 °C during the winter and 23.3 °C in the summer. The average relative humidities are approximately the same [30]. For this simulation, five-year data from COMSOL is used. COMSOL only provides one-year data. Therefore, the one-year data is used five times. Figure 37 shows the results for Singapore in function of the time.

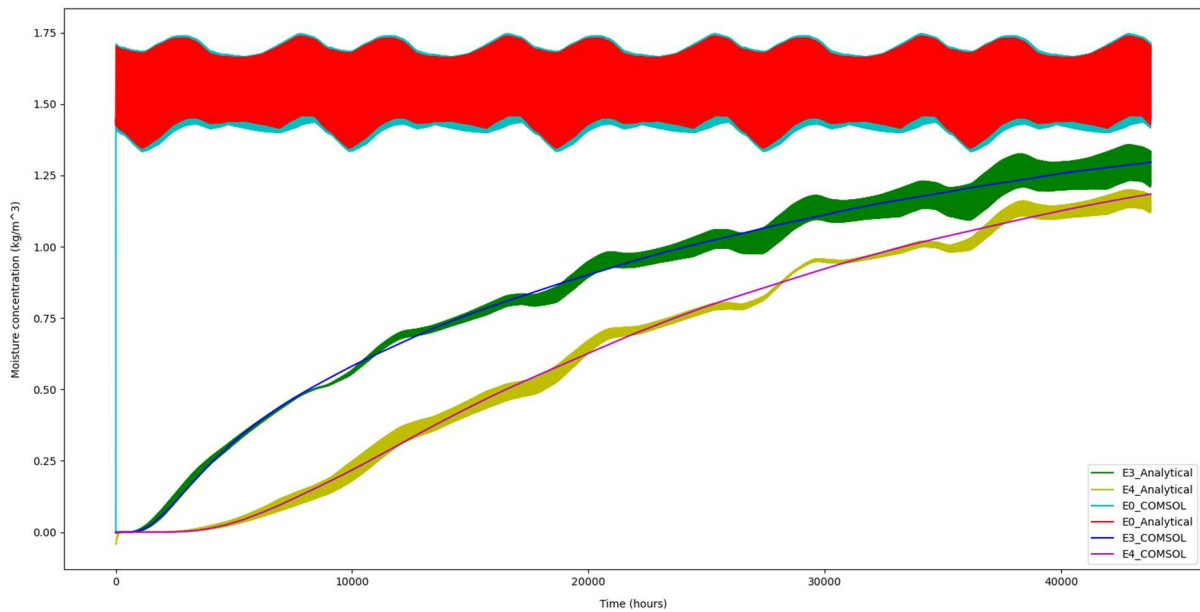


Figure 37: Five-year results Singapore glass backsheet model time depended

In Figure 37, three different locations are plotted for the glass backsheet PV module. These locations are the points E0, E3, and E4 of Figure 28. It can be seen that the edge of the PV module (E0) is immediately saturated while the other two graphs are saturated after nearly five years. The results correspond well with the results from COMSOL. The only difference is that the analytical model has more variation for quarter and half the width. Figure 38 shows the moisture concentration in function of the distance. Here, 0 m is at the edge of the PV module and 0.1 m is the half of the PV module.

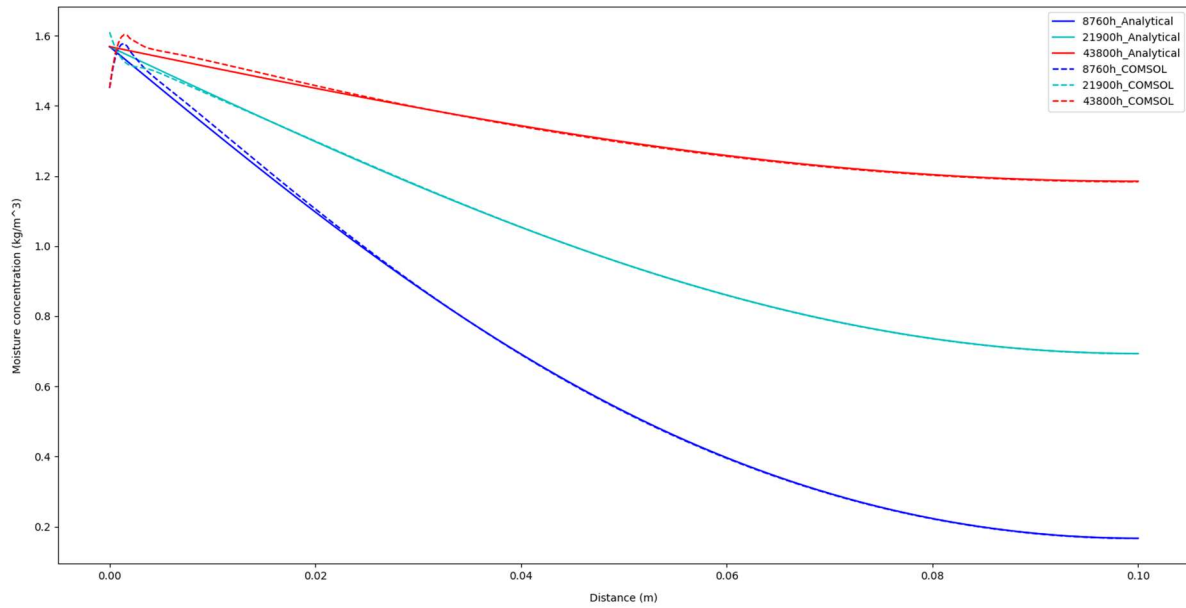


Figure 38: Results Singapore glass backsheet model distance depended

Figure 38 plots the results for 1 year (8 760 h), 2.5 years (21 900 h) and for 5 years (43 800 h). Here, the moisture concentration is the highest after five years. The two models correspond well. Only in the beginning there is difference. Here, the COMSOL model has some outliers. This is because COMSOL uses other boundary conditions as the analytical model. After that, the results for Brussels in function of the time are shown in Figure 39.

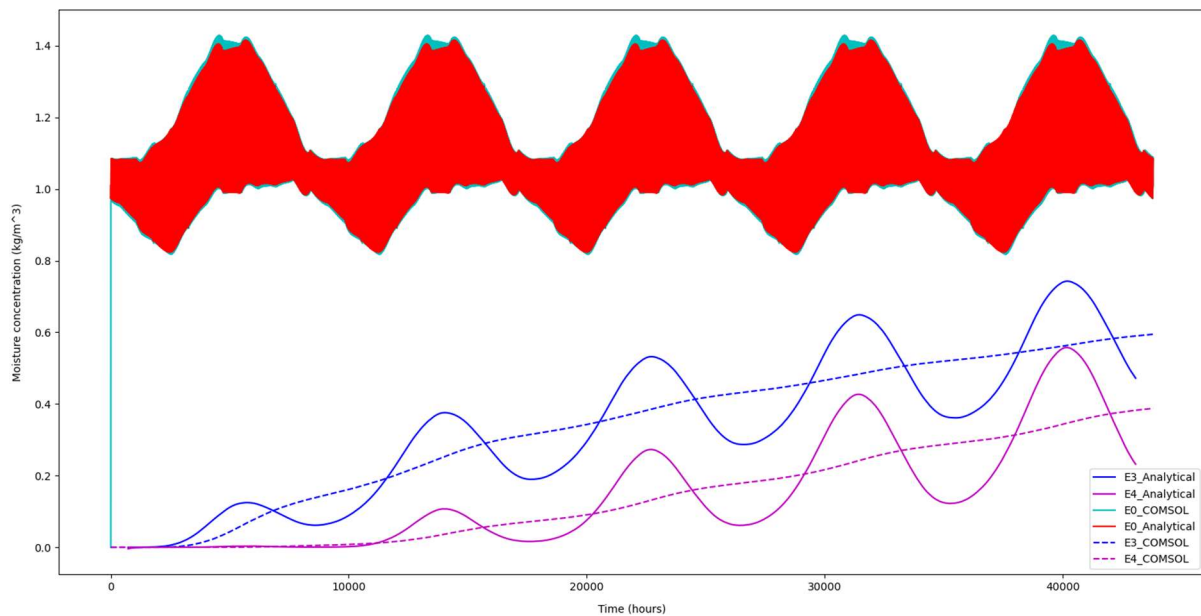


Figure 39: Five-year results Brussels glass backsheet model time depended

Figure 39 plots the moisture concentration at the edge and at quarter and half the width of the PV module. These graphs have more variation compared to the one for Singapore. This is because the ambient temperature in Singapore is almost constant during a year. Since, the diffusion coefficient and the solubility vary with temperature, this will have a significant influence on fluctuations of the

moisture concentration. According to equations (28) and (29), the diffusion coefficient and the solubility are high if the ambient temperature is high. Therefore, the moisture concentration is high during the summer ( $\pm 40\,000$  h) and low during the winter ( $\pm 35\,500$  h). The same pattern was noticed in 3.3.2, where data of Delft was used. Due to the seasonal fluctuations, the saturation moisture concentration in Brussels is lower as in Singapore. Next, the moisture concentration in function of the distance is plotted in Figure 40.

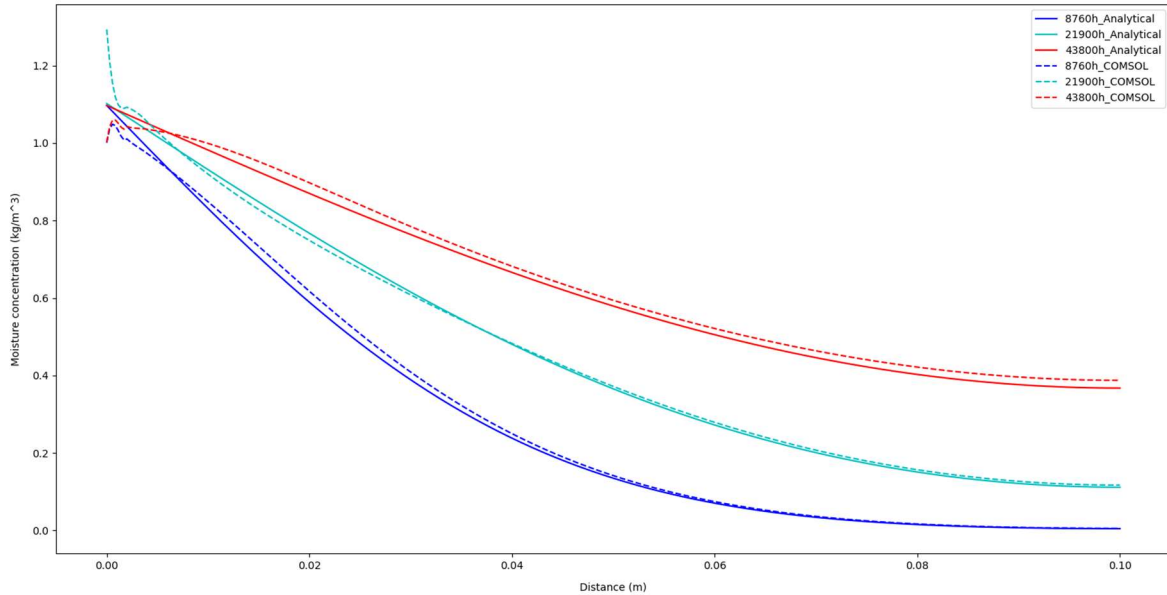


Figure 40: Results Brussels glass backsheet model distance depended

Figure 40 shows the same trend as Singapore. The moisture concentration in Brussels for 0.1 m is approximately 2.5 times lower than in Singapore for five years and four times lower for 2.5 years. The moisture concentration for one year is even near 0 kg/m<sup>3</sup>. Lastly, the five-year average moisture concentrations of Singapore and Brussels are respectively shown in Figure 41 and Figure 42.

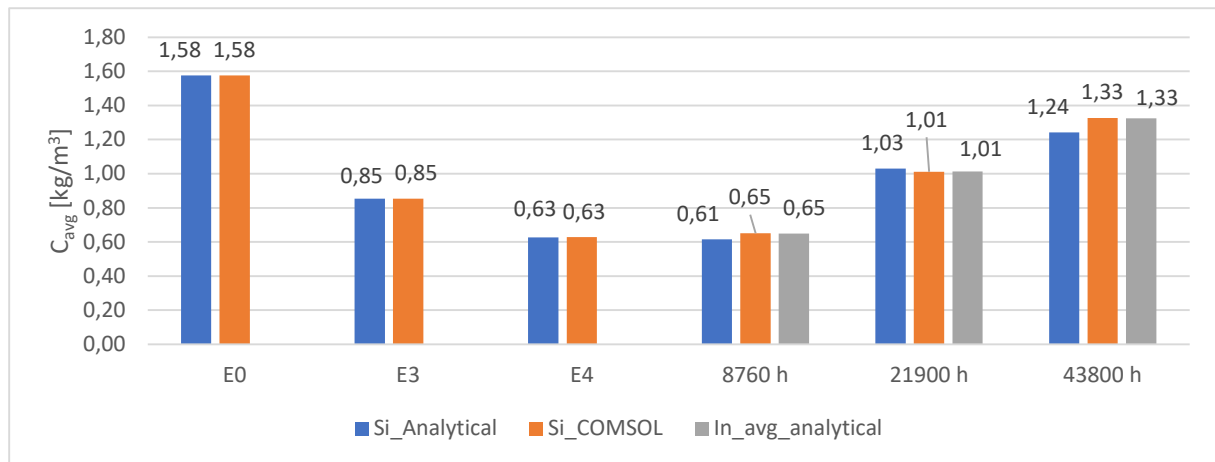


Figure 41: Five-year average moisture concentrations Singapore glass backsheet model

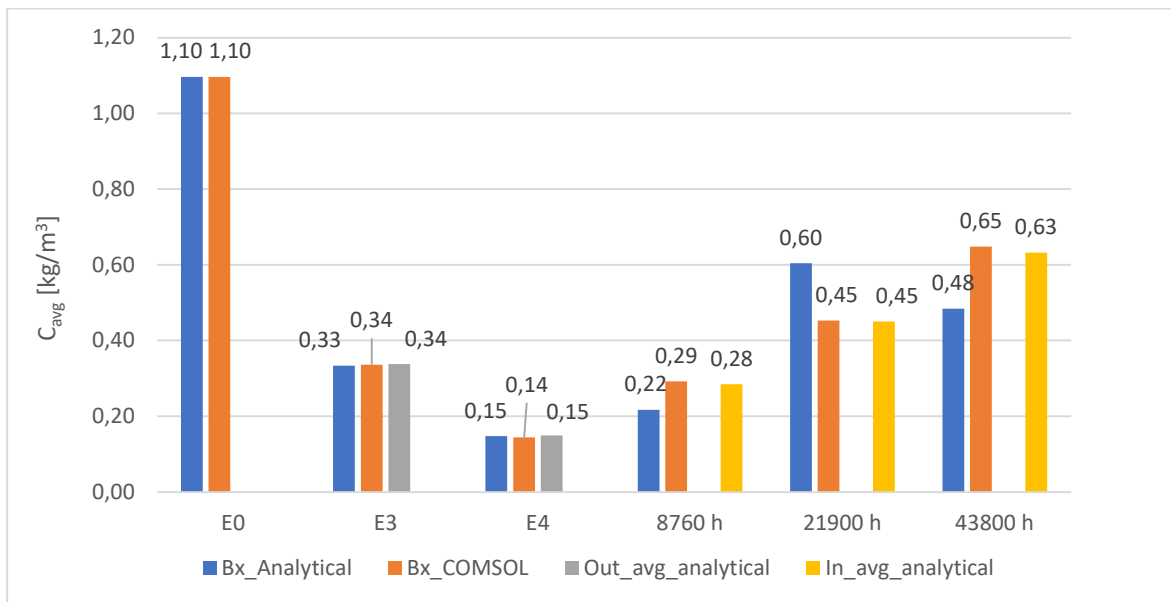


Figure 42: Five-year average moisture concentrations Brussels glass backsheet model

The five-year averages of the analytical model for the different simulations in Singapore correspond well with the averages of COMSOL. For Brussels, the difference between the five-year averages of the analytical model and COMSOL for 8 760 h, 21 900 h and 43 800 h are greater. These differences are respectively 0,07 kg/m<sup>3</sup>, 0,15 kg/m<sup>3</sup>, and 0,17 kg/m<sup>3</sup>. These differences are reduced by the 'in\_avg\_analytical'.

### 3.3.4 BIPV module

Lastly, the analytical model of the cavity and the analytical model of the PV module are combined so that the moisture concentration in a BIPV module can be simulated. Figure 43 shows a half year simulation of pathway 1 (Figure 26) for Singapore. Here, the temperature and the relative humidity in the cavity is used as the input parameters. The temperature in the cavity is simulated by imec's simulation framework.

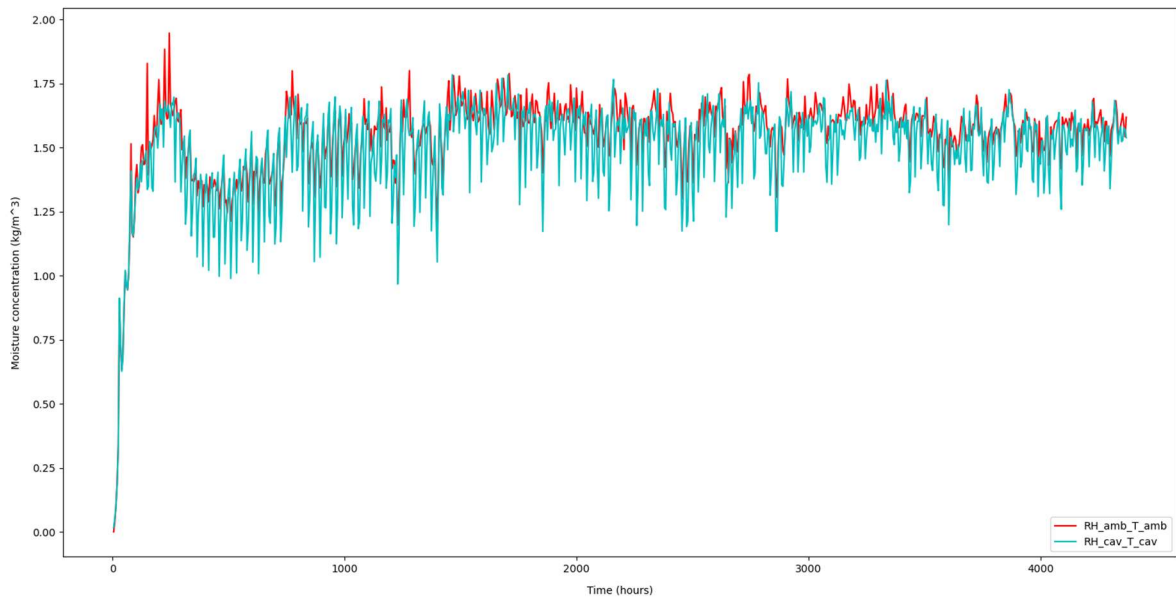


Figure 43: Half-year results BIPV module pathway 1

The red graph in Figure 43 plots the moisture concentration by using the ambient conditions while the blue graph plots the moisture concentration by using the cavity conditions. This indicates that the moisture concentration for the ambient conditions is higher. Figure 44 shows the results of pathway 2 (Figure 26) 0.05 m from the edge of the PV module (point E3 in Figure 28).

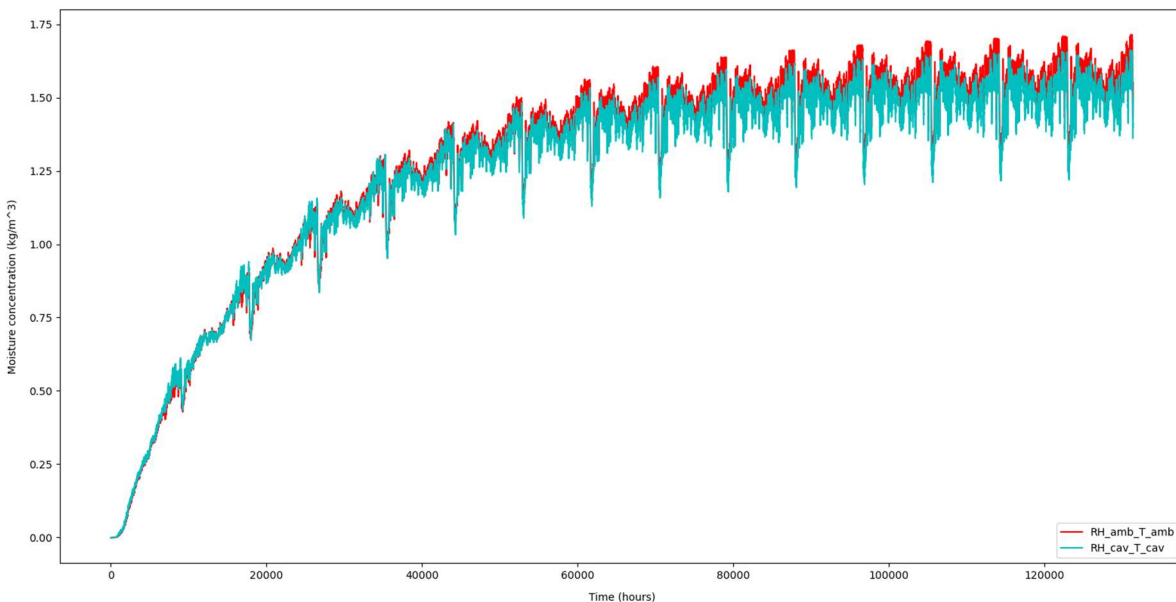


Figure 44: Fifteen-year results BIPV module pathway 2

In Figure 44 the moisture concentration is plotted for 15 years. After 15 years, the saturation concentration is almost reached. The graph for the cavity conditions has the same trend as the graph for the ambient conditions. In the beginning both moisture concentrations are almost identical, while the moisture concentrations for the ambient conditions are higher at the end of the simulation. This

results in an average moisture concentration of  $1.28 \text{ kg/m}^3$  for ambient conditions and  $1.25 \text{ kg/m}^3$  for cavity conditions.

### 3.4 Measurements

This section discusses the relative humidity measurements inside the PV modules. Firstly, the used measurement method and the measurement setup is explained. After that, the results of the calibration, the tested samples, and the RMC levels are shown.

#### 3.4.1 Indicator cards

As explained in the literature section 3.1.5, different type of measurement methods are available. The method used in this thesis was the indicator cards. The indicators cards use a blotting paper that is impregnated with cobaltous chloride. This causes it to change colour depending on the moisture concentration in the surrounding environment. The moisture from the environments gets absorbed or desorbed by the cards depending on the relative humidity, until it reaches an equilibrium. These indicator cards offer different dots that have different levels of cobaltous chloride. This causes the dots to react differently to the humidity depending on the level of cobaltous chloride [18]. As earlier mentioned, these cards offer important advantages in comparison to other methods. In Figure 45 the dots are visible before the lamination process.

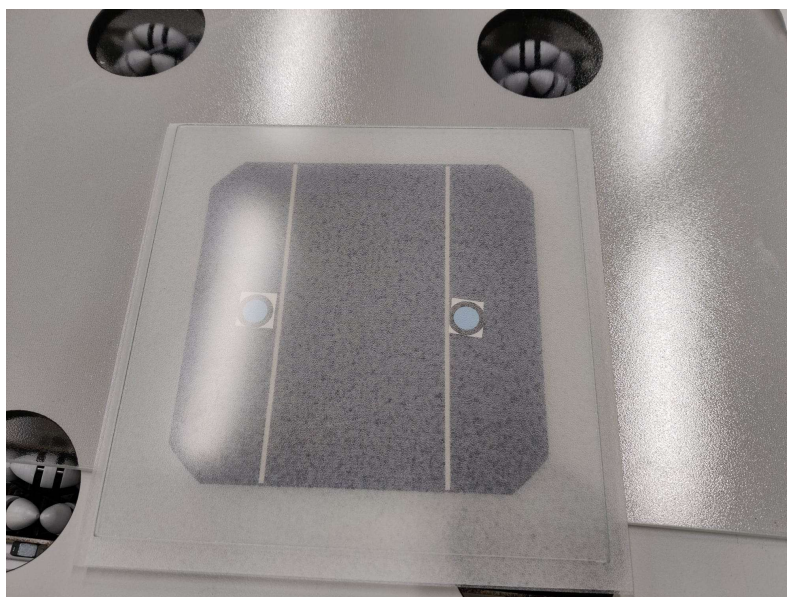


*Figure 45: Indicator card lamination*

Figure 45 shows the indicator cards before the lamination process. The two different dots are situated on the same distance from the edge. The dot on the left side is the 30% dot and the dot on the right is the 40% dot. These dots were chosen to ensure a visible colour change. The 30% dot has a faster reaction rate than the 40% dot but will also be less effective at high humidity levels. The 40%

dot will ensure a noticeable change on higher moisture contents, but its colour change will be slower in low moisture contents. The other dots on the indicator cards will not be used in this paper as the lower percentage levels will saturate sooner and the higher percentage levels could result in a moisture ingress that is not noticeable. After the lamination the cards will have a dark-green colour instead of the blue that it has before lamination. The cards will still operate after lamination. However, a calibration is required because of the presence of the polymers.

3.4.2 Lamination process

As showed in Figure 45 the cards are embedded in the PV module stack before the lamination process. The lamination process will remove air out of the PV module and warm the PV module up. This ensures that the encapsulant melts to get a good adhesion in order to provide a better durability and protection against the environmental conditions. The lamination stack of a PV module with the indicator cards is shown in Figure 46.

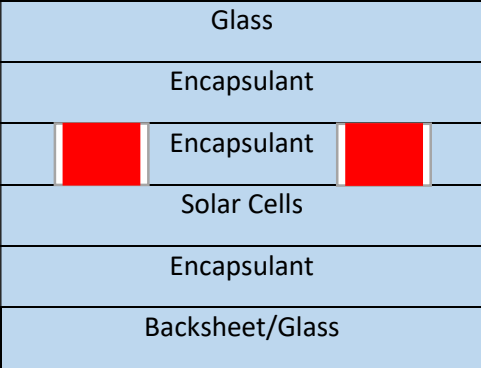


Figure 46: Lay-out lamination

With the use of the indicator cards illustrated as the red boxes an extra layer of encapsulant is needed as shown in Figure 46. This extra layer ensures that the cell does not crack. This is explained in section 3.1.5. Holes the size of an indicator card dot are cut-out in the encapsulant and positioned between the cell and indicator cards. The indicator cards are placed on top of the hole. Resulting in the back of the dot making direct contact with the cell. This ensures that the indicator cards measure the moisture content of the cell without the protection encapsulant having an effect on the moisture transport. The encapsulant that is used is TPO.

3.4.3 Measurement setup

The setup of the measurements plays a large role in ensuring a good repeatability of the pictures and helps with improving the time necessary for analysing the pictures. In Figure 47 the setup for the measurements is shown.



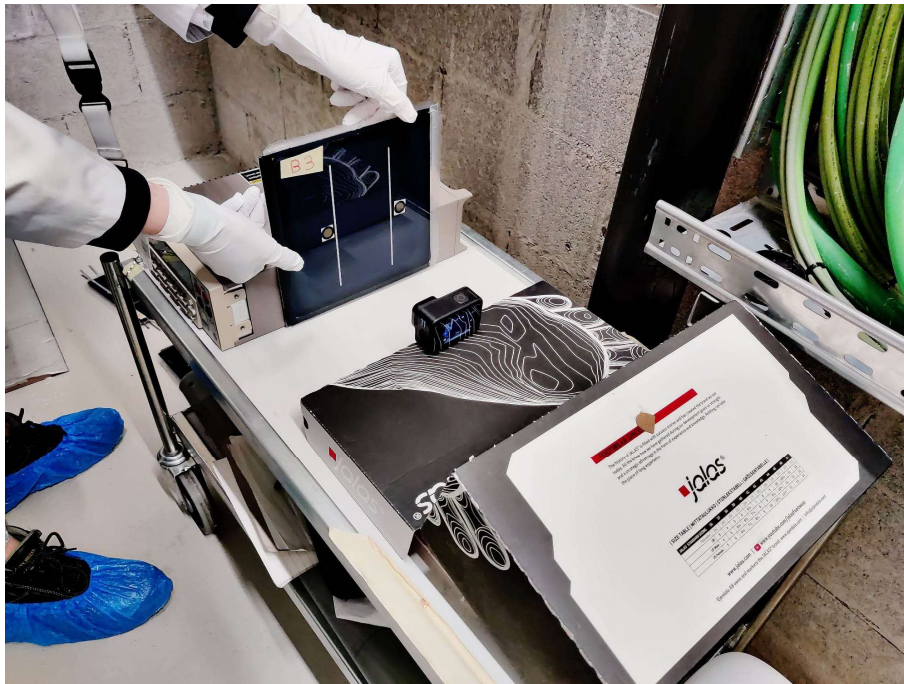


Figure 47: Measurement setup

The most important factor of the setup in Figure 47 is having a good repeatability. Due to the fact that the setup has to be reassembled every time, all parameters have to be as close to identical as possible. For instance, shadows play a large factor in taking the pictures. Due to this, certain precautions were made to ensure that there were no possible shadows on the PV module. These precautions consist of having a room with a light above the PV module and standing far enough away from the camera and setup. For the last precaution, the timer of the camera was set on three seconds. For the camera settings the linear mode was selected.

The lighting also has a large influence on the output of the analysis. For this reason, a room with a LED light was chosen. The LED light has less aging effect than a halogen bulb. The halogen bulb light wavelength changes more over time which can result in inaccuracy. The pictures were taken when the light was at least ten minutes on. This was done to decrease the chance of the LED lights changing colour over time after warming up. To ensure repeatable measurements, a stable support of the PV modules and the camera are used.

#### 3.4.4 Climatic chamber

High temperatures and high humidity are used to increase the moisture ingress. In normal outdoor circumstances the full saturation of a PV module can take multiple years. To increase the temperature and humidity in a controlled environment a chamber set in damp heat conditions is used. In Figure 48 the samples are shown in the chamber.



Figure 48: Damp heat chamber

The samples shown in Figure 48 are placed with the front glass panel down. This is done for the breathable samples and the calibration samples (not visible in this picture) resulting in a smaller chance of the protection sheet (brown sheet) interfering with the moisture ingress. The chamber for the glass backsheet and breathable modules is set at a constant relative humidity of 85% and a constant temperature of 85 °C. The relative humidity settings for the calibration is shown in Figure 49: Calibration planning.

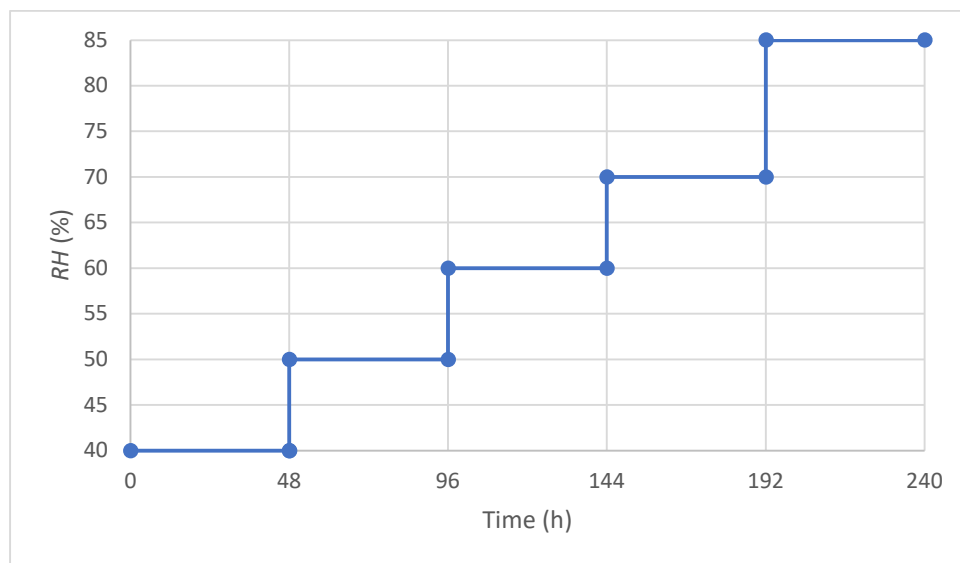


Figure 49: Calibration planning

The chamber for the calibration modules is set at a relative humidity of 40% and is then increased with 10% every 48 hours. The humidity interval will then be 40%-50%-60%-70%-85% at a constant temperature of 85 °C. The goal of the 48 hours is to ensure a full saturation at that humidity level. Measurements will then be done 48 hours after a relative humidity change. The measurements are taken immediately when the module is removed from the chamber. This is to decrease the chance of a variation in moisture concentration. Especially, the calibration samples can vary in moisture

concentration when exposed to normal environmental conditions for a long duration. To avoid this from happening the image acquisition setup was made before each measurement session.

### 3.4.5 Image processing

#### 3.4.5.1 Visual analysis

Due to the setup explained in section 3.4.3 pictures need to be acquired with the same lighting and environment. This ensures that the colour difference on the pictures is only affected by moisture and is not due to environmental changes. On Figure 50 and Figure 51 the pictures for glass backsheet module G4 are shown at 210 hours and at 1222 hours.



Figure 50: Picture G4 210h



Figure 51: Picture G4 1222h

On Figure 50 and Figure 51 it is visible that the lighting and reflections are very similar even though this was taken with more than 1000 hours in between. The most important thing when checking the quality of a picture is that the dots have no reflection. As this reflection directly affects the output of the python results. Another important thing to visually check after each measurement is that the three pictures of the same PV module is identical. This causes an inaccuracy in the pictures and will increase the standard deviation, as not the same pixels are accounted for the colour estimation. However, when replacing the PV module a change in positioning is normal and can be corrected in the python script.

#### 3.4.5.2 Python program

The python program used for the indicator cards was developed for the doctoral thesis of dr. Nikoleta Kyranaki and was created by dr. Nikoleta Kyranaki [18].

For each PV module at each time step there are three identical pictures taken. This is necessary to improve the sample size and to decrease the chance of faults. The initial placement of PV modules is

not important as this can be changed in the code. However, after the initial picture the camera should not move when taking the other two pictures. This is because the code uses the same pixel position for the three pictures. An example of a pixel dimension can be seen on Figure 52.

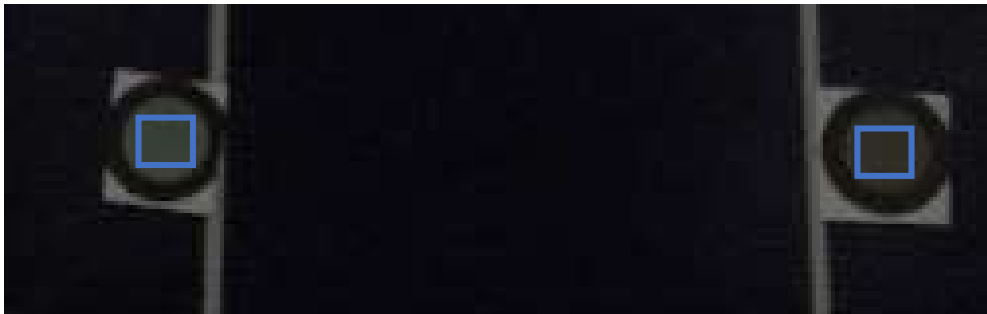


Figure 52: Zoomed in G4

The Figure 52 is a zoomed in picture of PV module G4. From this zoomed in figure a square of pixels will be chosen. For this the x and y coordinates of each dot must be selected using python. The square has to be made only for the colour part and not the black edge. This is because only the green part of the dots change colour depending on the moisture ingress. The size of this square is always 100 pixels by 100 pixels. These 10.000 pixels will be analysed per picture. This results in 30.000 pixels per PV module (three pictures per PV module).

The RGB (red, green, and blue) coordinates will then be generated for each dot of the three pictures. This is then averaged so that three RGB coordinates remain for the 30% dot and three RGB coordinates for the 40% dot. Python is then used to convert these values into a RGB colour plot. This colour plot will be shown in 3.4.7.1 and is a transformation to x and y coordinates. The standard deviation is also given to see the accuracy of the measurements.

### 3.4.6 Calibration curve humidity cards

Calibration is required for the indicator cards as these were initially designed for atmospheric conditions and not for encapsulation. For the calibration, the calibration samples were used, labelled as C3 and C4. These samples have a glass-encapsulant-indicator card-encapsulant layout seen in Figure 53.

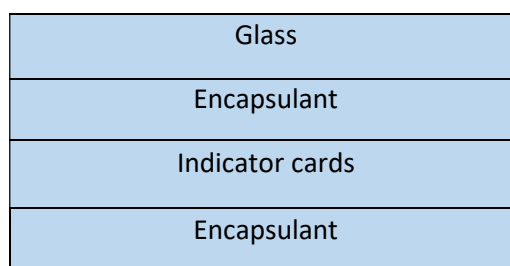


Figure 53: Lay-out calibration modules

This means that they do not have a backsheet. This lay-out is selected to decrease the time that is needed for the sample to fully saturate with moisture. However, the encapsulant and glass is necessary to make the test representative to the measurement with the PV modules [18].

In Figure 54 up to Figure 59 the different pictures at each humidity level are shown for the first calibration module.

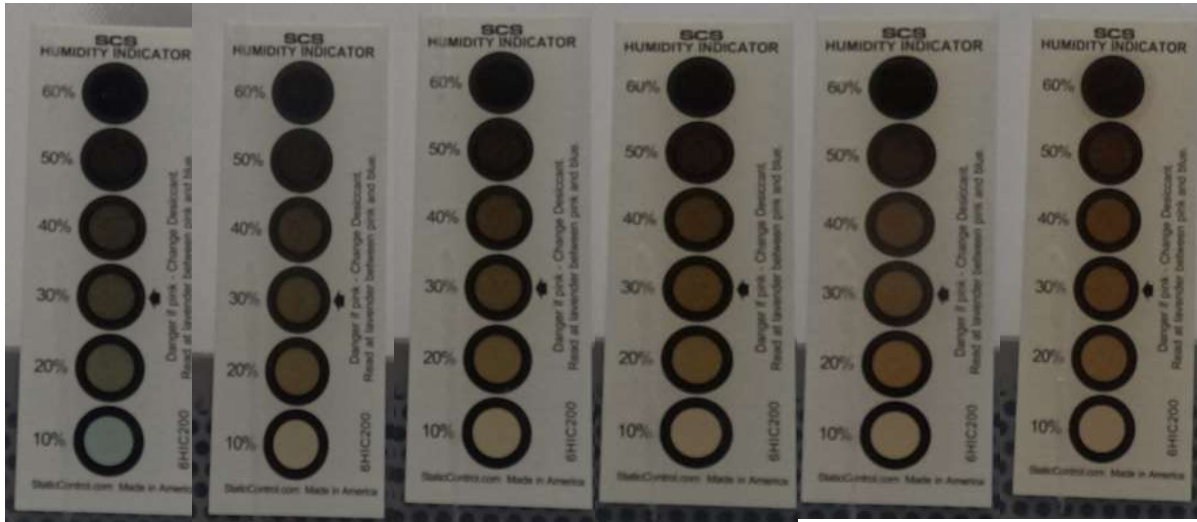


Figure 54: C3 before damp heat

Figure 55: C3 40%

Figure 56: C3 50%

Figure 57: C3 60%

Figure 58: C3 70%

Figure 59: C3 85%

The pictures shown in Figure 54 up to Figure 59 were taken at each humidity level. These humidity levels range from after lamination up to 85% relative humidity in steps of 10%, as explained in section 3.4.4 and shown in Figure 49. Here, the difference for each dot at each humidity level is visible. The 10% dot is saturated after the first humidity increase. This is why this dot was not used. The 20% dot has the same effect as the 10% dot. However, the 20% dot is slower. The 30% dot shows a consistent change in colour, as does the 40%. For this reason, these dots were chosen. The 50% and 60% show little change. Therefore, these dots were not used.

### 3.4.7 Results

#### 3.4.7.1 Explanation result method

To analyse the difference between the PV modules a RGB colour plot is generated. This shows the change in colour when the indicator cards absorb moisture. In Figure 60 an example of an RGB colour plot is given.

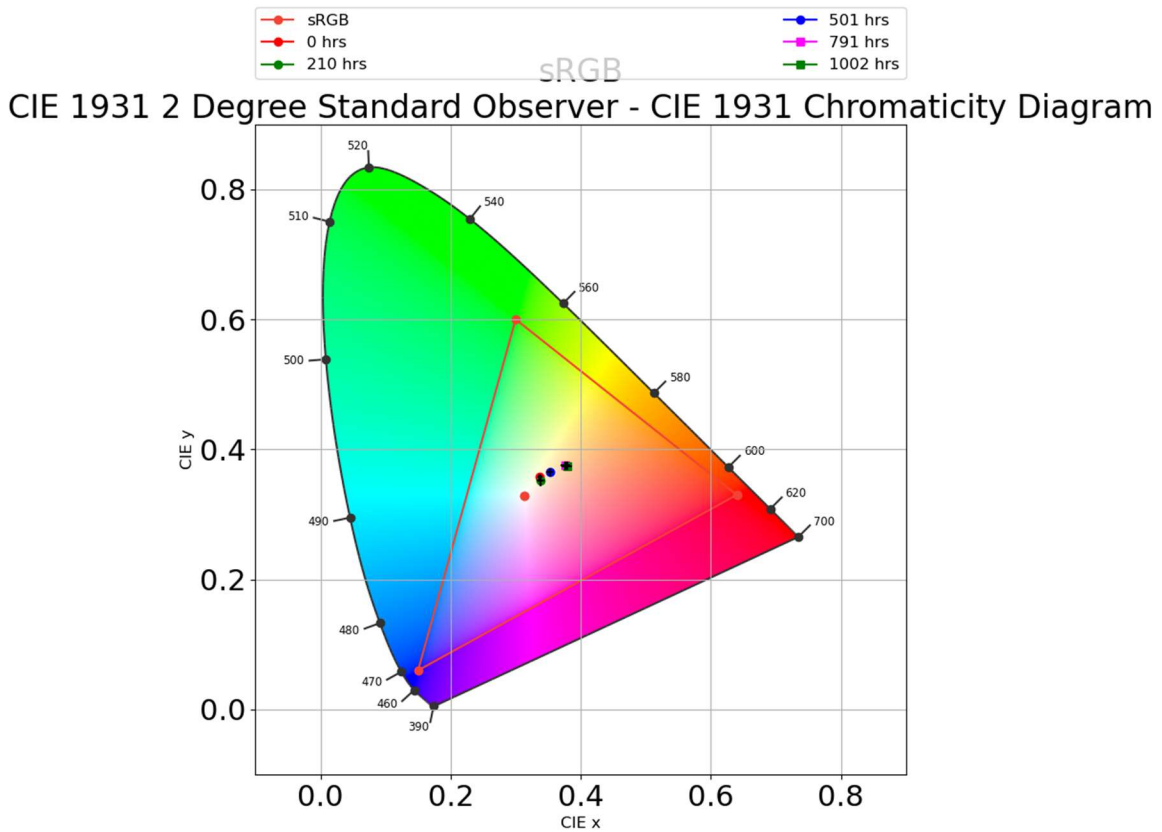


Figure 60: Example colour plot

In Figure 60 a colour plot for the 30% dot of a B3 module is given after 1002 hours. The B3 indicates that this is the first module with a breathable backsheet (number one and two were given to TU Delft for their testing). On this plot six points are shown. The first point is the sRGB point which is used to illustrate the white colour. The next five points were all measured by taking pictures at a given time and are then converted into RGB coordinates. After that, the RGB coordinates are converted into x and y coordinates. The samples that are measured are shown and explained in Table 8.



Table 8: Explanation samples

Module	Description	Status
C1	Calibration sample	Delivered to TU Delft
C2	Calibration sample	Delivered to TU Delft
C3	Calibration sample	Tested in this thesis
C4	Calibration sample	Tested in this thesis
B1	PV module breathable backsheet	Delivered to TU Delft
B2	PV module breathable backsheet	Delivered to TU Delft
B3	PV module breathable backsheet	Tested in this thesis
B4	PV module breathable backsheet	Tested in this thesis
G1	PV module glass backsheet	Delivered to TU Delft
G2	PV module glass backsheet	Delivered to TU Delft
G3	PV module glass backsheet	Tested in this thesis
G4	PV module glass backsheet	Tested in this thesis

Table 8 shows all the different samples with the different type of lay-outs and the planning for each. Half of the samples were sent to TU Delft and half were used for this thesis. The calibration samples were mentioned in section 3.4.6. The glass and breathable backsheet modules are two similar types of modules with the only change being the type of backsheet.

### 3.4.7.2 Result calibration samples

The results of calibration sample four (C4) are demonstrated in Figure 61 and Figure 62.

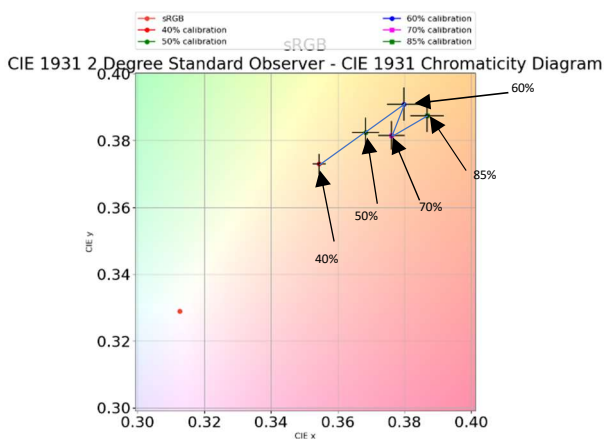


Figure 61: C4 30% dot

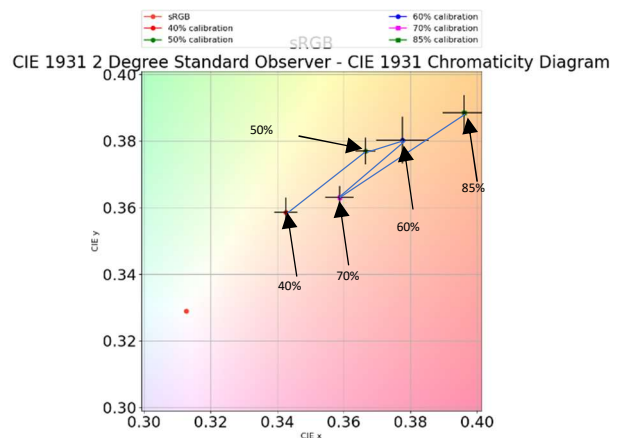


Figure 62: C4 40% dot

Figure 61 shows the colour plot for the 30% dot. Here it is visible that the colour is linear migrating to the top right for the 40%, 50% and 60% humidity levels. However the 70% and 85% humidity levels show that the dot is saturated and therefore deliver unusable results.

Figure 62 shows the colour plot for the 40% dot. This dot has a more linear approach and shows an accurate representation even at higher humidity levels. The 70% humidity level colour seems to be

unusable. This can be due to a difference in lighting or an error in the damp heat chamber. Therefore, further calibration will be done without the use of the 70% relative humidity colour dot.

In Figure 63 and Figure 64 the new calibration plot without the 70% relative humidity dot for the C4 module are shown.

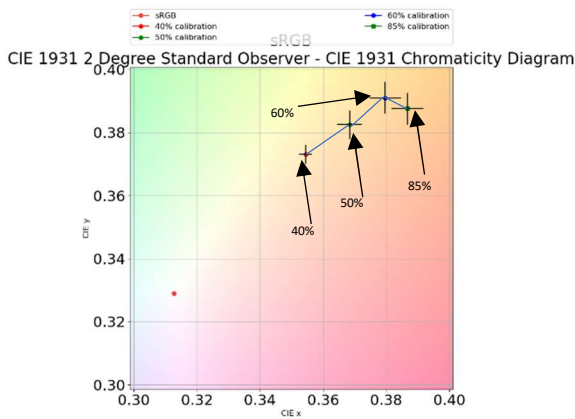


Figure 63: C4 30% without 70% RH

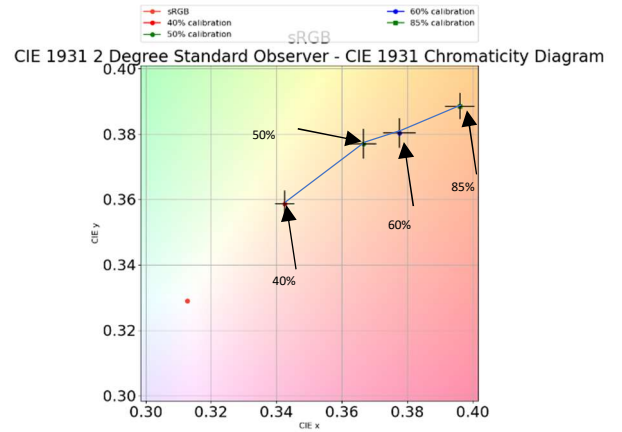


Figure 64: C4 40% without 70% RH

Figure 63 shows the 30% dot after the removal of the 70% relative humidity colour dot. This dot saturates faster and has little change after the 60% relative humidity. Figure 64 demonstrates the 40% dot after the removal of the 70% relative humidity. This shows a more linear change depending on the relative humidity and does not saturate. For further calibration the data without the 70% relative humidity will be used.



### 3.4.7.3 Result B3

The results of the first breathable backsheet module (B3) are given in Figure 65 and Figure 66.

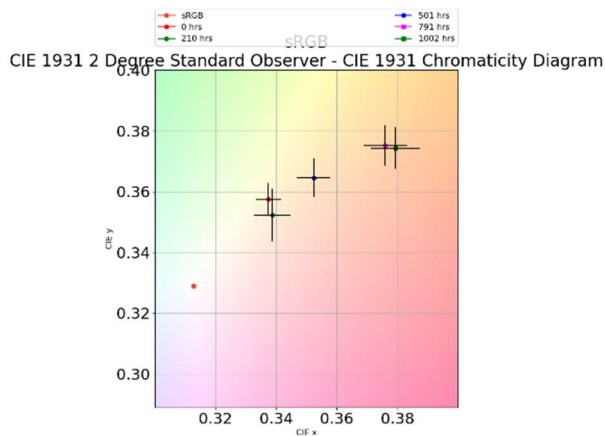


Figure 65: B3 30% dot

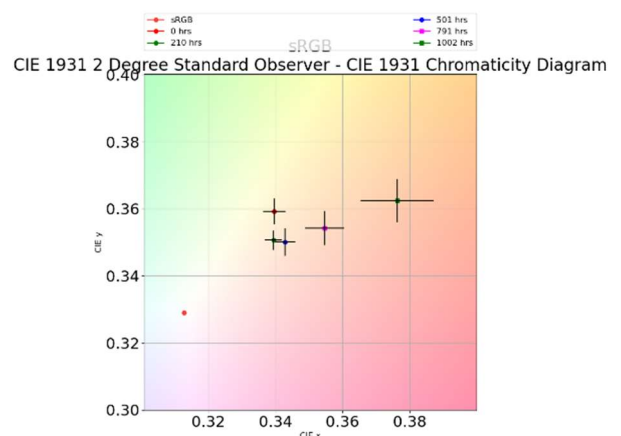


Figure 66: B3 40% dot

Figure 65 shows the colour plot for the 30% dot of the first breathable backsheet PV module. Here, it is shown that a longer time in a high humidity and temperature environment causes a change in colour of the indicator cards. This colour change illustrates that the PV module has a higher moisture concentration than before the colour change. The colour change expected for the indicator cards are from green to brown for a 60% dot [18]. As brown is a mix of red, yellow and blue which is visible around the 580 nm wavelength. For the 30% dot it is expected to end in a light brown colour. This is visible in the measurements as the dots gradually move to the top right.

Figure 66 shows the colour plot for the 40% dot of the first breathable backsheet PV module. The start value is different than the 30% dot. This is to be expected as the 40% dot in Figure 27 is slightly darker than the 30% dot. The 40% dot however does act slower in the beginning than the 30% dot, but the 30% dot saturates faster. Therefore, the 40% dot shows better that there is still moisture transport into the PV module after a longer duration. The cross lines are the standard deviation. These are used to check if the selected square dimension in the code is correct by checking the deviation between all the selected pixels. The higher duration (i.e. darker colour) dots have a higher deviation than the lower duration dots.

### 3.4.7.4 Result B4

The results of the second breathable backsheet module (B4) are given in Figure 67 and Figure 68.

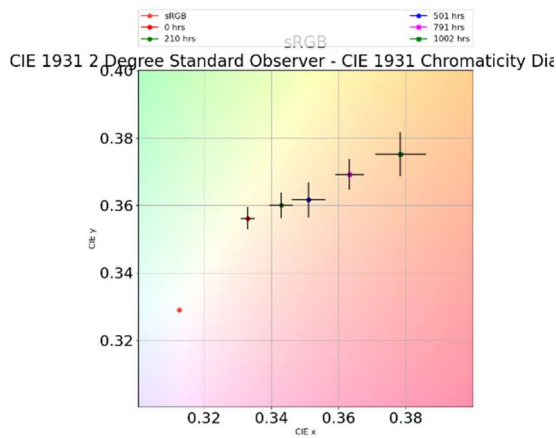


Figure 67: B4 30% dot

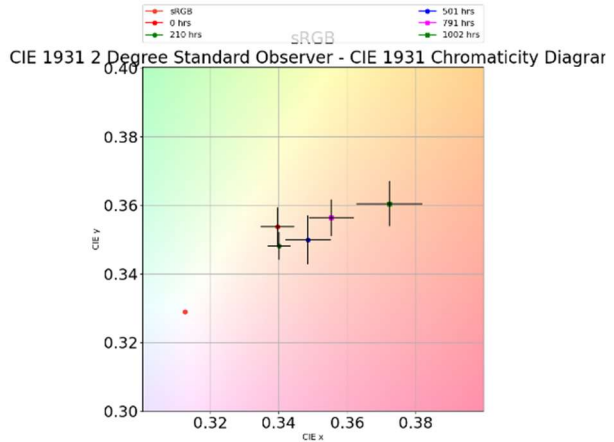


Figure 68: B4 40% dot

Figure 67 shows the colour plot for the 30% dot of the second breathable backsheet PV module. The start value of the 30% dot is similar to the 30% dot of the B3 module in Figure 65. The 210 and 792 hour mark is slightly different in the B4 in comparison to the B3 for the 30% dot, but the pattern of the movement stays consistent. This change can be explained by the B4 module having soldered busbars that exit the PV module. This can cause a change in moisture pathway.

Figure 68 shows the colour plot for the 40% dot of the second breathable backsheet PV module. These values are consistent with the values seen in B3 and show a closer comparison. This can be due to the colour of the 40% dot changing slower than the 30% dot.

### 3.4.7.5 Result G3

The results of the first glass backsheet module (G3) are given in Figure 69 and Figure 70.

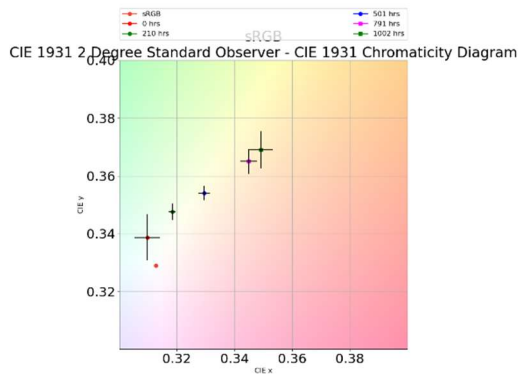


Figure 69: G3 30% dot

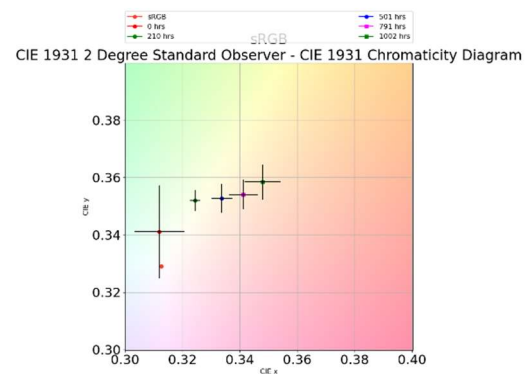


Figure 70: G3 40% dot

Figure 69 shows the colour plot for the 30% dot of the first glass backsheet PV module. The start value of the 30% should be similar to the 30% dots on the B3 and B4 modules. However this is not the case. This can be explained by an artifact in the lamination process. Therefore, a calibration is necessary to calibrate the values to the same start point as the B3 and B4 modules. This will later be explained in section 3.4.7.7.

Figure 70 demonstrates the colour plot for the 40% dot of the first glass backsheet PV module. Here, the saturation of the 30% dot is also faster than the 40% dot. This was also the case for the breathable backsheet PV modules as explained in 3.4.7.3.

### 3.4.7.6 Result G4

The results of the second glass backsheet module (G4) are given in Figure 71 and Figure 72.

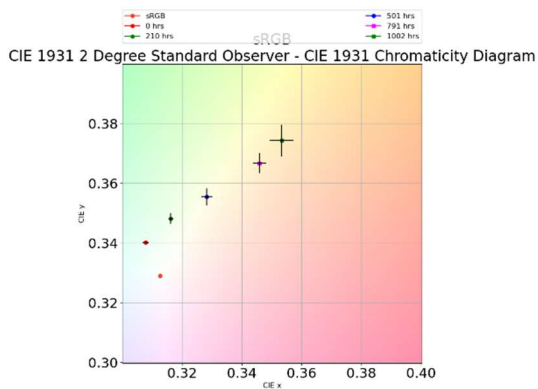


Figure 71: G4 30% dot

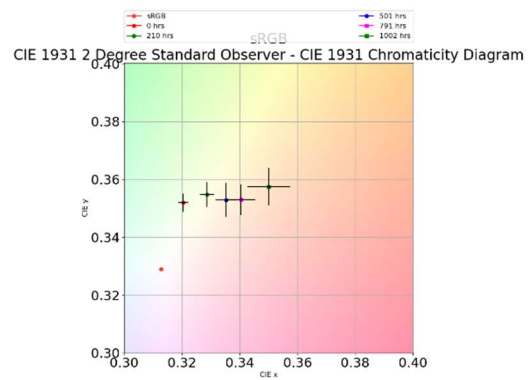


Figure 72: G4 40% dot

Figure 71 shows the colour plot for the 30% dot of the second glass backsheet PV module. The start values are similar with those of the G3 module. This indicates that this PV module also needs to be calibrated to the values of the breathable backsheets. However, the result without calibration seems to indicate that it has a good correlation with the results for the G3. This is to be expected as the glass backsheet modules do not have one PV module with busbars exciting the PV module. This was not the case with the comparison between the B3 and B4.

Figure 72 shows the colour plot for the 40% dot of the second glass backsheet PV module. These values are consistent with the values seen in G3 and show a closer comparison. Except for the measurement at 0 hours. The measurement at 0 hours in the G3 module shows a larger than usual standard deviation. This was due to a large reflection of the background that moved during the picture taking process. This only affected this PV module at 0 hours.

### 3.4.7.7 Comparing glass backsheets modules

As shown in Figure 69 and Figure 71 the start values of G3 and G4 are not similar to the start values of B3 and B4. These initial values were measured before any moisture ingress, directly after the lamination process. Therefore, these values are expected to be approximately the same. In Figure 73 - Figure 76 the initial values for the 30% and 40% dots of G1, G2, G3 and G4 are shown.

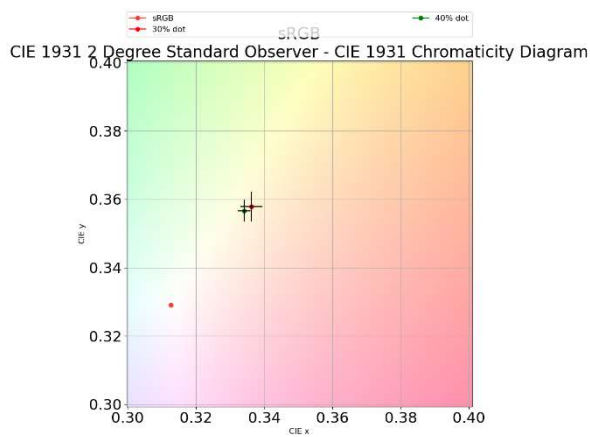


Figure 73: G1 TU delft

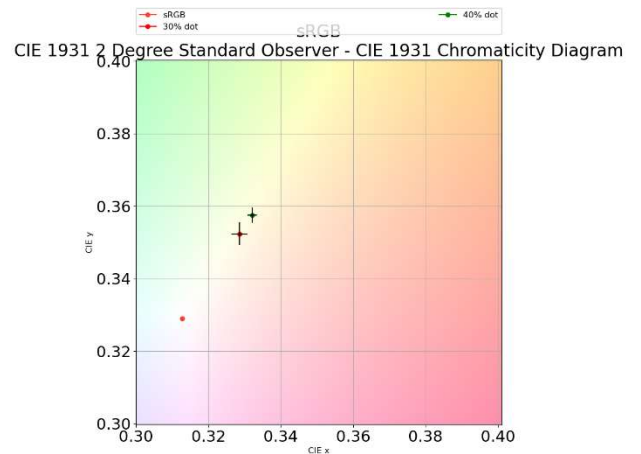


Figure 74: G2 TU Delft

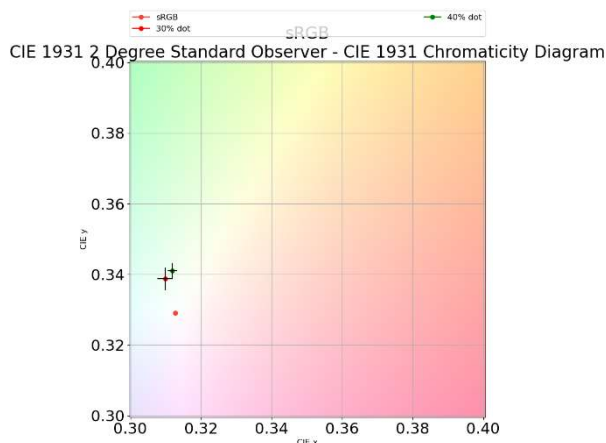


Figure 75: G3

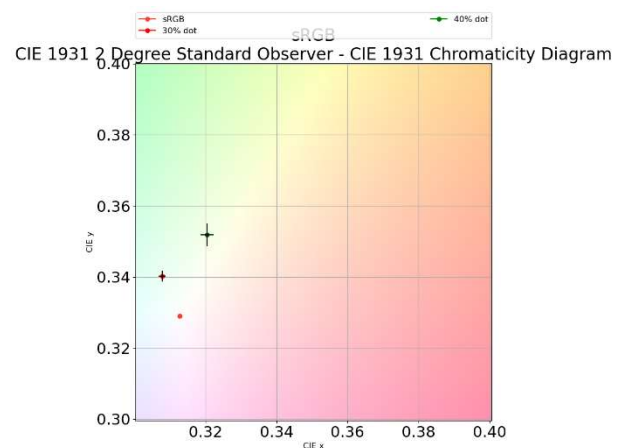


Figure 76: G4

Figure 73 and Figure 74 show the colour plot for 0 hours for the glass backsheet samples that were send to TU Delft, while Figure 75 and Figure 76 show the colour plot of the glass backsheet samples tested in this thesis. The G1 and G2 modules are samples made in this thesis but were send to TU Delft after lamination. TU Delft will have their own damp heat test (75°C, 85%). However, before the transportation measurements were done to these samples to get a baseline. The pictures used to generate these plots were taken at the same time as the G3 and G4. This should result in the initial values of the four modules being similar to each other. When the G1 and G2 are compared to the start values of G3 and G4 it is visible that both the 30% and 40% dot are not similar and have different start values. The start values for the samples that were send to TU Delft show a good comparison to the start values of the B3 and B4 modules shown earlier. This indicates that a calibration of G3 and G4 is necessary.

For this calibration, the initial values before aging and the final values, after moisture saturation of the samples, are compared to the values of the glass backsheet module, as they should be the same. After calculating and applying the respective colour differences, the middle values in the dataset of the glass backsheet module will be fitted. This will result in a new dataset which can deliver an accurate representation of the glass backsheet modules.

3.4.7.8 Relative moisture content (RMC)

Finally, the relative moisture content (RMC) for each time step is calculated. For this, the RMC level of the calibration curve that is the closest to the measured data point of a specific time step is calculated. This is achieved by calculating the smallest difference between the data point and the calibration curve. The results are shown in Figure 77 and Figure 78.

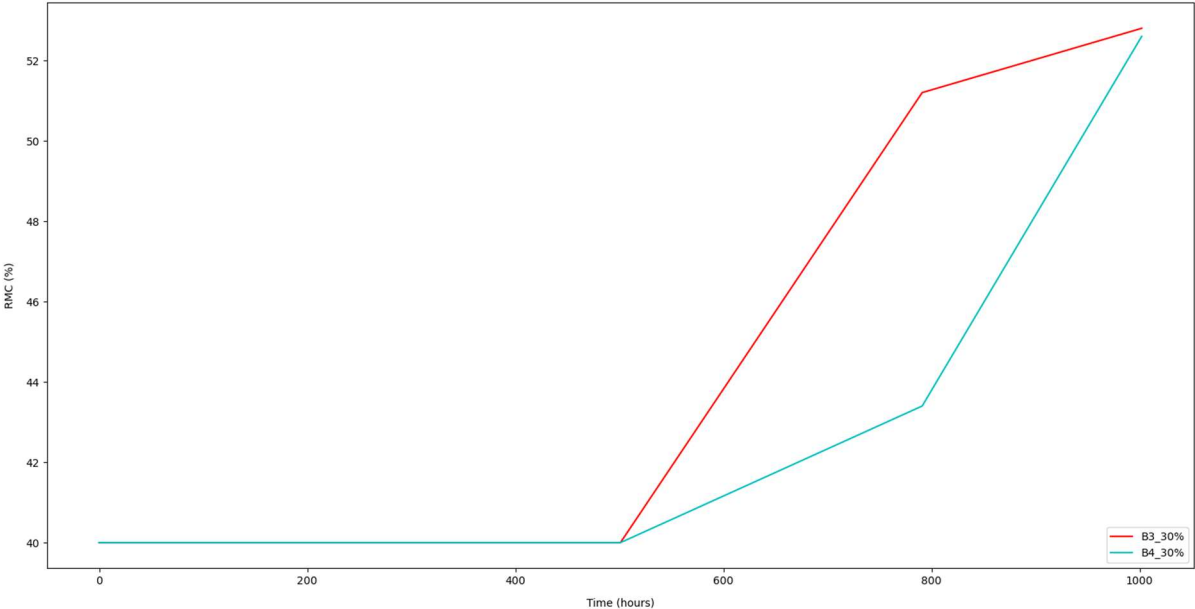


Figure 77: RMC levels B3 and B4 30%

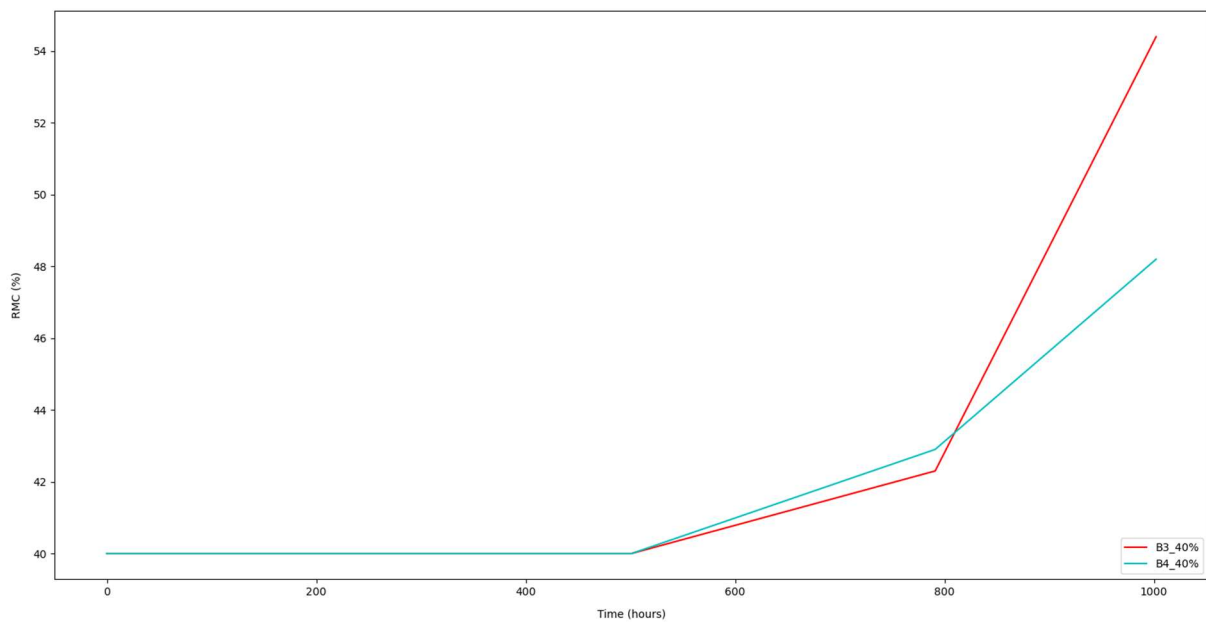


Figure 78: RMC levels B3 and B4 40%

Figure 77 and Figure 78 plots the RMC levels in function of the time for the 30% and 40% dot for both breathable backsheets PV modules. The RMC level stays 40% till 500 hours. This is because the first point of the calibration curve is at 40% so lower RMC levels are not shown. After that, the RMC level will increase. At 1002 hours, the RMC level of the 30% dot for both breathable backsheets PV modules reaches around 52.7%. Here, the 40% dot of B3 reaches 54.4%, while the 40% dot of B4 reaches 48.2%. Further research is necessary for the calibration and for the RMC levels of the glass backsheets PV modules.

### 3.5 Conclusion BIPV module

For the simulation of the moisture ingress in a PV module, a difference is made between a glass backsheets PV module and a PV module with a breathable backsheets. In a glass backsheets PV module, moisture can only enter from the sides while in a breathable module, moisture can also enter along the backsheets. In a breathable backsheets, two different pathways are considered. Pathway 1 describes the moisture transport from the backsheets to the encapsulant. At the end of pathway 1, the diffusing species change direction and move in lateral direction (Pathway 2) [19].

The analytical models are validated with the finite element software COMSOL made by TU Delft. Both the analytical model for the glass backsheets module and the breathable module have the same trend as the COMSOL model, but the analytical model has more variation. This problem is solved by using a moving average. The loss of values due to the moving average is small compared with the amount of data. Also, the average values of the analytical models correspond well with the average values of COMSOL. The overall averaged percent error when using the moving average is 0.5% for pathway 1 and 12.4% for pathway 2 of the breathable model. For the glass backsheets model this is 0.9%. The reason for the large error in pathway 2 can be due to the comparison of a 2D model with a 1D model. For this, further research is needed.

Lastly, the analytical model of the cavity and the analytical model of the PV module are combined so that the moisture concentration in a BIPV module can be simulated.

The measurements indicate that the problems of accurately measuring the moisture content is heavily affected by the measuring device and the calibration. The difference between the two dots show that the 30% dot better follows the moisture content for the beginning of the measurements. The 40% dot works better for the higher moisture contents. This indicates that the 30% dot saturates much faster than the 40%. For the comparison between the breathable backsheet and glass backsheet further research is necessary to calibrate the results. Additionally, further research is necessary to compare these results with the results from TU Delft to investigate the importance of the temperature in moisture ingress for the same modules.





## 4 Conclusion

The conclusions of the two objectives were previously explained in section 2.5 and 3.4. The three errors of the first goal showed that the model is a viable solution for modelling the cavity with the three errors being less than 5%. The atmospheric simplification was shown to have errors that were significantly higher. The percentage error of the second model showed that the analytical version was comparable to the FEM analysis with errors for both the pathway 1 and glass backsheet model being less than 1%. Pathway 2 showed a significant error. This is mainly due to comparing the 2D model of COMSOL with the 1D analytical version. This pathway requires further research.

The goal of this thesis was to create two models that each separately showed an accurate representation of their counterparts (measurement or FEM analysis). Therefore, the combination of these models result in a model that is able to accurately calculate the moisture content for a lifetime prediction. The incorporation of said model can heavily influence the accuracy of a lifetime prediction. The difference in accuracy between the current framework for a lifetime prediction of a PV module and the framework that incorporates the moisture ingress requires further research.



## References

- [1] “Imec.” <https://www.imec.be/nl> (accessed Oct. 05, 2022).
- [2] “Energyville.” <https://www.energyville.be> (accessed Oct. 05, 2022).
- [3] “Sino voltaics.” <https://sinovoltaics.com> (accessed Oct. 10, 2022).
- [4] A. Dadaniya and N. V. Datla, “Water diffusion simulation in photovoltaic module based on the characterization of encapsulant material using in-situ gravimetric technique,” *Sol. Energy Mater. Sol. Cells*, vol. 201, no. July, p. 110063, 2019, doi: 10.1016/j.solmat.2019.110063.
- [5] O. K. Segbefia, A. G. Imenes, and T. O. Sætre, “Moisture ingress in photovoltaic modules: A review,” *Sol. Energy*, vol. 224, no. October 2020, pp. 889–906, 2021, doi: 10.1016/j.solener.2021.06.055.
- [6] M. J. Ritzen, Z. A. E. P. Vroon, R. Rovers, and C. P. W. Geurts, “Comparative performance assessment of a non-ventilated and ventilated BIPV rooftop configurations in the Netherlands,” *Sol. Energy*, vol. 146, no. 2017, pp. 389–400, 2017, doi: 10.1016/j.solener.2017.02.042.
- [7] J. E. Gonçalves, T. van Hooff, and D. Saelens, “The influence of convection on the behaviour of a ventilated BIPV module: A sensitivity analysis,” *Build. Simul. Conf. Proc.*, vol. 7, pp. 4393–4400, 2019, doi: 10.26868/25222708.2019.210278.
- [8] J. E. Goncalves, T. van Hooff, and D. Saelens, “A physics-based high-resolution BIPV model for building performance simulations,” *Sol. Energy*, vol. 204, pp. 585–599, 2020, doi: 10.1016/j.solener.2020.04.057.
- [9] M. Van Belleghem, M. Steeman, A. Janssens, and M. De Paepe, “Heat, air and moisture transport modelling in ventilated cavity walls,” *J. Build. Phys.*, vol. 38, no. 4, pp. 317–349, 2015, doi: 10.1177/1744259114543984.
- [10] “Calculation of moisture content,” pp. 1–45.
- [11] L. Hoyos, “calctool,” *Air density calculator*, 2022. <https://www.calctool.org/atmospheric-thermodynamics/air-density> (accessed Nov. 02, 2022).
- [12] D. Camuffo, “Theoretical Grounds for Humidity,” *Microclim. Cult. Herit.*, pp. 49–76, 2014, doi: 10.1016/b978-0-444-63296-8.00002-0.
- [13] “Engineering ToolBox,” *Moisture Transport through Walls and Roofs*. [https://www.engineeringtoolbox.com/moisture-transport-walls-d\\_163.html](https://www.engineeringtoolbox.com/moisture-transport-walls-d_163.html) (accessed Oct. 25, 2022).
- [14] NIST, “Summary tables of useful fractional factorial designs.” <https://www.itl.nist.gov/div898/handbook/pri/section3/pri3347.htm> (accessed Nov. 10, 2022).
- [15] “Approximation error.” [https://en.wikipedia.org/wiki/Approximation\\_error](https://en.wikipedia.org/wiki/Approximation_error) (accessed Dec. 30, 2022).
- [16] M. Padhma, “End-to-End Introduction to Evaluating Regression Models,” 2021. <https://www.analyticsvidhya.com/blog/2021/10/evaluation-metric-for-regression-models/> (accessed Dec. 30, 2022).
- [17] “PVGIS online tool.” [https://joint-research-centre.ec.europa.eu/pvgis-online-tool\\_en](https://joint-research-centre.ec.europa.eu/pvgis-online-tool_en) (accessed Feb. 27, 2023).

- [18] N. Kyranaki, "Corrosion in crystalline silicon photovoltaic modules and the influence on performance," no. August, 2020.
- [19] S. Marwaha and K. Ghosh, "Analytical Modeling of Diffusion of Moisture in Silicon Photovoltaic Module under Damp Heat Testing Condition," *Silicon*, vol. 14, no. 9, pp. 4757–4766, 2022, doi: 10.1007/s12633-021-01156-7.
- [20] M. Jankovec *et al.*, "In-Situ Monitoring of Moisture Ingress in PV Modules Using Digital Humidity Sensors," *IEEE J. Photovoltaics*, vol. 6, no. 5, pp. 1152–1159, 2016, doi: 10.1109/JPHOTOV.2016.2583779.
- [21] J. Slapšak, S. Mitterhofer, M. Topic, and M. Jankovec, "Wireless System for in Situ Monitoring of Moisture Ingress in PV Modules," *IEEE J. Photovoltaics*, vol. 9, no. 5, pp. 1316–1323, 2019, doi: 10.1109/JPHOTOV.2019.2918044.
- [22] M. D. Kempe, "Modeling of rates of moisture ingress into photovoltaic modules," *Sol. Energy Mater. Sol. Cells*, vol. 90, no. 16, pp. 2720–2738, 2006, doi: 10.1016/j.solmat.2006.04.002.
- [23] E. Gregersen, "Diffusion," *Britannica*. [Online]. Available: <https://www.britannica.com/science/diffusion>.
- [24] "Permeability," *Britannica*. [Online]. Available: <https://www.britannica.com/science/permeability-physics>.
- [25] "Arden Buck equation," *Wikipedia*. [Online]. Available: [https://en.wikipedia.org/wiki/Arden\\_Buck\\_equation](https://en.wikipedia.org/wiki/Arden_Buck_equation).
- [26] S. Mitterhofer, "Modelling and monitoring of moisture transport phenomena in polymeric materials and photovoltaic modules," 2021.
- [27] S. Domjan, L. Petek, C. Arkar, and S. Medved, "Experimental Study on Energy Efficiency of Multi-Functional BIPV Glazed Façade Structure during Heating Season," pp. 1–19, 2020, [Online]. Available: [https://mdpi-res.com/energies/energies-13-02772/article\\_deploy/energies-13-02772.pdf?version=1591002125](https://mdpi-res.com/energies/energies-13-02772/article_deploy/energies-13-02772.pdf?version=1591002125).
- [28] M. D. Kempe, D. L. Nobles, L. Postak, and J. A. Calderon, "Moisture ingress prediction in polyisobutylene-based edge seal with molecular sieve desiccant," *Prog. Photovoltaics Res. Appl.*, vol. 26, no. 2, pp. 93–101, 2018, doi: 10.1002/pip.2947.
- [29] Saxenaanjali239, "How to Calculate Moving Averages in Python?," *geeksforgeeks*, 2021. <https://www.geeksforgeeks.org/how-to-calculate-moving-averages-in-python/> (accessed Jun. 10, 2023).
- [30] "Climate comparison." <https://www.worlddata.info/climate-comparison.php?r1=be-brussels-capital&r2=singapore> (accessed May 30, 2023).

## Appendices

Appendix A: Diffusion coefficients.....	84
Appendix B: Sensitivity analysis.....	84

## Appendix A: Diffusion coefficients p.24 [13]

Material	Diffusion Coefficient - Z	
	$GPa s m^2/kg$	$GPa s m^2/kg m$
Aluminum foil	5000	
Asphalt 1 coat	150	
Asphalt 2 coats	2000	
Asphalt paper, 0.5 kg/m <sup>2</sup>	750	
Asphalt paper, 2.5 kg/m <sup>2</sup>	1700	
Concrete		150
Gypsum		40
Glass		infinite
Mortar		80
Cork		100
Wallpaper	0.3	
Air, still		5
Metals		infinite
Rock wool		5
Polyethylene	125	
Polystyrene		75
Bricks		25
Wallboard, hard		500
Wallboard, soft		15
Paint for walls, matt	2-5	
Paint, alkyd	20 - 40	
Paint, oil	10	

## Appendix B: Sensitivity analysis p.25

The Table below shows the 16 experiments that were done for the sensitivity analysis.

RH_out	RH_in	T_out	T_cav	T_in	v_air	RH_cav
-1	-1	-1	-1	-1	-1	64.54
1	-1	-1	-1	-1	1	265.607
-1	1	-1	-1	1	1	38.455
1	1	-1	-1	-1	1	110.598
-1	-1	1	-1	1	1	4.81
1	-1	1	-1	-1	1	7607.706
-1	1	1	-1	-1	-1	516.285
1	1	1	-1	1	-1	5764.312
-1	-1	-1	1	-1	1	0.009
1	-1	-1	1	1	1	0.649
-1	1	-1	1	1	-1	10.644
1	1	-1	1	-1	-1	3.559
-1	-1	1	1	1	-1	1.33
1	-1	1	1	-1	-1	25.804
-1	1	1	1	-1	1	0.073
1	1	1	1	1	1	47.802

Each input parameter is set at minimum (-1) or maximum (1) depending on the pattern from the engineering statistics handbook. By setting the input parameters at minimum or maximum in the formula for the relative humidity in the cavity, the output will have a certain value. This value will be evaluated with a regression analysis from Excel. This regression analysis is shown in the table below.

Summary output				
<i>Regression Statistics</i>				
Multiple R	0.672865383			
R Square	0.452747823			
Adjusted R Square	0.087913039			
Standard Error	2183.252172			
Observations	16			
ANOVA				
	<i>df</i>	<i>SS</i>	<i>MS</i>	
Regression	6	35491077.5	5915179.583	
Residual	9	42899310.41	4766590.046	
Total	15	78390387.91		
<i>Coefficients</i>				
Intercept	903.8864375		<i>RH_out</i>	effects 1648.736 % effects 28.81266
<i>RH_out</i>	824.3681875		<i>RH_in</i>	184.8409 3.230206
<i>RH_in</i>	-92.4204375		<i>T_out</i>	1684.258 29.43342
<i>T_out</i>	842.1288125		<i>T_cav</i>	1785.305 31.19929
<i>T_cav</i>	-892.6526875		<i>T_in</i>	274.3706 4.794792
<i>T_in</i>	-137.1853125		<i>v_air</i>	144.7526 2.529639
<i>v_air</i>	72.3763125		Total	5722.264

The output of the regression analysis gives the coefficients that are needed in the equation to describe the relative humidity as a function of the input parameters. These coefficients are used to calculate the effect of each parameter on the relative humidity. Here, the effect is twice the coefficient. Each effect is now divided by the total effect to calculate the percentage effect. These percentages are plotted in the Pareto chart.